REPUBLIQUE DU CAMEROUN
Paix – Travail – Patrie
****
UNIVERSITE DE YAOUNDE I
FACULTE DES SCIENCES
DEPARTEMENT DE DE PHYSIQUES
****
CENTRE DE RECHERCHE ET DE FORMATION DOCTORALE EN SCIENCES, TECHNOLOGIES ET GEOSCIENCES

REPUBLIC OF CAMEROUN
Peace – Work – Fatherland
****
UNIVERSITY OF YAOUNDE I
FACULTY OF SCIENCE
DEPARTMENT OF OF PHYSICS
****
POSTGRADUATES SCHOOL OF SCIENCE, TECHNOLOGY AND GEOSCIENCES
LABORATORY OF NUCLEAR, ATOMIC, MOLECULAR PHYSICS AND BIOPHYSICS

Energy transport and localization in complex protein structures with long-range intermolecular interactions

THESIS
Submitted and defended in fulfillment of the requirements for the Degree of Doctorat/Ph.D in Physics

Par : **MADIBA EPANE Stéphane**
Master of Science in Physics, Option: Biophysics

Sous la direction de
EKOBENA FOUDA Henri Paul
Professor
Universitty of Yaounde I

Année Académique : 2020

UNIVERSITE DE YAOUNDE I
UNIVERSITY OF YAOUNDE I

FACULTE DES SCIENCES
FACULTY OF SCIENCE

DEPARTEMENT DE PHYSIQUE
DEPARTMENT OF PHYSICS

ATTESTATION DE CORRECTION DE LA THESE DE DOCTORAT/Ph.D

Nous, Professeur **BEN-BOLIE Germain Hubert**, Examinateur, et Professeur **NDJAKA Jean-Marie Bienvenu**, Président du jury de la Thèse de Doctorat/Ph.D de Monsieur **MADIBA EPANE Stéphane**, Matricule **05U083**, préparée sous la direction du Professeur **EKOBENA FOUDA Henri Paul** intitulée : « **Energy transport and localization in complex protein structures with long-range intermolecular interactions** », soutenue le **jeudi, 16 juillet 2020**, en vue de l'obtention du grade de Docteur/Ph.D en Physique, Spécialité **Physique nucléaire, Atomique, Moléculaire et Biophysique**, attestons que toutes les corrections demandées par le jury de soutenance ont été effectuées.

En foi de quoi, la présente attestation lui est délivrée pour servir et valoir ce que de droit.

Fait à Yaoundé le 17 JUL 2020

L'Examinateur

Pr. BEN-BOLIE Germain Hubert

Le Président du jury

Pr. NDJAKA Jean-Marie Bienvenu

Le Chef de Département de Physique

UNIVERSITE DE YAOUNDE I * FACULTE DES SCIENCES * Le Chef de Département DEPARTEMENT DE PHYSIQUE

Ndjaka Jean-Marie
Bienvenu
Professeur

Energy transport and localization in complex protein structures with long-range intermolecular interactions

Submitted in Partial Fulfillment of the Requirements

for the Degree of Doctor of Philosophy in Physics

Speciality: **Nuclear, Atomic, Molecular Physics and Biophysics**

Option: **Biophysics**

by

MADIBA EPANE Stéphane

M. Sc. in Physics

Registration Number: **05U083**

Under the supervision of

EKOBENA FOUDA Henri Paul

Professor

July 20, 2020

Dedication

↬ ***To the Almighty GOD for the health, intelligence, inspiration and graces he has always given me throughout my life***

↬ ***To my wife Mrs. Madiba, born Fouda Azeng Seraphine Estelle and my children Rachelle, Manuel, Dyclane, Evane and Chloé that they find here the justification of my absences throughout this work.***

↬ ***To my parents Mr. Madiba Justin and Mrs. Madiba, born Mrs. Dimwamwa Epanè Rachèl who spared no effort for my education, for their support and comfort during difficult times and for their kind guidance. The words are weak to show you my gratitude.***

Acknowledgments

My first thanks naturally go to my PhD supervisor, **Pr. Ekobena Fouda Henri Paul**, who has brought me over these years his complementary scientific skills to carry out this thesis. He also supported me and always guided me to carry out this work. Beyond the thesis, I want to thank him for his human qualities that have helped establish a calm and motivating work environment.

I would like to thank the members of jury who have accepted to evaluate the present work. The President of jury **Pr. Bienvenu Jean-Marie Ndjaka** and the other members of the jury **Pr. Germain Hubert Ben-Bolie**, **Pr. Hona Jeacques**, **Pr. Siéwé Siéwé Martin** and **Pr. Moukam Kakmeni François-Marie**.

I thank the Biophysics Laboratory of the Department of Physics of the Faculty of Sciences of the University of Yaoundé I and all its leading experts in knowledge for all the teaching and mentoring received from Level I to the present day. Sincerely thank **Pr. Kamgang Kabeyené Beyala Veronique**, Director of Higher Teacher Training College Bertoua who gave me the opportunity to teach as a temporary teacher in this school since its creation.

I would particularly like to thank **Pr. Conrad Bertrand TABI** very much for the confidence he has placed in me, as well as the many advice, explanations, scientific and human analyzes he has given me. I learned a lot from him and it was a great pleasure for me to work with him.

Pr. Effa Joseph Yves for his constant and unfailing support in the preparation of this thesis and for all our scientific discussions throughout this work.

I thank **Pr. Ema'a Ema'a**, **Dr. Djondiné Philippe**,respectively Deputy Director, Head of Physics Department and **Dr Belibi Belibi Placide** of Higher Teacher Training College Bertoua with whom i have a very good collaboration.

I would like to thank **Dr. Alain Mvogo**, **Dr. Dang Koko Adamou**, **Dr. Maïna**

Ibrahim, **Dr. Issa Sali**, **Dr. Mimshe Fewu Josué Clément**, **Dr. Ngoubi Hénock**, **Dr. Ondoua Rodrigue**, **Dr. Teuma Mbezi**, **Dr. Okali**, **Dr. Belobo** and **Dr. Mvondo Stanislas** with whom we created a cordial and warm environment, which was a determining factor for my success.

I thank my brothers and sisters: **Mrs Enyouma born Madiba Njollè** , **Madiba Ehonè**, **Madiba Moussoua Odile Leslie**, **Madiba Ebene Nkake Raoul** for their unfailing support and total confidence.

I thank brother-in-law **Colonel Enyouma Prothé**, **Um Laurent Patrice** and the whole **Enyouma** family for the support, hospitality, fraternity and friendliness they bring me.

I thank all my family-in-law to know the great **Ngoa** family of Ekali 3 on the road to Mbalmayo for their total trust and unimaginable support for me.

I would like to sincerely thank **Mr. and Mrs. Manon** for their presence and signicant contributions to my place and that of the whole family. May the Almighty grant them long life.

Finally, I would like to thank my sponsor **Ebonguè Ngoh Jean Jules** for his advice, his support and his daily interventions for my well-being.

I can not end without deeply thanking all those who have contributed directly or indirectly to my success and the outcome of this doctoral thesis, that they are honored.

Contents

List of Figures

List of Abbreviations

ATP: adenosine triphosphate

LRI: long-range interactions

NLS: nonlinear Schrödinger

sG: sine-Gordon

NLSEs: NLS equations

CNLS: coupled nonlinear Schrödinger

KdV: Korteweg and de Vries

MI: modulational instability

NLPDEs: nonlinear partial differential equations;

PDE: partial differential equation

IST: inverse scattering transform

Abstract

Based on a review of the literature, we have successfully constructed protein models, primarily based on the long-range interaction between peptide units of alpha-helical proteins. One of the models is a generalization of the Davydov model of alpha-helix proteins and comprises three strands, instead of just one as envisioned in the original model. This particular model has been shown to be fully described by a set of discrete, coupled and modified nonlinear Schrödinger equations involving long-range interactions between peptide groups along the protein strands. Using the method of modulation instability, it has been shown that the competition between non-linearity and long-range intermolecular interactions modifies the field of plane wave instability. The impact of competition between non-linearity and long-range interactions on the energy transport and storage process was also discussed numerically. It has been shown that non-linearity and long-range coupling can contribute to the emergence of solitonic structures trains, when the parameters are well chosen in the field of the instability of the plane waves. The relevance of the improved model as well as the biological implications of the long-range intermolecular interactions account have been discussed in the transport and energy storage contexts in molecular structures related to hydrogen in general, and in the proteins of α-helix in particular. In a second plane, the Schrödinger coupled fractional nonlinear equations were derived from two excitons energy transfer model of alpha-helical proteins. The terms fraction of space are due to the presence of long-range intermolecular interactions. Analysis of the linear stability of plane wave solutions has revealed the existence of regions of instability, in which solitary waves may appear as a result of the competition between nonlinear and dispersive effects. The parametric expansion of the instability growth rate has been shown to be sensitive to changes in fractional order and nonlinear coupling coefficient parameters. Numerical evidence of analytic predictions has been provided via the emergence and long-term behavior of solitonic structures, whose characteristics have changed with changes in fractional parameters.

Keywords: α-helical proteins, nonlinear excitations, solitons, long-range interactions.

Résumé

En se basant sur une revue de la littérature, nous avons réussi à construire des modèles de protéines, principalement basés sur l'interaction à longue portée entre les unités peptidiques d'hélice-alpha des protéines. L'un des modèles est une généralisation du modèle de Davydov d'hélice-alpha des protéines qui comprend trois brins, au lieu d'une seule comme envisagé dans le modèle initial. Il a été montré que ce modèle particulier était complètement décrit par un ensemble d'équations de Schrödinger non linéaires discrètes, couplées et modifiées, impliquant des interactions à longue portée entre des groupes peptidiques le long des brins de protéines. Au moyen de la méthode de l'instabilité modulationnelle, il a été montré que la compétition entre la non-linéarité et les interactions intermoléculaires à longue portée modifiait le domaine de l'instabilité des ondes planes. L'impact de la concurrence entre la non-linéarité et les interactions à longue portée, sur le processus de transport et de stockage de l'énergie, a également été abordé numériquement. Il a été démontré que la non-linéarité et les couplages à longue portée peuvent concourir à l'émergence de trains de structures solitoniques, lorsque les paramètres sont bien choisis dans le domaine de l'instabilité des ondes planes. La pertinence du modèle amélioré ainsi que les implications biologiques du compte des interactions intermoléculaires à longue portée ont été discutées dans les contextes de transport et de stockage d'énergie dans les structures moléculaires liées à l'hydrogène en général, et dans les hélice-α des protéines en particulier. Dans un deuxième plan, les équations non linéaires fractionnées couplées de Schrödinger ont été dérivées d'un modèle de transfert d'énergie à deux excitons d'hélice-alpha des protéines. Les termes fraction d'espace sont dus à la présence d'interactions intermoléculaires à longue portée. L'analyse de la stabilité linéaire des solutions d'ondes planes a révélé l'existence de régions d'instabilité, dans lesquelles des ondes solitaires pourraient apparaître à la suite de la concurrence entre effets non linéaires et dispersifs. L'expansion paramétrique du taux de croissance de l'instabilité s'est révélée être sensible aux variations des paramètres d'ordre fractionnel et du coefficient de couplage non linéaire. Des preuves numériques sur les prédictions analytiques ont été fournies via l'émergence et le comportement de la longue portée sur les structures solitoniques, dont les caractéristiques se sont modifiées avec les variations des paramètres d'ordre fractionnaire.

Mots clés: hélice-α des protéines, excitations nonlinéaires, solitons, interactions à longue portée.

General Introduction

The work of Fermi, Pasta and Ulam, Zabusky and Kruskal has given rise to many studies of the dynamics of nonlinear excitations in atomic networks. Nonlinear excitations in diatomic chains have received a lot of attention because of their applications to many physical systems. Indeed, diatomic chain models have been used as prototypes to describe the energy transport, the conductivity of proton mobility in hydrogen-bonded chains. Davydov's mechanism for locating and transporting energy in proteins relates to the α-helix often found in membranes. The hydrolysis of ATP (adenosine triphosphate) releases a neighboring energy two quanta $\hbar\omega$ from the vibrational model of the carbon-oxygen bond. This vibration is therefore a natural candidate for storing the hydrolysis energy of ATP. Moreover, since the hydrogen atom is engaged in a hydrogen bond which contributes to maintaining the geometry of the helix, it may be thought that the excitation of the oxygen carbon bond is coupled to the mode of deformation of the propeller. This is proposed by Davydov's model, which considers that the energy transmitted to the carbon-oxygen bond contributes to locally deforming the helix. This distortion tends to slightly modify the vibration frequency of the excited carbon-oxygen bond which ceases to be reasoning with the other oxygen carbon bonds of the neighborhood. It is important to know that many biological processes such as muscle contraction, active transport and enzymatic catalysis rely on energy. This energy, which is released by the hydrolysis of adenosine triphosphate (ATP), is mainly transported and stored by proteins. The understanding of subsequent phenomena, related to energy management by proteins, has been an active research topic since the pioneering work of Davydov **[1]**. Based on a simple formulation of the problem, Davydov showed that energy is transported by solitonic structures, thus establishing the relationship between these entities and the distortions of the network. In particular, considering the structure of the helix-α, Davydov and Kislukha **[2, 3]** proteins used the exciton formalism to explain the automatic trapping of the oscillations of the amide-I, as a consequence of the interaction between exciton vibrations and the distor-

tion of the protein structure resulting from the presence of the exciton. They established that due to the interaction between non-linearity and dispersion, the self-trapped amide-I vibratory energy, coupled with the deformation of the protein structure, could travel as a soliton in the protein strand **[4, 5]**. Previous models on the subject of energy transport and storage in protein chains focused on a single-stranded structure of hydrogen-bonded peptide units, both in the discrete regime and in the continuous regime **[6–8]**. These models have been hotly debated because of their inconsistent formulation in the Davydov soliton life-time predictions and, more importantly, their stability at 300 K biological temperature **[9–16]**. Nevertheless, numerical simulations have revealed that such solitons could be stable at 300 K, but these studies have been conducted from a purely classical point of view, with no consistent argument to prove their stability **[4, 5, 17–22]**. In order to solve this problem, the adoption of a description of the protein helix-α, in the form of a biological system stabilized by three quasi-linear strands has proved to be a good idea. Most of the pioneering analytical and numerical contributions in this direction can be found in references **[5, 23, 24]**. In the same sense, Daniel and Latha **[25]**, discussed slightly modified Davydov models of the helix-α proteins, in which discrete and continuous regimes were studied with particular interest for the influence of the backbone, coupling and its consequences on the transport and metabolism process. energy storage between the spines. Based on the fact that the process of Modular Instability (MI) is a direct mechanism leading to solitons and the formation of nonlinear structures **[26–30]**, Tabi et al. **[31–33]** have shown that this process could also be considered in the context of three-stranded molecular structures. More recently, a generalized model of helix-α protein chains, including competition between diagonal and non-diagonal couplings, has been proposed **[34]**. Subsequent energy modes proved to be very sensitive to the nonlinear effects introduced by the two types of coupling. In reference **[33]**, using the Hennig model **[35]**, Tabi et al. have shown that during the energy transport process, the covalent bonds can be compressed, while the hydrogen bonds exhibit oscillating behaviors leading to favorable conditions for the transport and storage of energy in the coupled spines via polaronic structures . Based on X-ray protein analysis data, it has also been shown that the three-dimensional structure is favorable for the transfer of energy and particles into proteins, due to the important presence of hydrogen bridges between them. thorns **[36–38]**. In other words, the polarons appearing in the dynamics of the proteins can correspond to the energy related to the transport of the electrons, as a function of

the force of coupling to the vibratory movements **[39]**. In addition, recent studies have suggested that long-range dispersive (LR) interactions may be responsible for interesting dynamic behaviors, particularly in molecular systems such as DNA and proteins **[40–42]**, neural **[43,44]** and the cell **[45]**. This thesis is dedicated to the transport and localization of energy in complex protein structures with long-range intermolecular interactions. Our main objective here is to show that dispersive LR interactions can enhance the efficiency of energy transport and storage in three-stranded molecules with inter-spin coupling. The organization of work is as follows: chapter one presents the generalities of protein chains on the biological and physical aspects, with particular emphasis on their dynamics. The methods of investigation will be presented in chapter two. We will first present the preliminaries during which we will discuss models with long-range energy modes in helix-α networks with inter-spin coupling and models with long-range interaction effects; then we will talk about the analytical method used; and finally, we will talk about the numerical method used. We will conclude with chapter three on results and discussions. We will not be able to complete this work without making a general conclusion and perspectives.

Chapter 1

Literature review, the soliton concept and the Davydov model

Introduction

Biology tells us that proteins are essential for the body because they participate in virtually every process in cells. In this chapter, we will talk about the information about protein chains, the origin of the concept of soliton and the theory of Davydov soliton that he proposed a long time ago explaining the mechanism of transport and storage. of energy in the protein molecules.

1.1 Protein chains

Proteins are biological macromolecules found in all living cells. They are formed of one or more polypeptide chains. Each of these chains consists of the sequence of amino acid residues linked together by peptide bonds. Proteins provide a multitude of functions within the living cell and in tissues. These are enzymatic proteins (enzymes) that catalyze the chemical reactions of synthesis and degradation necessary for the metabolism of the cell. Other proteins provide a structural role within the cytoskeleton or tissues (actin, collagen), some are molecular motors that allow mobility (myosin), others are involved in the conditioning of DNA (histones), the regulation of gene expression (transcription factors) or the transmission of cellular signals (membrane receptors).
The protein chains are synthesized in the cell by the ribosomes, from the information coded

in the genes, which determine the order in which the 22 amino acids, called proteinigenic, which are incorporated directly during the biosynthesis of proteins. The sequence of amino acids is called the polypeptide sequence. Post-translational modifications may occur after the protein has been synthesized, which may have the effect of modifying its physical or chemical properties. It is also common for non-protein molecules, called prosthetic groups, to bind stably to proteins and play a decisive role in their biological functions: this is the case, for example, with heme in hemoglobin, without which this protein could not carry oxygen in the blood. Proteins adopt a three-dimensional structure that allows them to perform their biological function. This particular structure is determined primarily by their amino acid sequence whose various physico-chemical properties lead the protein chain to adopt a stable folding.
In the laboratory, they can be separated from other cellular constituents using various techniques such as ultracentrifugation, precipitation, electrophoresis and chromatography. Genetic engineering has introduced a large number of methods to facilitate the purification of proteins. Their structure can be studied by immunohistochemistry, site-directed mutagenesis, X-ray crystallography, nuclear magnetic resonance and mass spectrometry. Proteins are an important component of animal nutrition, they are degraded in the digestive tract and the released amino acids are then reused by the body.

1.1.1 Aminoacids and peptide bond

Due to the chemical structure of different acids amino acids, the protein chain has directionality. The end of the protein with a free carboxylic group is known as than C-terminus or carboxy terminus, while the end witha group of free animated is known as N-terminus or amine terminus. The words protein, polypeptide, and peptide are few an ambiguous and can overlap in meaning. the protein is generally used to refer to the biological molecule complete in a stable conformation, while peptide is typically reserved for oligomers of a short aminoacid often lack a stable three-dimensional structure. However, the boundary between the twois not well defined and is usually not close to 20-30 residues. Polypeptide can refer to any linear string simple aminoacids, usually independently of the length **[1]**.

1.1.2 Protein structures

Four levels of structural complexity are used to describe the three-dimensional shapes of proteins. Most proteins are folded in athree-fold structuredimensions. The form in which a proteinfoldsof course isknown as its native state. Althoughmanyproteinscanbend-without help, simply by the chemicalproperties of theiraminoacids, othersrequiremolecular help to bend in their initial states. Biochemistsoftenrefer to four distinct aspects of the structure:

1.1.2.1 Primary structure: aminoacidorder structure

Most proteins have a linear primary structure Each amino acid is linked to the next by a peptide bond, which is formed when the carboxylic group of a first amino acid reacts with the amino group of a second, with elimination of water. When amino acids are incorporated into a chain (called a polypeptide chain), they are called residues. The polypeptide chain is not connected; it forms a single stretched filament. By convention, the first amino acid in the chain is designated as being the one whose amino group remains free; it is said that it is in 5 or else that it constitutes the N-terminus or the N-terminus. The last residue of the chain is the one whose carboxylic group remains free; it is said at 3, or at the C-terminus.

There are circular proteins: By focusing on the active ingredient of a Congolese medicinal tea that facilitates uterine contractions, it was discovered in the 90's that it was a small protein with a circular structure, stable enough to resist boiling. and ingestion. This protein, the B1 kalata, was just the first of a series of circular proteins we had to discover, and now have more than a hundred members in their ranks (we think there could even be several thousands). Their structure gives them great stability and many of them have insecticidal or antimicrobial activities. (Other non-protein circular peptides exist, such as the cyclosporine we discussed in 1.6.2). Some have a topological structure in node (this is the case of kalata B1); they are called cyclotides.

Circular proteins seem to be produced from large linear precursors, but the enzymes that allow their maturation and cyclization are poorly known. In the case of mammalian defensin RTD-1, two independent precursors are cut and ligated together at both ends to form a circle. In the case of kalata B1, two separate parts of the same precursor are first cut, then leagued at their ends to form a circle. But in the case of AS-48 bacteriocin, only

one precursor is cut and its two ends united to close the circle.
The advantage of being circular for one protein is, among other things, not to offer a terminal end to the exopeptidases. The stability is thus increased. It is also more difficult to permanently denature them by heat or pH changes.

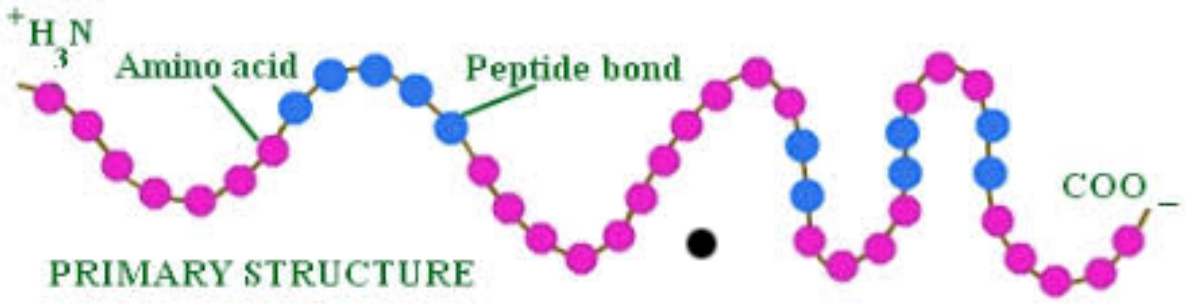

Figure 1.1: *Amino-acids sequence. Image taken from Jewel Medley, biologiste associé, Austin Community College (2017)*

1.1.2.2 Secondary structure

The secondary structure of a protein is the local spatial arrangement of a polypeptide backbone atoms without regard to the conformations of its side chains. Protein secondary structure includes the regular polypeptide folding patterns such as helices, sheets, and turns. The secondary structure exhibits two regular structure: the α-helix and the β-sheet. regularly repetition of local structures is stabilized by hydrogen bonds. Since the structures secondary are local, many structural regions different secondary maybe present in the same molecule of protein (Figure 1.2)

1.1.1.2.1 The α-helix

The α-helix is right-handed; that is, it turns in the direction that the fingers of a right hand curl when its thumb points in the direction that the helix rises. The α-helix has 3.6 residues per turn and a pitch (the distance the helix rises along its axis per turn) of 5.4 Å **[5, 46]**. The α-helices of proteins have an average length of $\sim$12 residues, which corresponds to over three helical turns, and a length of $\sim$18 Å. The real α-helix structure of protein molecules consists of three spines (chains) of hydrogen bonded peptide groups in the longitudinal direction. Each spine contains peptide groups (HNCO) periodically placed, connected by hydrogen bonds "...H-N-C=O...H-N-C=O...H-N-C=O...", where the

dotted lines represent hydrogen bonds and C=O the amide-I bond, as shown in Fig. 1.2. Most of the investigations are based on the assumption that they are approximately parallel and independent.

In the α-helix, the backbone hydrogen bonds are arranged such that the peptide C=O bond of the nth residue points along the helix axis toward the peptide N-H group of the (n+4)th residue. This results in a strong hydrogen bond that has the nearly optimum N...O distance of 2.8 Å. Amino acid side chains project outward and downward from the helix, thereby avoiding steric interference with the polypeptide backbone and with each other. The core of the helix is tightly packed; that is, its atoms are in Van der Waals contact.

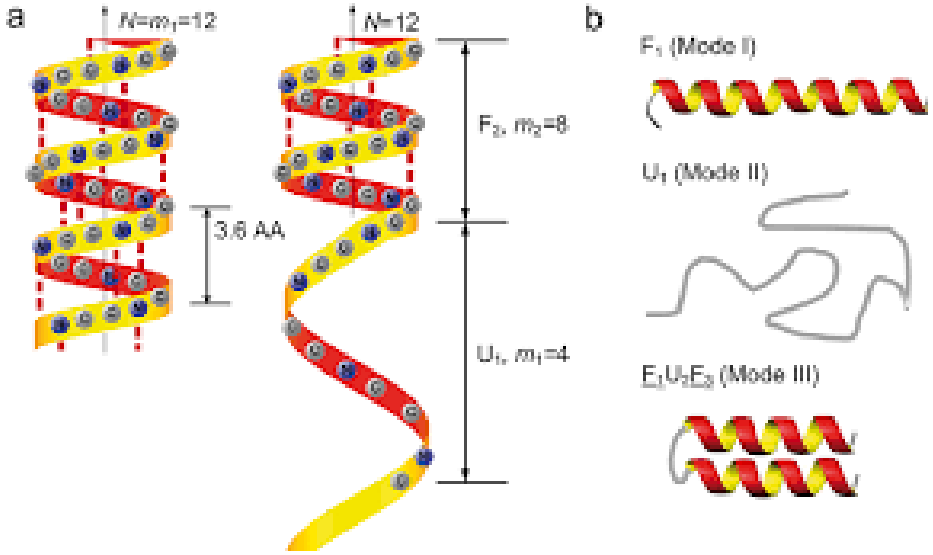

Figure 1.2: secondary structure of α-*helix* . *Image taken from wikipedia*

1.1.1.2.2 The β-sheet

In 1951, the same year Pauling proposed the α-helix, Pauling and Corey postulated the existence of a different polypeptide secondary structure, the β-sheet. Like the α-helix, the β-sheet uses the full hydrogen-bonding capacity of the polypeptide backbone. In β-sheets, however, hydrogen bonding occurs between neighboring polypeptide chains rather than within one as in an α-helix. Sheets come in two varieties:

1. The antiparallel β-sheet, in which neighboring hydrogen-bonded polypeptide chains run in opposite directions.

2. The parallel β-sheet, in which the hydrogen-bonded chains extend in the same

direction. The conformations in which these structures are optimally hydrogen bonded vary somewhat from that of the fully extended polypeptide shown in Fig. 1.3. They therefore have a rippled or pleated edge-on appearance and for that reason are sometimes called pleated sheets. Successive side chains of a polypeptide chain in a β-sheet extend to opposite sides of the sheet with a two-residue repeat distance of 7.0 Å.

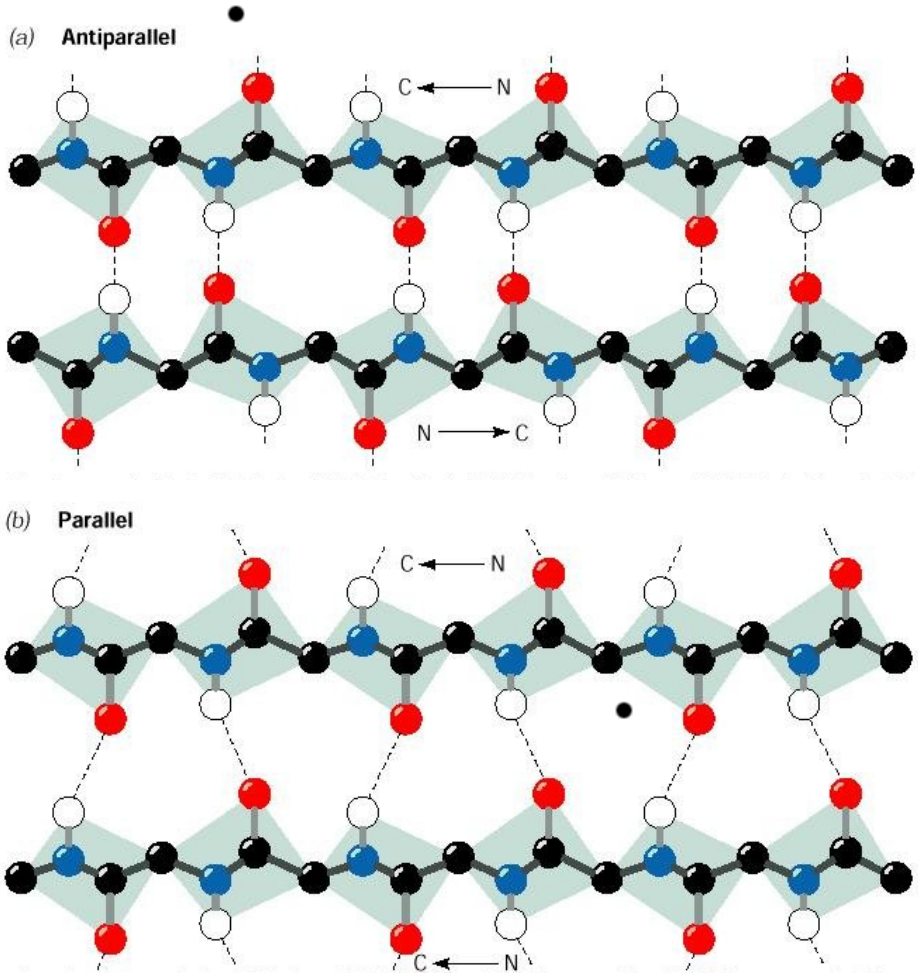

Figure 1.3: *β-sheet structure of proteins. Image taken from Scool of Biomedical Sciences Kiki*

1.1.2.3 Tertiary structure

The global form of a molecule simple protein is the spatial relationship of structures secondary to one another. The tertiary structure is usually stabilized by nonlocal interactions, but also across as alt bridge, hydrogen bonds, difulphide bonds, and level post-translational modifications. The term "tertiary structure" is often used as synonymous

with the fold limit.

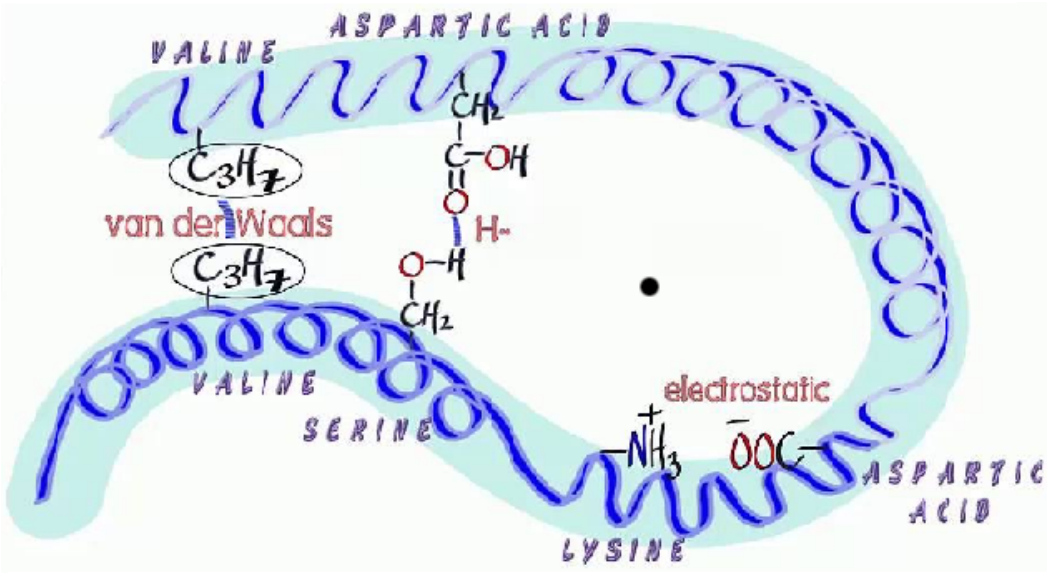

Figure 1.4: *Tertiary structure of proteins. Image taken from Frankly Chemestry, 11 july 2016 (Youtub)*

1.1.2.4 Quaternary structure

Shape or structure results from the interaction of more than one molecule of protein, usually called protein subunits in this context,that function as part of the larger assembly or protein complex. Proteins are not the molecules completely rigid. In addition to these levels of structure,proteins can shift betweens ever al related structures while they perform their biological function. In the context of these functional rearrangements, these structures tertiary or quaternary are usually referred to as "conformations, "and transitions between them are called conformation changes. Such changes are often induced by the attachment of a substrate molecule to an enzyme active location, or the physical region of the protein that participates in chemical catalysis. In solution all the proteins also undergo the variation of the structure by the vibration, thermal and collision with other molecules, see animation on the right side. Proteins can be unofficially divided into three main classes, which correlate with typical tertiary structures: proteins globular, fibrous proteins, and membrane proteins.Almost all globular proteins are soluble and many are enzymes. Fibrous proteins are often structural; of protein membrane serve oftenreceptorsor provide channels for polar or charged molecules to go through the cell

membrane.A special box of intramolecular hydrogen sticks in proteins, poorly protected from water attack and therefore to promote their own dehydration, are called dehydrons (Figure 1.2), **[3]**

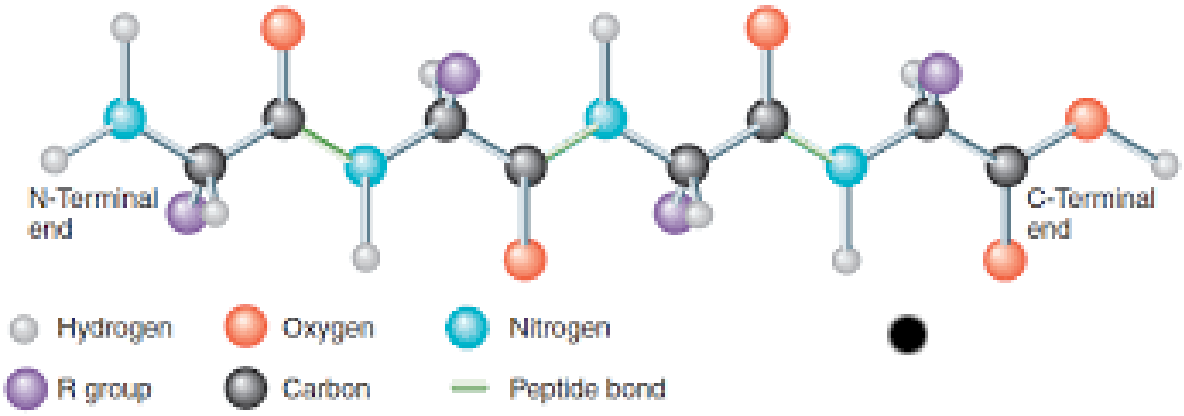

Figure 1.5: *Quaternary structure of proteins. Image taken from Kevin Ahern's Biochemestry (BB450/550) at organstate edu.*

1.1.3 Structure determination

Discovering the tertiary structure of a protein, or structure quaternary complex, can provide important clues about how the protein performs its function. The common experimental methods of structure determination include X-ray crystallography and NMR spectroscopy, at which can produce the atomic information resolution.Cryoelectron microscopy is used to produce low-resolution structural information about very complex large amounts of protein, including reunited viruses **[1]**; variant known as electron crystallography canals op ro duce high resolution information in some cases, especially for two-dimensional crystals membrane proteins **[2]**. Resolved structures are usually deposited in Protein Data Bank (PDB), a resource freely available from the form of which one can get structural data about thousands of cartesian coordinate proteins for each atom in the protein. Many more gene sequences are known than protein structures. In addition, the set of resolved structures is bi as ed towards proteins that can easily under reserves the conditions required in X-ray crystallography, one of the main methods of structure determination. In particular, globular proteins are comparatively easy to crystallize for the purpose of ray crystallography X. Membrane proteins, on the other hand, are difficult

to crystallize and are under-represented in PDB **[3]**.

Genomics structural initiatives have tried to remedy these inadequacies in systematically solving the structures representative of the main classes of folds. Forecast of protein structure the methods try to provide ways to produce a plausible structure for proteins whose structures have not been experimentally determined. Proteins are organic molecules consisting of a certain amino acid sequence linked together by a binding peptide. The carbonyl group (C = O) and the amine group (-NH) of the peptic link look for a configuration of low energy. One of the ways to minimize the internal energy of the molecule, and thus to stabilize it, consists of creating hydrogen bonds **[1]**. But the group amine of a peptide bond located in position n canto contract a bond of this type with the amine group of a other chemical la is on located 4 amino acids further downstream in chain. And so on: n + 1 creates an H link with n + 5. These hydrogen bonds force the protein to adopt a helical conformation. When the bond involves the acids amines n and n + 4, we speak of alpha helix. When it concerns the amino acids n and n + 3, we speak of helix 310 and when it concerns the amino acids n and n + 5, we speak Propeller.

It can be considered that the beta sheet is actually a very stretched propeller. The alpha helix therefore allows, as we have just see it, decrease the overall energy of the protein. Why some regions of the protein adopt this configuration rather thana not her remains the object of research. Only certain trends that certain amino acid sequences have have been noted as appearing more often, statistically, in a alpha helix. This is due in large part to the fact that peptides can "choose" to satisfy their hydrogen bond with side chains of amino acids rather than with the peptide bonds.

There is however a case where the sequence Amino acid must adopt the helical conformation: when This is the part of a membrane protein that crosses the membrane. Indeed, in this hydrophobic medium, the only way to make H bonds is to adopt a helical conformation (or beta leaflet, but we saw that the beta leafletis a special case of the propeller). There are several types of helices in proteins: The alpha helices, whose direction of gyration is hourly. He is by far the most represented helical structure in proteins. Weals of ind propellers 310 right and alpha helices. These three types of propellers are allowed by the Ramachandran diagram. The alpha helix being optically active **[3]**, circular dichroism measurements are used to determine the "elicitation rate" of a protein in solution **[47]**. The three forms of DNA: A, B, Z. We distinguish on the form B,center, the small furrow in the center of the image, and two parts of the bigfurrowat the top and bottom of the

image. Nucleic acids organize themselves into double helices to satisfy the links between bases. This structure has the effect of making a stack of bases on each other, thereby minimizing the energy of the system excluding water. This stacking is also the origin of the hyperchromic effect of DNA (increase in the fluorescence emission of DNA when two strands complementary separates).
In a DNA helix, we have a hydrophobic core constituted by the stacking of the bases above the others and a skeleton formed by the bridges phosphorus and sugars (deoxyribose) rather hydrophilic. The propeller type B, the most common, defines a large furrow and a small furrow. Access to the bases contained in the great groove and in the little furrow is different. In addition, certain proteins DNA-binding regulation show a higher tropism for one of the furrows. Depending on the conditions of the environment (salinity, content in water), but also to a certain extent depending on the composition in bases, nucleic acids adopt one of the three conformations: Propeller B double helix right Helix A double helix right Helix Z double helix left Presents the different levels of compaction from DNA to chromosome These three types of helix are found in the DNA that we call then B-DNA, A-DNA and Z-DNA. The most represented is B-DNA. RNA adopts helix A.

1.2 Types of Proteins

There are two types of proteins namely fibrous proteins and globular proteins.

1.2.1 Fibrous proteins

The main fibrous proteins are collagen, keratin, fibrinogen and muscle proteins.

1.2.1.1 Collagen

Collagen is the most abundant protein in vertebrates. It is found in bones, skin, tendons and cartilage. Its molecule usually contains three long polypeptide chains, each composed of about one thousand amino acids. These chains curl into a regular triple helix, responsible for the elasticity of the skin and tendons. When collagen fibrils are degraded by intense heating, their chains shorten to form gelatin.

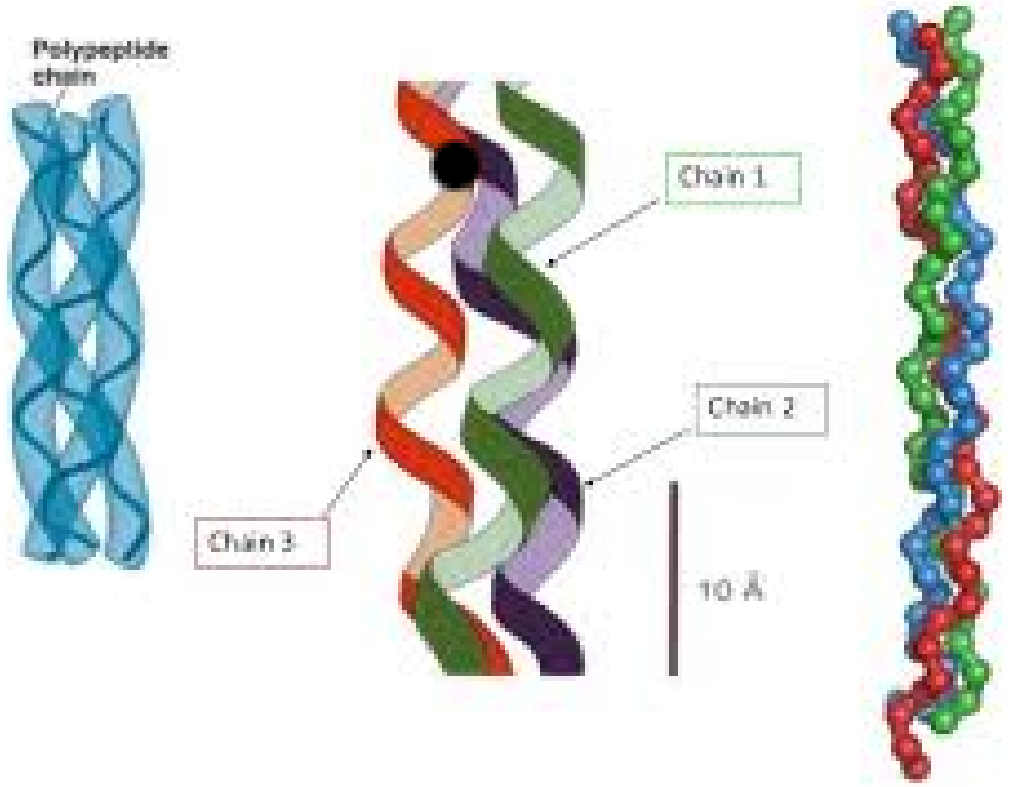

Figure 1.6: *Collagen structure.Image taken from wikimedia commons*

1.2.1.2 Keratin

Keratin, present in the upper layers of the epidermis, in the hair, nails, scales, hooves and feathers, wraps in a regular twist called "alpha helix". Charged with protecting the body against the external environment, keratin is completely insoluble in water. Its numerous disulfide bonds make it an extremely stable protein able to resist the action of proteolytic enzymes.

1.2.1.3 Fibrinogen

Fibrinogen is a plasma protein that causes blood clotting. Due to the action of thrombin, fibrinogen is converted into fibrin molecules, an insoluble protein that clumps together to form a clot.

1.2.1.4 Muscle proteins

Myosin binds to actin, another muscle protein, to give actomyosin. Filaments of actomyosin can shorten and cause contraction of muscles.

1.2.2 Globular proteins

Unlike fibrous proteins, globular proteins are spherical and highly soluble. They play an important role in metabolism. Albumins, globulins, casein and protein hormones are globular proteins. Albumins and globulins are abundant in animal cells, blood serum, milk and eggs. Hemoglobin is a protein that carries oxygen in the body. She is responsible for the color of the red blood cells. More than one hundred different human hemoglobins have been discovered, including hemoglobin S, responsible for sickle cell anemia, a hereditary disease endemic in black Africa. Sickle cell anemia is a form of anemia caused by an alteration of the shape of red blood cells (RBCs), which take on the appearance of a sickle. This is due to the presence of an abnormal form of hemoglobin, the protein responsible for the transport of oxygen.

1.2.2.1 Enzymes

All enzymes are globular proteins that bind rapidly with other substances, called "substrates", to catalyze the many chemical reactions of metabolism. These molecules have catalytic sites on which the substrates are placed, as a key in a lock, and are transformed into specific products.

1.2.2.2 Protein hormones

These proteins, which come from the endocrine glands, do not act like enzymes. They stimulate target organs that, in turn, control important activities such as metabolic efficiency or enzyme production. Insulin, secreted by pancreatic islets, regulates carbohydrate metabolism by controlling blood glucose levels. Thyroglobulin, produced by the thyroid gland, regulates the entire metabolism. Calcitonin, also produced by the thyroid, lowers the level of calcium in the blood.

1.2.2.3 Antibody

Also known as "immunoglobulins", antibodies are proteins present in the blood serum whose role is to bind to antigens (substances or foreign bodies invading the body). A single antigen can induce the production of many types of antibodies that neutralize it by binding to it and facilitating its degradation.

1.2.2.4 Microtubules

The globular proteins can also assemble into tiny hollow tubes, serving both as a cell skeleton and an intracellular transport vehicle. Each of these microtubules consists of two types of proteins that are linearly linked to form a tube of great length. Microtubules make up the internal structure of cellular eyelashes, appendages through which microorganisms move in their environment.

1.3 Origin of the soliton concept

In 1834, a young engineer named John Scott Russell (1808-1882) while conducting experiments to determine the most efficient design for canal boats, made a remarkable scientific discovery **[48]**. As he described it in his Report on Waves: I was observing the motion of a boat which was rapidly drawn along a narrow channel by a pair of horses, when the boat suddenly stopped - not so the mass of water in the channel which it had put in motion; it accumulated round the prow of the vessel in a state of violent agitation, then suddenly leaving it behind, rolled forward with great velocity, assuming the form of a large solitary elevation, a rounded, smooth and well-defined heap of water, which continued its course along the channel apparently without change of form or diminution of speed. I followed it on horseback, and overtook it still rolling on at a rate of some eight or nine miles an hour, preserving its original figure some thirty feet long and a foot to a foot and a half in height. Its height gradually diminished, and after a chase of one or two miles I lost it in the windings of the channel. Such, in the month of August 1834, was my first chance interview with that singular and beautiful phenomenon which I have called "the Wave of Translation. This event took place on the Union Canal at Hermiston, very close to the Riccarton campus of Heriot-Watt University, Edinburgh.

The simulation of the observations made by J. S. Russell was been possible in 1995, at the Heriot-Watt University at a conference dedicated to the solitons and for their

applications, which took place in Edinburgh in 1982. Figure 1.4 shows it. On this figure, we can see an example of the solitary wave.

John Scott-Russell first discovered the soliton phenomenon in 1834, and further research led to understanding solitons as solutions to the KdV, modified KdV, and Sine-Gordon equations **[49, 50]**. Zabusky and Kruskal **[51]** in 1965 investigated soliton solutions of the KdV equation **[49]**. They demonstrated that solitons exist in one-dimensional space. Gardner *et al.* **[52]** introduced the inverse scattering technique for solving the KdV equation and proved that this equation is completely integrable. In 1972, Zakharov and Shabat **[53]** found another integrable equation and finally it turned out that the inverse scattering technique can be applied successfully to a whole class of equations (e.g. the nonlinear Schrödinger and sine-Gordon equations). From 1965 up to about 1975, a common agreement was reached to reserve the term soliton to pulse-like solitary solutions of conservative nonlinear partial differential equations that can be solved by using the inverse scattering technique.

1.3.1 Different classes of soliton

The soliton is a wave packet that maintains its shape while it travels at constant speed. Solitons are caused by a cancelation of nonlinear and dispersive effects in the medium. The term "dispersive effects" refers to a property of certain systems where the speed of the waves varies according to frequency. They arise as the solutions of a widespread class of weakly nonlinear dispersive partial differential equations describing physical systems **[50]**. They also have particle like behavior i.e., preserving their forms in space or in time or both in space and time resulting in spatial, temporal or spatiotemporal solitons, respectively. There are two types of solitons: the non-topological soliton and the topological soliton **[50]**.

1.3.1.1 Non-topological solitons

A soliton is non-topological when the propagation medium remains in the same state before and after the wave has passed. These types of soliton are those observed in hydrodynamics (although some are also observed in solid mechanics). In hydrodynamics environment, the non-topological soliton can be described by the KdV equation **[49, 50]**.

$$\frac{1}{c_0}\frac{\partial \eta}{\partial t} + \frac{\partial \eta}{\partial x} + \frac{3\eta}{2h}\frac{\partial \eta}{\partial x} + \frac{h^2}{6}\frac{\partial^3 \eta}{\partial x^3} = 0 \tag{1.1}$$

where $c_0 = \sqrt{gh}$ is the speed of propagation of linear waves in the limits of great wavelengths, h the depth and η the height of the liquid surface above the level of balance.

The KdV equation has the following soliton solution **[49, 50]**

$$\eta = \eta_0 \mathrm{sech}^2[\frac{1}{2h}\sqrt{\frac{3\eta_0}{h}}(x - c_0[1 + \frac{\eta_0}{2h}]t)], \tag{1.2}$$

where the width of the soliton $L = \sqrt{2/A}$ varies with the amplitude A. It decreases when the amplitude A increases and tend to the infinity when the amplitude tends to zero. The KdV equation is one of the prototypes of the theory of solitons because it has remarkable mathematical properties.

1.3.1.2 Topological solitons

A soliton is topological when the propagation medium is in different states before and after the passing of the wave. The soliton can be described in this state by the sine-Gordon (sG) equation **[50]**. This sG equation, which is derived from a chain of pendulum of mass m and length l is given by

$$\frac{\partial^2 \theta}{\partial t^2} - c_0^2 \frac{\partial^2 \theta}{\partial x^2} + \omega_0^2 \sin(\theta) = 0, \tag{1.3}$$

where $\omega_0^2 = \frac{mgl}{I}$ is the frequency, $c_0^2 = \frac{Ca^2}{I}$ is the velocity and g is the gravity; I is the moment of inertia, C is the constant of torsion of the spring and a is the distance between the pendulum. As the KdV equation, this equation is completely integrable and admits exact soliton solutions. A soliton solution of this equation is **[49, 50]**:

$$\theta(x,t)_{\pm} = 4\arctan[\exp(\pm\frac{x - ct}{L})], \tag{1.4}$$

where $L = \frac{c_0}{\omega_0}\sqrt{1 - \frac{c^2}{c_0^2}}$ measures the spatial extension of the solution.

1.3.2 Some applications of solitons

The remarkable properties of solitons have been used to explain many yet unexplained phenomena such as the Fermi-Pasta-Ulam paradox **[54]**, and to discover and establish new theories in many aspects of science and technology **[50, 55, 56]**. In elastic tubes for

example, the soliton results from the balance between nonlinearity from the hydrodynamics of blood flow and dispersion related to the elasticity of the artery wall **[57]**. The soliton model in neuroscience is a recent developed model that attempts to explain how signals are conducted within neurons. This model proposes that the signals travel along the cell's membrane in the form of pulse solitons **[58, 59]**. As such the model presents a direct challenge to the widely accepted Hodgkin-Huxley model **[60]** which proposes that signals travel as action potentials. In hydrodynamics, tsunamis and rogue waves are well known manifestations of solitons. Solitons are very important in telecommunications, especially in data transmission system.

1.4 Davydov's model

In 1973 scientists gathered at the New York Academy of Sciences to discuss an unanswered question in bioenergetics: How is chemical energy transduced and transported in biological systems?. In the same year, Davydov projected a nonlinear mechanism for the storage and transfer of vibrational energy in protein molecules **[8]**. The Davydov model describes energy transfer in the hydrogen-bonded spines that stabilize protein α-helices. Exploiting the regularity in the structure of α-helical proteins, he showed that simplified models of these proteins could self-focus, or trap energy in stable pulse-like waves known as solitons. The Davydov model is based on the assumption that transport of amide-I bond energy along the α-helical proteins is the same as transport in a molecular crystal **[8, 61, 62]**.

The idea is that the energy liberated in the hydrolysis of adenosine triphosphate (ATP) creates up to two quanta of amide-I, an excited vibrational state in the peptide group that is essentially a stretching vibration in the C=O bond. This vibration excitation propagates from one group to the next because of the dipole-dipole interaction between the groups. But it also interacts with the neighboring hydrogen bonds, leading to a deformation of the lattice and a lower energy state. This new state, which is constituted by an amide-I excitation and its associated hydrogen bond distortion, is the Davydov soliton. The Davydov model which is otherwise known as the Davydov soliton, is able to predict that nonlinear interactions between phonons and amide-I vibrations can produce a long-lived combined excitation, which propagates along the α-helical proteins.

Solitons in the Davydov model are formed as a result of the dynamical balance between

the dispersion due to the resonant interaction of internal vibrations and the nonlinearity provided by the interaction of these vibrations with the local displacements of the equilibrium positions of the peptide groups.

However, the Davydov model, due to its simplicity, has been thought to reduce the whole dynamics of the complex α-helical protein to only one spine, as it was assumed that the results for one hydrogen bonding spine summarizes the features of the whole α-helix duplex. The nonlinear model proposed by Davydov is able to rationalize long distance energy transduction. Davydov accommodated his idea by the following Hamiltonian

$$H = H_{ex} + H_{ph} + H_{int}, \tag{1.5}$$

where H_{ex} is the Hamiltonian for the amide-I vibrational excitations, which describes the dynamics of intramolecular excitations or simply excitons. H_{ph} is the Hamiltonian for the displacements of the peptide groups also known as lattice vibrations and H_{int} is the Hamiltonian for the interaction between the amide-I excitations and the displacements of the peptide groups. H_{ex} is given by

$$H_{ex} = \sum_n \left[E_0 B_n^+ B_n - J(B_n^+ B_{n-1} + B_n^+ B_{n+1})\right], \tag{1.6}$$

where the term $E_0 B_n^+ B_n$ defines the amide-I excitation energy, while $B_n^+(B_n)$ is the boson creation (annihilation) operator for the intramolecular vibrations and the constant E_0 the exciton energy on the n^{th} site. These operators satisfy the commutation relations $[B_n, B_m^+] = \delta_{mn}$ and $[B_n, B_m] = 0$. The constant J is the intersite transfer energy constant produced by the dipole-dipole interactions. $B_n^+ B_{n-1}$ and $B_n^+ B_{n+1}$ represent transfer of amide-I energy from site n to $n \pm 1$ due to the dipole-dipole interactions.

The energy H_{ph} associated with displacing the peptide groups away from their equilibrium positions is given in the harmonic approximation by

$$H_{ph} = \sum_n \left[\frac{p_n^2}{2M} + \frac{K}{2}(u_n - u_{n-1})^2\right], \tag{1.7}$$

where K is the spring constant or elasticity coefficient of the hydrogen bonds forming the linear chain. M is an effective mass of the peptide group. The operator u_n is the longitudinal displacement of the peptide group parallel to the helical axis from its equilibrium position. p_n is the momentum operator conjugate to u_n. The operators u_n and p_n satisfy the commutation relations $[u_n, p_n] = i\hbar$.

The exciton-phonon interaction Hamiltonian is given by

$$H_{int} = \sum_n \left[\chi(u_{n+1} - u_{n-1})B_n^+ B_n\right], \tag{1.8}$$

where the coupling constant χ arises from modulation of the one-site energy by the molecular displacements.

To understand the dynamics arising from the above Hamiltonian, the following ansatz has been introduced **[63]**

$$|\phi(t)>=\sum_n a_n(t)B_n^+ \exp\{-\frac{\mathrm{i}}{\hbar}\sum_n[\beta_n(t)p_n - \pi_n(t)u_n]\}|0>, \tag{1.9}$$

where $\hbar$ is the Planck's constant and $|0>$ the ground-state vector. a_n (a_n^*) is the coherent state representation of the operators B_n (B_n^+) and the function $|a_n|^2$ characterizes the probability amplitude for finding a quantum of Amide-I energy in a particular amino acid satisfying the normalization condition.

$$<\phi(t)|\phi(t)>=\sum_n |a_n|^2 = 1. \tag{1.10}$$

The coherent state representations for u_n and p_n are β_n and π_n, respectively. We can write the coherent states operators for B_n, B_n^+, u_n and p_n as

$$a_n(t) =<\phi(t)|B_n|\phi(t)> \tag{1.11a}$$

$$a_n^*(t) =<\phi(t)|B_n^+|\phi(t)> \tag{1.11b}$$

$$\beta_n(t) =<\phi(t)|u_n|\phi(t)> \tag{1.11c}$$

$$\pi_n(t) =<\phi(t)|p_n|\phi(t)>. \tag{1.11d}$$

From the time-dependant Schrödinger equation

$$H|\phi>=\mathrm{i}\hbar\frac{d}{dt}|\phi>, \tag{1.12a}$$

and the relations

$$\mathrm{i}\hbar\frac{d}{dt}<\phi(t)|u_n|\phi(t)>=<\phi(t)|[u_n,H]|\phi(t)> \tag{1.12b}$$

$$\mathrm{i}\hbar\frac{d}{dt}<\phi(t)|p_n|\phi(t)>=<\phi(t)|[p_n,H]|\phi(t)>, \tag{1.12c}$$

the equations of motion satisfied by $a_n(t)$ and $\beta_n(t)$ are written as

$$\mathrm{i}\hbar\frac{da_n}{dt} = (E_0 + W)a_n - J(a_{n+1} + a_{n-1}) + \chi(\beta_{n+1} - \beta_{n-1})a_n \tag{1.13a}$$

$$M\frac{d^2\beta_n}{dt^2} = K(\beta_{n+1} + \beta_{n-1} - 2\beta_n) + \chi(|a_{n+1}|^2 - |a_{n-1}|^2), \tag{1.13b}$$

where $W = \frac{1}{2}\sum_n \left[\frac{\pi_n^2}{M} + K(\beta_{n+1} - \beta_n)^2\right]$ represents the lattice phonon energy.

The Davydov idea has attracted a lot of interest, which has increased even further after the appearance of a paper **[61]** in which Davydov and Kislukha demonstrated that the corresponding system of equations for a molecular chain, in the continuum approximation admits a solitonic solution.

In the continuum approximation, Eqs. (1.13) read

$$\mathrm{i}\hbar a_t(x,t) = [E_0 + W - 2J]a(x,t) - Jd^2 a_{xx}(x,t) + 2\chi\beta_x(x,t)a(x,t) \tag{1.14a}$$

$$M\beta_{tt}(x,t) = Kd^2\beta_{xx}(x,t) + 2\chi_1 d(|a(x,t)|^2)_x, \tag{1.14b}$$

where d is the lattice constant. Subscripts x and t represent partial derivatives with respect to x and t, respectively.

We derive Eq. (1.13b) with respect to x once and define a new variable $\xi = x - Vt$, where V represents the velocity of the wave in the system. Then, Eq. (1.13b) becomes

$$\beta_{\xi\xi} = -\frac{2\chi}{K(1-S^2)d}(|a|^2)_\xi, \tag{1.15}$$

where $S = \frac{V}{V_0}$ and $V_0 = d\sqrt{\frac{K}{M}}$ is known to be the longitudinal sound velocity in the chain. We integrate two times this equation with respect to ξ, while annulling the integration constants. We reconsider the variable x and obtain

$$\beta_x = -\frac{2\chi}{K(1-S^2)d}(|a|^2)_x, \tag{1.16}$$

We define a new function ψ such as $a = \psi\exp[-i\frac{(E_0+W-2J)}{\hbar}t]$, Eqs. (1.13) reduce to a sole NLS equation

$$\mathrm{i}\hbar\psi_t(x,t) + P\psi_{xx}(x,t) + Q|\psi(x,t)|^2\psi(x,t) = 0, \tag{1.17}$$

where $P = Jd^2$ and $Q = \frac{4\chi^2}{K(1-S^2)}$.

Equation (1.17) is the well-known completely integrable NLS equation and which has soliton solutions. The one-soliton solution of this equation is **[64]**

$$\psi(x,t) = A\,\mathrm{sech}[B(x-vt)]e^{-i(\kappa x - wt - \sigma)}, \tag{1.18}$$

where A and B are the amplitude and the inverse width of the soliton, respectively. This solution describes a self-trapped quasiparticle (a lump of vibrational Amid-I energy) that propagates at constant velocity and is accompanied by a self-consistent chain deformation.

The velocity v of the soliton is related to the wave number κ by

$$v = \frac{d}{dt}\left(\frac{\int_{-\infty}^{\infty} x|\psi|^2 dx}{\int_{-\infty}^{\infty} |\psi|^2 dx}\right) = -2P\kappa \tag{1.19}$$

and the frequency w by

$$w = P(B^2 - \kappa^2), \tag{1.20}$$

while the relation between the soliton amplitude A and the inverse width B is

$$B = A\sqrt{\frac{Q}{2P}}. \tag{1.21}$$

The relation (1.21) introduces the constraint

$$PQ > 0. \tag{1.22}$$

Equation (1.17) has infinitely many conserved quantities. The first two of them are the energy E and linear momentum M that are respectively given by

$$E = \int_{-\infty}^{\infty} |\psi|^2 dx = 2A \tag{1.23}$$

and

$$M = \frac{i}{2}\int_{-\infty}^{\infty} (\psi\psi_x^* - \psi^*\psi_x)dx = -2\kappa A. \tag{1.24}$$

Note that the value of these conserved quantities are computed by the one-soliton solution that is given by Eq. (1.18).

The Davydov model has been applied in a molecular theory of force generation in muscle contraction **[8,65,66]**. It is well known that the active units in muscle contraction are two molecules, a thicker one called myosin, with protruding parts called the heads, which bind to the other unit, called actin and push against it. A proposal has been made that the energy released by the hydrolysis of ATP can be transferred from one myosin head

to the next via the actin molecule. If actin is substituted for myosin tail, this proposal becomes very similar to that of Davydov. The Davydov theory for muscular contraction relies on the coherent motion of the lattice contraction associated by the Davydov soliton. The theory explains the attachment, pulling and detachment of the myosin heads as the effect of the traveling of an asymmetric Davydov soliton along the α-helix bundles in the myosin tails **[65, 66]**. An asymmetric soliton leads to a kink in an α-helix, centered at the point where the quantum excitation is located. As the excitation moves, the kink moves with it and first pushes the myosin heads against actin, then drags actin with it and then, as the kink moves away, the heads detach from actin. The Davydov theory of muscle contraction constitutes a mechanism for the transduction of chemical energy into mechanical energy with a level of detail that has not been achieved even by other theories of muscle contraction.

1.5 Concerns with the Davydov Model

The Davydov soliton model has been a subject of intensive investigations during the last four decades. Just to cite a few, it has been generalized by taking into account the long-range nature of exciton transfer and by considering amide-I solitons in acetanilide **[67–70]**. Furthermore, extensive numerical calculations and slight modifications have been done to refine the Davydov soliton model **[71, 72]**. The Davydov Hamiltonian has been modified by Scott **[73]** by changing the relative lattice coordinates for the out-of-phase motion of the hydrogen bond proton of each peptide group in order to remove the unimportant dispersion of the phonon modes. Along the same lines, Takeno **[74, 75]** has developed a theory of vibron solitons to show that the Davydov model can be formulated in a more reasonable and quantitatively correct form by employing a nonlinear coupled oscillator-lattice system. On this background, Simo and Kofané **[76]** further modified the Davydov model by taking into account two intramolecular vibrations (excitons) coupled to longitudinal displacements of the molecules from their equilibrium positions

Other work has been done on proteins such as those of Mvogo and all that have focused on inhomogeneities and others on long range **[41]**; those of Mimche and all of which they have taken into account interspine coupling **[32]**; those of Ondoua and all of which, they have taken account of the terms of rotation **[34]**; we will not forget the work of Issa Sali and all who have focused on the saturation of proteins **[77]**.

Experimentally, the first evidence for a Davydov-like state was obtained in the crystalline polymer acetanilide (($CH_3CONHC_6H_5$)X), or (ACN), an organic solid close to a biological molecule, which includes hydrogen-bonded chains identical to those found in proteins **[70]**.

1.6 Experiment and applications of Davydov models

1.6.1 Experiment of acetanilide

The most convincing experimental evidence for the existence of solitons in proteins does not come from protein or living cell spectra, but from the spectrum of the crystalline acetanilide polymer ((CH3CONHCgH)) or ACN. ACN is organized into hydrogen-linked chains that are held together transversely by Van der Waals forces. ACN was used as an analgesic in the nineteenth century (its modern chemical cousin is Tylenol), but its interest in our subject is its remarkable similarity to the chain structure of hydrogen-bonded peptide groups in helical proteins. In the late 1960s, Careri noticed that the lengths and angles of peptide bonding in ACN were very close to those of natural proteins. He began an experimental program at the University of Rome to determine if ACN would show unexpected physical properties that could be biological. Her intuition was rewarded in 1973 by observing an abnormal line in the ACN infrared absorption spectrum. Numerous attempts by Careri and his colleagues to find a conventional assignment for this new line failed throughout the 1970s. Then, in 1982, when Scott became aware of Careri's data, Careri's group and he suggested that the abnormal line was due to a new type of soliton, resulting from the coupling of the arnid-I vibration to a displacement out of the plane. The soliton resulting from this coupling with the lower mass of the proton can be excited directly by electromagnetic radiation, an ingredient necessary to explain the ACN data.One of the unsolved problems of the Davydov soliton as the carrier of energy transport along the helical structure of protein molecules remained it stability at physiological temperature. Most studies conducted at absolute zero. In 1985, experiments conducted at 300 K showed that Davydov solitons lasted for only a few picoseconds, and so could not explain energy transfer **[78]**. In 1994 counter-arguments using quantum mechanics suggest that Davydov solitons may have a longer lifespan **[79, 80]**.

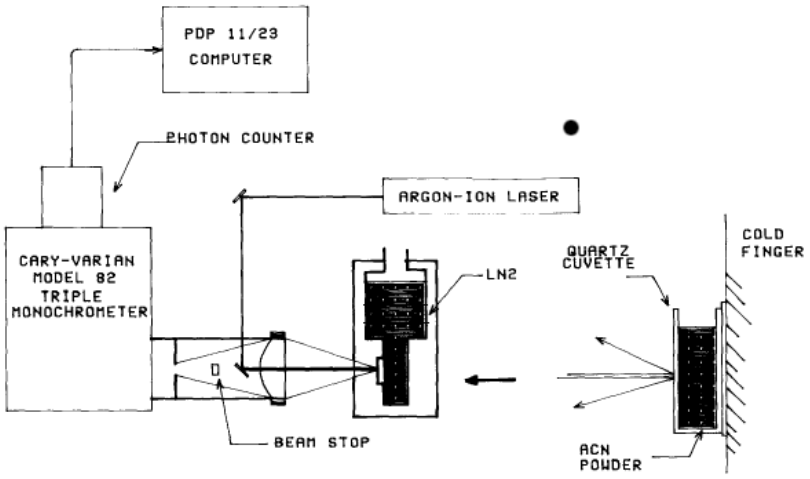

Figure 1.7: *Front-scatter geometry for collecting Raman scattering from solid samples. Excitation beam reflections were blocked by a beamstop, while the wider angle scattering from the sample was passed to the monochromotor.* ***[81]***

1.6.2 Mechanism for General Anesthesia

The first general anesthesia for human surgery was performed at Massachusetts General Hospital in Boston in 1846. The patient was asleep by breathing diethyl ether into a glass vesicle and the surgeon quickly dissected a tumor under the jaw. After completing the operation, the surgeon remarked to his audience, "Gentlemen, this is not a fool." Since this first successful demonstration of diethyl ether, researchers have discovered more than twenty drugs that induce general anesthetic effects. These drugs have physical properties and very diverse chemical structures; as a whole, they give little knowledge of the properties of their mechanism of action. In order to overcome this perplexity, H. Meyer and E. Overton (about the year 1900) originally proposed that the anesthetic potency might be related to the solubility of lipids. Several other proposals followed; but the simplest idea is that they act by binding directly to a particularly sensitive protein, which may or may not be located in a lipid membrane and inhibit its normal function. In this discussion, we will focus on a large class of general intravenous anesthetics that are only slightly soluble in lipids and are capable of forming hydrogen bonds. These agents are mainly represented by barbiturates. In Figure 1.8, it is easy to see that a barbiturate contains four H-N-C = O groups in its ring. These H-N-C = 0 groups are very similar to the peptide groups of proteins that play an important role in the propagation of solitons. The other drugs

shown in Figure 1.8 also contain H-N-C = O groups, but to a lesser extent than the barbiturates. Hydantoins contain three peptide groups, glutethimides and succinimides contain two, and urethanes contain one. These drugs are not used as general anesthetics as such, but nevertheless have a similar inhibitory effect on the central nervous system. The potency of these six drugs seems to be directly related to the number of H-N-C = O groups in the molecule. This is corroborated by the fact that N-methylated barbiturates (which contain two H-N-C = O groups) are shorter.

Conclusion

In this chapter, we have discussed the generalities of molecular proteins, soliton theory, and the Davydov soliton model. Davydov reports for interactions between vibrons and phonons of proteins. These interactions induce a nonlinear dynamic that counterbalances the dispersion created by the dipole dipole coupling. It gives the concept of Davydov soliton whose dynamics is described by the NLS equation. As a result, the soliton appears as a powerful vehicle capable of transferring bioenergy. However, it appears that the LRI between peptide units due to dipole-dipole interactions, inhomogeneities due to defects caused by the presence of additional molecules such as drugs, carcinogens, mutants and dyes in specific sites of the helical alpha protein sequence bring significant changes in the equations governing soliton dynamics in Helical Proteins-α. This aspect of the problem will be studied throughout this work. In the next chapter, we will present the investigative methodology used to obtain our results.

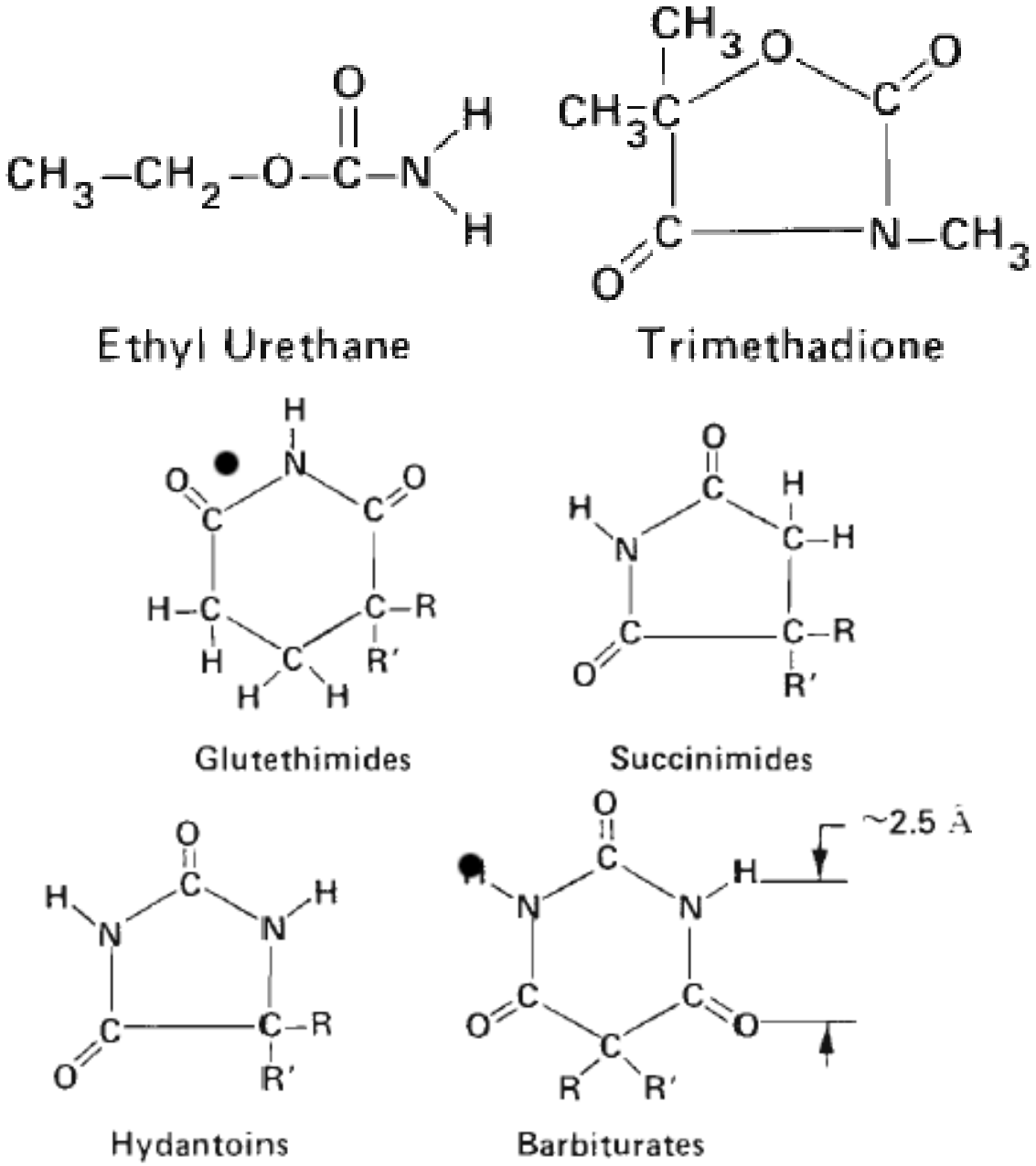

Figure 1.8: *The six drugs shown above, all of which contain H-N-C=0 groups, inhibit the central nervous system. Hydantoins, succinimides, and trimethadione are used primarily as antiepileptic agents, whereas glutethimides are used as sedatives. Ethyl urethane is a common veterinary general anesthetic but is not used in humans because its actions are not smooth. The presence of an alkyl or my1 group at R and R' confers increasing lipid solubility, and, generally, increased lipid solubility promotes cm increased drug potency.* ***[82]***

Chapter 2

Methodology of investigations

Introduction

The Davydov model as mentioned in the introduction is only the most idealized model to explain the energy transfer along backbone of protein molecules. Our main objective is to investigate the effect of LRI in the dynamics of solitons propagating trough the α-helical proteins. In order to accomplish our aims, we employ some analytical and numerical methods. Generally, from the proposed models, we show that the dynamics of the system is governed by the NLS equation, the perturbed NLS equation or CNLS equations, sometimes of which the dispersive coefficient depends on the LRI parameter. Some of these equations are difficult to be solved and where sometimes the solutions need to be approximated. There are many analytical methods which are used to obtain these solutions. These analytical methods lead to many behaviors of the solutions. The numerical methods are used to consolidate the analytical results. In the first part of this chapter, we present the characteristics of our models. In the second part, we give general information about our analytical methods; the third part is devoted for the presentation of the numerical methods.

2.1 Preliminary

2.1.1 Models with long-range energy modes in $\alpha-$helix lattices with inter-spine coupling

Protein molecules are in contact with many factors, which should be taken into account in the study of their nonlinear dynamics. For example, protein enzymes catalyze the millions of chemical reactions occurring each moment in biological system, but they do so in a molecular crowded environment and not as isolated entities. The effects of the environment of the molecule is due to essentially of the variation of physical factors (temperature and pressure) and chemical factors (pH). For this reason, one key of controlling and manipulating biological molecules is to understand theses inhomogeneous processes and systems from the fundamental point of view. Therefore, the protein dynamics can be explained more viably through for example in an inhomogeneous model, rather than with the homogeneous case. In recent years, the study of waves propagation, especially solitons trough inhomogeneous or disordered one dimensional models of α-helical proteins has attracted a lot of interest **[83–88]**. For instance, the effect of mass inhomogeneities on the energy transfer by solitons in the α-helical proteins have been studied by Simo **[83]**, where it has been shown that in the cases light and heavy-mass-induced impurities, oscillatory motion can be introduced by cn and dn-type solitons, respectively. The origination of the Davydov soliton in the linear polymer chain of α-helical proteins, both ideal and with a single impurity has been studied by Todorovic *et al.* **[84, 85]** applying numerical analysis to discrete equations of motion. It has been demonstrated that the soliton velocity is inversely proportional to the soliton amplitude **[84]** and that two exciton-phonon coupling constants influence separately the soliton behavior **[85]**. Wang *et al.* have investigated the effects of linear inhomogeneity in a generalized fourth-order nonlinear Schrödinger equation describing the inhomogeneous α-helical proteins **[86]**. Since the inhomogeneous coefficient of the equation $h = \alpha x + \beta$, the soliton takes on the parabolic profile during the evolution. The soliton velocity, amplitude and width have been found related to α and the soliton position to β. The results obtained in all above studies rather encourage us to extend the study in another cases. This will be attempted in Chapter 3. The inhomogeneities in the α-helical proteins will be supposed on the one hand due to defects caused by the presence of additional molecules such as drugs, mutants and carcinogens

in specific sites of amino acid sequence, or due to the environment of the molecule on the other hand. The following three-dimensional Hamiltonian describing the energy transport and localization in α-helical proteins by Madiba and all **[89]** is investigated

$$H = H_{exc} + H_{vib} + H_{int}, \tag{2.1}$$

where H_{exc} is the energy associated with intramolecular excitations, H_{vib} is the contribution from the displacements of peptide groups also known as lattice vibrations; H_{int} is the interaction energy between the amide-I excitations and the displacements of peptide groups. The energy H_{exc} is defined as:

$$H_{exc} = \sum_{n,\alpha} \left[E_0 \beta^{\dagger}_{n,\alpha} \beta_{n,\alpha} - \sum_{m \neq n} J_{n-m} \beta^{\dagger}_{n,\alpha} \beta_{m,\alpha} + L \left(\beta_{n,\alpha+1} + \beta_{n,\alpha-1} \right) \beta^{\dagger}_{n,\alpha} \right], \tag{2.2}$$

with the subscript n referring to the lattice index along a strand (or chain) α, where $\alpha = 1, 2, 3$. The expression of H_{exc} suggests that an individual amino acid will be identified by the index pair (n, α), such that $\beta_{n,\alpha}$ ($\beta^{\dagger}_{n,\alpha}$) are boson creation (annihilation) operators associated with intramolecular vibrations of the nth peptide group in the strand α. These operators satisfy the usual commutation relations for bosons i.e. $[\beta_{n,\alpha}, \beta^{\dagger}_{m,\alpha}] = \delta_{m,n}$ and $[\beta_{n,\alpha}, \beta_{m,\alpha}] = 0$. E_0 is the local amide-I vibrational energy, in this context the term $E_0 \beta^{\dagger}_{n,\alpha} \beta_{n,\alpha}$ is the vibrational energy at the site (n, α). The term $\sum_{m \neq n} J_{n-m} \beta^{\dagger}_{n,\alpha} \beta_{m,\alpha}$ is the energy related to the LR interactions between molecular excitations on sites n and m, belonging to the same chain. The coupling parameter J_{n-m} is the LR transfer integral between sites n and m, here considered of the form:

$$J_{n-m} = J_0 |n - m|^{-r}, \tag{2.3}$$

with J_0 the strength of the transfer integral and r a parameter range whose values are in the interval $[1, +\infty[$. However r covers different physical contexts, depending on its value. For example if $r \to \infty$ the LR interaction reduces to nearest-neighbor couplings, a case corresponding to the models studied in Refs. **[33,35]**. For $r = 5$ the LR interaction is of a dipole-dipole type, while for $r = 3$ the LR interaction is of the Coulomb type. We should stress that the strongest interaction effects are due to smaller values of r. Therefore, the case $r = 1$ is a particular one that implies strong LR forces among the peptide groups that constitute the protein lattice. This may have some direct biological consequences on the structural dynamics of the molecule and on the localization of energy. Some other

contributions have recently considered the finite range interaction using the Kac-Baker potential to model intermolecular interactions, an proposed strong LR coupling to be responsible for stabilizing the protein chain structure **[90]**.

The parameter L in formula (3.22) is the linear coupling energy between covalently bonded peptide groups between different strands. H_{vib} describes the vibronic dynamics of the molecular system, and includes both the radial and longitudinal displacements of the peptide units from their equilibrium positions. Note that radial and longitudinal displacements are related to the changes in radius $R \to R + v_{n,\sigma}$ and the pitch $b \to b + u_{n,\sigma}$, and feature the distortions of the covalent and hydrogen bonds respectively. This contribution to the total Hamiltonian is written as:

$$H_{vib} = \frac{1}{2}\sum_{n,\alpha}\left\{\frac{\left(P^{u}_{n,\alpha}\right)^{2}}{M} + \frac{\left(P^{v}_{n,\alpha}\right)^{2}}{M} + \kappa\left(u_{n,\alpha} - u_{n-1,\alpha}\right)^{2} + \frac{1}{4}\varpi\left(v_{n,\alpha} - v_{n,\alpha-1}\right)^{2}\right\}. \tag{2.4}$$

M is the mass of a peptide group, κ and ω are the elasticity coefficients of the hydrogen and covalent bonds, respectively. $u_{n,\alpha}$ is the longitudinal displacement of the molecule parallel to the helical axis, and $v_{n,\alpha}$ the displacements along the helix radius. The quantities $P^{u}_{n,\alpha}$ and $P^{v}_{n,\alpha}$ are the momentum conjugate to $u_{n,\alpha}$ and $v_{n,\alpha}$ respectively. The vibrational and excitonic parts interact through the Hamiltonian

$$H_{int} = \sum_{n,\alpha}\left[\chi(u_{n+1,\alpha} - u_{n,\alpha}) + \frac{1}{2}\eta(v_{n,\alpha+1} - 2v_{n,\alpha} + v_{n,\alpha-1})\right]\beta^{+}_{n,\alpha}\beta_{n,\alpha}. \tag{2.5}$$

In Eq.(3.25), the terms associated with the parameters χ and η represent the diagonal coupling between the excitonic amplitude and the displacement of the peptide groups in the longitudinal and radial directions, respectively. Otherwise, the adjacent bonds oscillations are affected by the dynamics of the exciton as discussed in Refs. **[33–35]**.

The following quantum state vector can be used to understand the collective excitation of the system

$$|\psi(t)\rangle = \sum_{n,\alpha} A_{n,\alpha}(t)\beta^{\dagger}_{n,\alpha}\left\{\exp\left[-\frac{i}{\hbar}\sum_{n,\alpha}\left[b_{n,\alpha}(t)P^{u}_{n,\alpha} - \phi_{n,\alpha}(t)u_{n,\alpha}\right] + \left[c_{n,\alpha}(t)P^{v}_{n,\alpha} - \pi_{n,\alpha}(t)v_{n,\alpha}\right]\right]\right\}|0\rangle, \tag{2.6}$$

where $\hbar$ is the Planck constant and $|0\rangle$ is the ground-state vector. $A_{n,\alpha}(A^{*}_{n,\alpha})$ is the coherent state representation of the operators $\beta_{n,\alpha}$ $(\beta^{\dagger}_{n,\alpha})$. We have introduced $b_{n,\alpha}$ and $c_{n,\alpha}$ as the coherent state representations of $u_{n,\alpha}$ and $v_{n,\alpha}$ respectively, and $\phi_{n,\alpha}$ and $\pi_{n,\alpha}$ for their conjugate momenta $P^{u}_{n,\alpha}$ and $P^{v}_{n,\alpha}$. Moreover, the coherent state representations

of the operators for $\beta_{n,\alpha}$, $\beta^{\dagger}_{n,\alpha}$, $u_{n,\alpha}$, $v_{n,\alpha}$, $P^{u}_{n,\alpha}$ and $P^{v}_{n,\alpha}$ are written as

$$\begin{aligned} A_{n,\alpha}(t) &= \langle\psi(t)|\beta_{n,\alpha}|\psi(t)\rangle, \quad A^{*}_{n,\alpha}(t) = \langle\psi(t)|\beta^{\dagger}_{n,\alpha}|\psi(t)\rangle, \\ b_{n,\alpha}(t) &= \langle\psi(t)|u_{n,\alpha}|\psi(t)\rangle, \quad c_{n,\alpha}(t) = \langle\psi(t)|v_{n,\alpha}|\psi(t)\rangle, \\ \phi_{n,\alpha}(t) &= \langle\psi(t)|P^{u}_{n,\alpha}|\psi(t)\rangle, \quad \pi_{n,\alpha}(t) = \langle\psi(t)|P^{v}_{n,\alpha}|\psi(t)\rangle. \end{aligned} \tag{2.7}$$

Ansatz Eq. (3.27) satisfies the normalization condition $\langle\psi(t)|\psi(t)\rangle = \sum\limits_{n,\alpha}|A_{n,\alpha}|^{2} = N$, where $|A_{n,\alpha}|^{2}$ characterizes the probability amplitude for finding a quantum of Amide-I energy in a particular amino acid. The Hamiltonian that gives the coherent states is written in the form

$$\langle H\rangle = \langle\psi(t)|H|\psi(t)\rangle, \tag{2.8}$$

which is written in the more expanded form

$$\begin{aligned} \langle H\rangle = \sum_{n,\alpha}\Bigg\{ A^{*}_{n,\alpha}\Bigg[(E_0+W)A_{n,\alpha} - \sum_{m\neq n}J_{n-m}A_{m,\alpha} - L(A_{n,\alpha+1}+A_{n,\alpha-1})\Bigg] \\ + \chi(b_{n+1,\alpha}-b_{n-1,\alpha})A^{*}_{n,\alpha}A_{n,\alpha} + \frac{1}{2}(c_{n,\alpha+1}-2c_{n,\alpha}+c_{n,\alpha-1})A^{*}_{n,\alpha}A_{n,\alpha}\Bigg\}, \end{aligned} \tag{2.9}$$

with

$$W = \frac{1}{2}\sum_{n,\alpha}\left\{\frac{(\phi_{n,\alpha})^{2}}{M} + \frac{(\pi_{n,\alpha})^{2}}{M} + \kappa\left(b_{n,\alpha}-b_{n-1,\alpha}\right)^{2} + \frac{1}{4}\varpi\left(c_{n,\alpha}-c_{n,\alpha-1}\right)^{2}\right\}. \tag{2.10}$$

The dynamics of the system is easily understood by constructing the Heisenberg's equation of motion, i.e.,

$$i\hbar\frac{\partial}{\partial t}\langle X_{n,\alpha}\rangle = \langle[X_{n,\alpha}, H]\rangle, \tag{2.11}$$

where X stands for the dynamic variables $A_{n,\alpha}$, $b_{n,\alpha}$, $c_{n,\alpha}$, $\phi_{n,\alpha}$ and $\pi_{n,\alpha}$ satisfying the commutation relations $[X, X^{*}] = 1$ and $[\beta_{n,\alpha,P_{n,\alpha}}] = [b_{n,\alpha}, \phi_{n,\alpha}] = [\gamma_{n,\alpha}, P_{n,\alpha}] = [c_{n,\alpha}, \pi_{n,\alpha}] = i\hbar$. This leads to the following set of coupled equations:

$$\begin{aligned} i\hbar\frac{d}{dt}A_{n,\alpha}(t) &= \chi(b_{n+1,\alpha}-b_{n-1,\alpha})A_{n,\alpha} + \frac{\eta}{2}(c_{n,\alpha+1}+2c_{n,\alpha}+c_{n,\alpha-1})A_{n,\alpha} \\ &- L(A_{n,\alpha+1}+A_{n,\alpha-1}) - \sum_{m\neq n}J_{n-m}A_{m,\alpha} \end{aligned} \tag{2.12}$$

$$\frac{d^{2}}{dt^{2}}b_{n,\alpha}(t) = -\kappa(b_{n+1,\alpha}-2b_{n,\alpha}+b_{n-1,\alpha}) + \chi(|A_{n+1,\alpha}|^{2}-|A_{n-1,\alpha}|^{2}) \tag{2.13}$$

$$\frac{d^{2}}{dt^{2}}c_{n,\alpha}(t) = -\frac{\varpi}{4}(c_{n,\alpha+1}+c_{n,\alpha-1}-2c_{n,\alpha}) - \frac{\eta}{2}\left(|A_{n,\alpha+1}|^{2}+|A_{n,\alpha-1}|^{2}+2|A_{n,\alpha}|^{2}\right) \tag{2.14}$$

Another fact that is not negligible in the present model is that the velocity of the intermolecular transport of excitonic energy is much lower than the velocity of sound of the

acoustic bond oscillations. This causes the terms of inertia to be negligible, leading to the following adiabatic approximations:

$$\begin{aligned} b_{n,\alpha} - b_{n-1,\alpha} &= -\frac{\alpha}{\kappa}\left(A^*_{n,\alpha}A_{n-1,\alpha} + A^*_{n-1,\alpha}A_{n,\alpha}\right) + \frac{\chi}{\kappa}\left(|A_{n-1,\alpha}|^2 + |A_{n,\alpha}|^2\right) \\ b_{n+1,\alpha} - b_{n,\alpha} &= -\frac{\alpha}{\kappa}\left(A^*_{n,\alpha}A_{n+1,\alpha} + A^*_{n+1,\alpha}A_{n,\alpha}\right) + \frac{\chi}{\kappa}\left(|A_{n+1,\alpha}|^2 + |A_{n,\alpha}|^2\right) \\ c_{n,\alpha+1} + c_{n,\alpha-1} - 2c_{n,\alpha} &= \frac{2\eta}{\varpi}\left(|A_{n,\alpha+1}|^2 + |A_{n,\alpha-1}|^2 + 2\,|A_{n,\alpha}|^2\right), \quad \alpha = 1,2,3, \end{aligned} \tag{2.15}$$

upon which the following set of coupled equation is obtained

$$\begin{aligned} i\frac{\partial A_{n,\alpha}}{\partial t} =& -\frac{\chi^2}{\kappa}\left[|A_{n+1,\alpha}|^2 + |A_{n-1,\alpha}|^2 + 2|A_{n,\alpha}|^2\right]A_{n,\alpha} - \frac{2\eta^2}{\kappa}\left[|A_{n,\alpha-1}|^2 + |A_{n,\alpha+1}|^2 + 2|A_{n,\alpha}|^2\right]A_{n,\alpha} \\ & - \sum_{l=1}^{\infty} J'_l(A_{n+l,\alpha} + A_{n-l,\alpha}) + L(A_{n,\alpha+1} + A_{n,\alpha-1}), \quad \alpha = 1,2,3, \end{aligned} \tag{2.16}$$

which has been obtained after introducing the scaled quantities $\chi \longrightarrow \frac{\hbar}{\sqrt{M}J_0^{3/2}}\chi$, $\varpi \longrightarrow \frac{\hbar^2}{MJ_0^2}\varpi$, $\kappa \longrightarrow \frac{\hbar^2}{MJ_0^2}\kappa, \eta \longrightarrow \frac{\hbar^2}{MJ_0^2}\eta, L \longrightarrow \frac{L}{J_0}, t \longrightarrow \frac{J_0}{\hbar}t$. In Eqs.(3.36), we have simplified the LR term by considering $l = n-m$ so that the dispersion term becomes $\sum_{l=1}^{\infty} J'_l(A_{n+l,\alpha} + A_{n-l,\alpha})$, with $J'_l = |l|^{-r}$. Eqs.(3.36) are an ensemble of three CDNLS equations. In the same chain, there are in fact two types of couplings, i.e., the nonlinear coupling term $\frac{\chi^2}{\kappa}\left[|A_{n+1,\alpha}|^2 + |A_{n-1,\alpha}|^2 + 2|A_{n,\alpha}|^2\right]A_{n,\alpha}$ and the linear or LR coupling term $\sum_{l=1}^{\infty} J'_l(A_{n+l,\alpha} + A_{n-l,\alpha})$. Obviously, the nonlinear coupling term is restricted to nearest-neighbor peptide groups. Interestingly, interaction among adjacent spine is insured by a linear term, $L(A_{n,\alpha+1}+A_{n,\alpha-1})$, and the nonlinear term $\frac{2\eta^2}{\kappa}\left[|A_{n,\alpha-1}|^2 + |A_{n,\alpha+1}|^2 + 2|A_{n,\alpha}|^2\right]A_{n,\alpha}$. Based on this, there is indeed a competition between nonlinear and dispersive terms. However, this is not enough to confirm the emergence of solitonic structures in the proposed model. This requires more investigation related to the MI as done in the next section. For the rest of the calculations, the following set of parameter values will be used **[4, 33, 34]**: $E_0 = 0,205\text{eV}{=}1,55 \times 10^{-22}$ Nm, $\kappa = 19.36$N, $L = 2.46 \times 10^{-22}$N.m, $\varpi = [91.0 - 155.5]\text{Nm}^{-1}$ $J = 15.47 \times 10^{-23}$J, $I = [91.0 - 155.5]\text{N.m}^{-1}$, $M = 1.9 \times 10^{-25}$ Kg, $\chi = [2-6] \times 10^{-11}$N, $\eta = [0.7 - 1.2] \times 10^{-11}$ N.

2.1.2 Models with long-range interaction effects

A great interest has been ported in the study of energy transfer trough nonlinear excitations along the backbones of bio-molecules. By considering higher order excitations and

interactions between internal molecular excitations, the nonlinear dynamics of α-helix has been studied both at the discrete and continuum levels **[87, 88, 91–97]**. These studies include molecular excitations along a single hydrogen bonding spine of the α-helical proteins **[87, 91, 95–97]** and also the interspine coupling **[87, 88, 92, 93]**. However, in the above studies only the nearest or next nearest-neighbor interactions of molecular excitations have been taken into account, neglecting the fact that in the biomolecules, a group of molecules interacts with more than its nearest and next nearest-neighbors. On this subject, some authors have shown that the study of the LRI in nonlinear lattice models is very relevant, mainly in molecular chains and DNA molecules where Coulomb and dipole-dipole interactions are of physical importance. In particular, it has been shown by many authors that LRI play an active role in the stability of protein molecules. Rau and Parsegian **[98]** studied experimentally the evidence for long-range attractive hydrogen forces and emphasized that many forces could be responsible for LRI in the biomolecules. Chen and Chaudhari **[99]** have shown that the establishment of protein secondary structure, especially the regions of β-sheets, involves LRI between amino acids. The results by Nagano **[100]** have strongly suggested that the topological pathway of the polypeptide chain in three-dimensional space might be decided by the LRI between an α-candidate and a β-candidate. On this background, the LRI have been used by Sarker and Krumhansl **[101]** to investigate the thermodynamic properties, in connection with topological solitons. Using a one-dimensional lattice with long-range coupling of Lennard-Jones type, Ishimori **[102]** showed in the continuum limit that the value of the force range parameter contributes to the dispersive terms in the equation of propagation. Saha and Kofane **[103]** have studied the LRI effect between adjacent and distant bases in a DNA and their impact on the ribonucleic acid polymerase-DNA dynamics. Recently, the dynamics of the one spine model for α-helical proteins with LRI of Kac-Baker type was developed by Grecu *et al.* **[104]**. The authors have obtained in the non-resonant case the NLS equation **[104]** while in the resonant case the Zakharov -Benney equations **[105]** have been found. Despite these rather interesting results, few work has been done so far and the subject appearing particularly difficult to address due to the complexity of the three dimensional α-helical structure.

In this work two types of LRI effects are used: The so-called Kac-Baber LRI and the power-law LRI.

2.1.2.1 Kac-Baber type long-range interactions

Beginning from the pioneering contributions by Baker **[106]**, and Kac and Helfand **[107]**, studies with the Kac-Baber LRI have been the subject of great interest for a long time. In the present work, it is taken in the form **[87, 88]**

$$J_{mn} = J\frac{1-r}{2r}r^{|m-n|}, \tag{2.17}$$

where the parameter J_{mn} is the coupling constant of the dipole-dipole interaction between two peptide groups n and m and J is the dipole-dipole constant interaction between the adjacent peptide groups along the hydrogen bonding spine. The parameter r with $0 \leq r \leq 1$ defines the range of interaction. The absolute difference $|m-n|$ measures the distance between peptide groups n and m. For $r = 0$, the model is reduced to a nearest-neighbor interaction. The limit $r = 1$, which should be taken only when the number of excitations is infinite, corresponds to the infinite range problem, also called the Van der Waals model since the behavior of the system in this limit is identical to a Van der Waals model **[106, 107]**. The pre-factor $1-r$ is chosen to ensure that the total potential experienced by one site due to all others is finite for all r, so that an energy limit exists **[108]**. Then we have

$$\sum_{m\neq n} J_{mn} = J. \tag{2.18}$$

Two models with the Kac-Baber LRI will be investigated in the present work: the first model for the one spine α-helical protein model and the second for the three-spines α-helical proteins model. The corresponding Hamiltonians are **[87]**

$$\begin{aligned} H &= \sum_n EB_n^+B_n - \frac{1}{2}\sum_{n\neq m} J_{mn}(B_n^+ + B_m^+)(B_n + B_m) \\ &\quad + \sum_n [\frac{p_n^2}{2M} + \frac{K}{2}(u_n - u_{n-1})^2] + \sum_n \chi(u_{n+1} - u_{n-1})B_n^+B_n \end{aligned} \tag{2.19}$$

and **[89]**

$$
\begin{aligned}
H &= \sum_{n,\alpha}(E_0 B^+_{n,\alpha}B_{n,\alpha} + E_1 B^+_{n,\alpha}B_{n,\alpha}B^+_{n,\alpha}B_{n,\alpha}) - \sum_{n\neq m,\alpha} J_{mn}(B^+_{n,\alpha}B_{m,\alpha} + B^+_{m,\alpha}B_{n,\alpha}) \\
&\quad - \sum_{n,\alpha} J_1(B^+_{n,\alpha}B_{n+1,\alpha}B^+_{n,\alpha}B_{n+1,\alpha} + B^+_{n,\alpha}B_{n-1,\alpha}B^+_{n,\alpha}B_{n-1,\alpha}) + \frac{1}{2}\sum_{n,\alpha}[\frac{p^2_{n,\alpha}}{M} \\
&\quad + \frac{S^2_{n,\alpha}}{M} + K(u_{n,\alpha} - u_{n-1,\alpha})^2 + I(v_{n,\alpha} - v_{n,\alpha-1})^2] + \sum_{n,\alpha}\{\chi B^+_{n,\alpha}B_{n,\alpha}(u_{n+1,\alpha} - u_{n,\alpha}) \\
&\quad + \lambda B^+_{n,\alpha}B_{n,\alpha}[(v_{n,\alpha+1} - v_{n,\alpha}) + (v_{n,\alpha-1} - v_{n,\alpha})]\}, \qquad (2.20)
\end{aligned}
$$

respectively. The subscript n counts unit cells ($H{-}N{-}C = O$) along the infinite hydrogen bonding spines while α specifies one of the three hydrogen bonding spines ($\alpha = 1, 2, 3$).

2.1.2.2 Power-law type long-range interactions

In this work, the power-law long-range interactions are taken of the form **[109]**

$$J_{n-m} = \frac{J}{|n-m|^r}, \qquad n \neq m, \qquad (2.21)$$

where in the present case the parameter r covers different physical situations: for the nearest-neighbor approximation $r \to \infty$, for the dipole-dipole interaction $r = 3$ and for the long-range Coulomb interaction $r = 1$. In this thesis, we will consider a wide class of LRI that give fractional system of equations attributed to complex media in the continuum limit.

The following Hamiltonian for the three-spines α-helical proteins model with the power-law LRI is investigated **[109]**

$$
\begin{aligned}
H &= \sum_{n,\alpha}\left\{E_0 B^+_{n,\alpha}B_{n,\alpha} - \sum_{m\neq n} J_{n-m}B^+_{n,\alpha}B_{m,\alpha} - L\left[B^+_{n,\alpha}(B_{n,\alpha+1} + B_{n,\alpha-1})\right]\right\} \\
&\quad + \frac{1}{2}\sum_{n,\alpha}[\frac{p^2_{n,\alpha}}{M} + \frac{S^2_{n,\alpha}}{M} + K(u_{n,\alpha} - u_{n-1,\alpha})^2 + I(v_{n,\alpha} - v_{n,\alpha-1})^2] \\
&\quad + \sum_{n,\alpha}\left[\chi_1(u_{n+1,\alpha} - u_{n-1,\alpha})B^+_{n,\alpha}B_{n,\alpha} + \chi_2(u_{n,\alpha} - u_{n-1,\alpha})(B^+_{n+1,\alpha}B_{n,\alpha} + B^+_{n,\alpha}B_{n+1,\alpha})\right] \\
&\quad + \lambda B^+_{n,\alpha}B_{n,\alpha}[(v_{n,\alpha+1} - v_{n,\alpha}) + (v_{n,\alpha-1} - v_{n,\alpha})]. \qquad (2.22)
\end{aligned}
$$

In this work, we show that the power-law LRI leads to a nonlocal integral term in the equations of motion. Indeed, the non-locality originating from the LRI results in the dynamic equations with space derivatives of fractional order.

2.2 Analytical method

In order to show effectively that energy can be localized and transferred in the α-helical proteins, we use sophistical mathematical methods, such that: the modulational instability, the perturbation soliton theory, the transform Fourier method and the Jacobian elliptic functions method, just to cite a few. In that follows, we will present some of these methods and the others will be applied directly in Chapter 3.

2.2.1 Modulational instability

Modulational instability is a universal process that is inherent to most nonlinear wave systems in nature. Many theoretical and experimental works have revealed that MI is the direct way through which localized patterns emerge in many nonlinear systems. It is a result of the interplay between nonlinearity and dispersion and arises in continuous as well as in discrete systems. The MI has been observed in many branch of physics such as plasma physics **[110]**, nonlinear optics **[111]**, nonlinear electrical transmission lines **[112]** and biological systems **[113–117]**. The increasing interest in the way energy spread in protein molecules is a consequence of its importance in biology. Solitons and localized structures have been intensively used during the recent years. The direct way to emerge solitons and localized structures from nonlinear systems is through the activation of modulational instability. MI consists in the input of continuous wave (with a constant amplitude, but with an amplitude dependence of the dispersion relation) which propagates through the system, which can become unstable for a small perturbation under specific conditions.

Procedure of modulational instability

The analysis on the stability starts by assuming the steady-state solution of a given equation which is an exact continuous wave solution in the form

$$\psi(x,t) = \psi_0 e^{i(kx-\omega t)}, \tag{2.23}$$

where ψ_0 is a real constant. The parameters k and ω are the wave number and the angular frequency of the carrier wave, respectively. Substituting the plane wave solution into the equation, we get the amplitude-dependent relationships between k and w known as the nonlinear dispersion relation.

The linear stability of the continuous wave solution (2.23) can be investigated by seeking a solution in the form

$$\psi(x,t) = [1 + B(x,t)]\psi_0 e^{i(kx-\omega t)}, \tag{2.24}$$

where the modulation of the amplitude $B(x,t)$ is assumed to be small in comparison with the corresponding parameters of the carrier wave. We substitute Eq. (2.24) into the basic equation and neglecting the nonlinear terms, we obtain the linear equation for the perturbation.

After, we assume the perturbation B, to be in the form of progressive and regressive wave such that

$$B(x,t) = \mu e^{i(Kx-\Omega t)} + \nu e^{-i(Kx-\Omega t)}, \tag{2.25}$$

where K and Ω represent the wave number and the frequency of the modulation, respectively. By inserting Eq. (2.12) into the linear equation for the perturbation and having performing the linearization, we end up with an eigenvalue problem for the perturbation frequency Ω.

The dispersion relation that determines Ω, as a function of K and k, and the MI gain $G = |Im\Omega(K,k)|$ is determined and solved numerically to determine the regions where the plane wave is instable.

It is shown in this work that the MI is precursor of solitons and localized structures formation in α-helical proteins even in the presence of thermal fluctuations of the environment. For the analysis, the following three coupled chains model of molecule will be considered **[89]**

$$\begin{aligned} H &= \sum_{n,\alpha}(E_0 B^+_{n,\alpha}B_{n,\alpha} + E_1 B^+_{n,\alpha}B_{n,\alpha}B^+_{n,\alpha}B_{n,\alpha}) - \sum_{n\neq m,\alpha} J_{mn}(B^+_{n,\alpha}B_{m,\alpha} + B^+_{m,\alpha}B_{n,\alpha}) \\ &- \sum_{n,\alpha} J_1(B^+_{n,\alpha}B_{n+1,\alpha}B^+_{n,\alpha}B_{n+1,\alpha} + B^+_{n,\alpha}B_{n-1,\alpha}B^+_{n,\alpha}B_{n-1,\alpha}) + \frac{1}{2}\sum_{n,\alpha}[\frac{p^2_{n,\alpha}}{M} \\ &+ \frac{S^2_{n,\alpha}}{M} + K(u_{n,\alpha} - u_{n-1,\alpha})^2 + I(v_{n,\alpha} - v_{n,\alpha-1})^2] + \sum_{n,\alpha}\{\chi B^+_{n,\alpha}B_{n,\alpha}(u_{n+1,\alpha} - u_{n,\alpha}) \\ &+ \lambda B^+_{n,\alpha}B_{n,\alpha}[(v_{n,\alpha+1} - v_{n,\alpha}) + (v_{n,\alpha-1} - v_{n,\alpha})]\}, \end{aligned} \tag{2.26}$$

where the subscript n counts unit cells (H-N-C=O) along the chains while j specifies one of the three chains.

2.2.2 F-expansion method

The exact solutions of nonlinear partial differential equations constitute a crucial factor in the progress of nonlinear dynamics and are a key access for the understanding of various phenomena governing by these equations. In the recent years, wide variety of effective methods to find all kinds of analysis solutions of NLPDEs have been investigated. Among these, the powerful mathematical tool for solving NLPDEs has been revealed to be the F-expansion method. Yomba **[118–120]** gave potential examples of the method to find the soliton solutions of some NLPDEs. Also, the F-expansion method is a unifying frame in which other methods could be presented as complementary viewpoints.

Basic idea of the method applied to coupled system of equations adapted with the three-spines α-helical protein model

We consider a general coupled NLPDEs of the form

$$L_1(u, u_t, u_x, u_{tt}, u_{xt}, u_{xx}, v, v_x, w, w_x, ...) = 0, \tag{2.27a}$$

$$L_2(v, v_t, v_x, v_{tt}, v_{xt}, v_{xx}, u, u_x, w, w_x, ...) = 0. \tag{2.27b}$$

$$L_3(w, w_t, w_x, w_{tt}, w_{xt}, w_{xx}, u, u_x, v, v_x, ...) = 0. \tag{2.27c}$$

Using a traveling wave transformation

$$\xi = k(x - ct), \tag{2.28}$$

where k and c are constants. We can write Eqs. (2.27) as the following nonlinear ordinary differential equations:

$$M_1^{'}(u, u^{'}, u^{''}, u^{'''}, v, v^{'}, w, w^{'}...) = 0, \tag{2.29a}$$

$$M_2^{'}(v, v^{'}, v^{''}, v^{'''}, u, u^{'}, w, w^{'}...) = 0, \tag{2.29b}$$

$$M_3^{'}(w, w^{'}, w^{''}, w^{'''}, u, u^{'}, v, v^{'}...) = 0, \tag{2.29c}$$

where the prime denotes the derivative with respect to ξ. According to the method, we assume that the solutions can be expressed in the form

$$u_\xi = \sum_{j=0}^{n_1} a_j f^j(\xi), \tag{2.30a}$$

$$v_\xi = \sum_{j=0}^{n_2} b_j g^j(\xi), \tag{2.30b}$$

$$w_\xi = \sum_{j=0}^{n_3} c_j h^j(\xi). \tag{2.30c}$$

To determine the values of n_1, n_2 and n_3, we balance the linear term of highest order in Eqs. (2.29) with the highest order nonlinear term.

The F-expansion method requires that we map the solutions of Eqs. (2.30) with those of a ϕ^4 model as shown below:

$$f_\xi^2 = P_1 f^4(\xi) + Q_1 f^2(\xi) + R_1, \tag{2.31a}$$

$$g_\xi^2 = P_2 g^4(\xi) + Q_2 g^2(\xi) + R_2, \tag{2.31b}$$

$$h_\xi^2 = P_3 h^4(\xi) + Q_3 h^2(\xi) + R_3. \tag{2.31c}$$

We have introduced P_j, Q_j, and R_j (j=1,2,3) and different functions of $f(\xi)$, $g(\xi)$ and $h(\xi)$ in order to determine different combinations of Jacobian elliptic functions in the three spines. We can express the solutions in spines 2 and 3 in terms of the solution in spine 1, inspired by the fact that there is always a relation among two Jacobian elliptic functions **[88]**. Thus, we assume the following relations between $g(\xi)$, $h(\xi)$ and $f(\xi)$

$$g^2(\zeta) = \nu_1 f^2(\xi) + \nu_2, \tag{2.32a}$$

$$h^2(\zeta) = \eta_1 f^2(\xi) + \eta_2. \tag{2.32b}$$

Substituting Eqs. (2.32) into Eqs. (2.31), leads to

$$\nu_1 = \frac{P_1}{P_2}, \tag{2.33a}$$

$$\nu_2 = \frac{Q_1 - Q_2}{3P_2} \tag{2.33b}$$

$$\eta_1 = \frac{P_1}{P_3} \tag{2.33c}$$

$$\eta_2 = \frac{Q_1 - Q_3}{3P_3} \tag{2.33d}$$

$$Q_1^2 + Q_1 Q_2 - 2Q_2^2 + 9P_2 R_2 = 0, \tag{2.33e}$$

$$Q_1^2 - Q_2^2 - 3P_1 R_1 + 3P_2 R_2 = 0, \tag{2.33f}$$

$$Q_1^2 + Q_1 Q_3 - 2Q_3^2 + 9P_3 R_3 = 0, \tag{2.33g}$$

$$Q_1^2 - Q_3^2 - 3P_1 R_1 + 3P_3 R_3 = 0. \tag{2.33h}$$

Substituting Eqs. (2.33) and (2.31) into Eqs. (2.27) and setting to zero all the coefficients of different power of $f^j(\xi)g^n(\xi)$, $f^j(\xi)h^n(\xi)$ $(j = 0, 1, 2, 3, n = 0, 1)$, we obtain a set of algebraic equations, which solving by Mathematica, k, c, a_j, b_j, c_j can be expressed in terms of P_j, Q_j, R_j, ν_1, ν_2. To illustrate clearly the method.

2.3 Numerical method

It is worth that the stability of the solutions is a necessary condition for them to be experimentally feasible. To confirm our analytical approaches, we verify the stability of the solutions obtained. Many different methods have been proposed and used in an attempt to solve accurately various types of ordinary and partial differential equations such as the Runge-Kutta method. These methods discretize the differential system to produce a discrete system of equation or map. In this work, we use the fourth order Runge-Kutta method.

2.3.1 Fourth order Runge-Kutta method

The fourth order Runge-Kutta method is a much more locally accurate method. Suppose that we have an equation of the form;

$$\frac{dU}{dt} = f(t, U), \tag{2.34}$$

with $U(t_0) = U_0$. Then if we know U_n and set $t = (n-1)h$, the value of U_{n+1} is given by the sequence of operations

$$U_{n+1} = U_n + \frac{1}{6}(k_1 + 2k_2 + 2k_3 + k_4) \tag{2.35}$$

where k_1, k_2, k_3 and k_4 are the coefficients of the fourth order Runge-Kutta given by the system below

$$\begin{cases} k_1 = hf(t, U_n) \\ k_2 = hf(t + \frac{h}{2}, U_n + \frac{k_1}{2}) \\ k_3 = hf(t + \frac{h}{2}, U_n + \frac{k_2}{2}) \\ k_4 = hf(t + h, U_n + k_3), \end{cases} \tag{2.36}$$

where h is the normalized integration time step. This method has many advantages:

- It is easy to use and no equations need to be solved at each stage;
- It is highly accurate for moderate h values;
- It is a one step method i.e. U_{n+1} only depends on U_n;
- It is easy to start and easy to code.

2.3.2 Split-step method

The Split-step method is based on the pseudo-spectral method **[121]**. This method involves calculating the dispersive and nonlinear terms in the dynamical equations governing the protein chain using fast Fourier transforms and then propagating the resulting ordinary differential equations forward in time t in Fourier space using the fourth order Runge-Kutta method. In numerical analysis, the split-step (Fourier) method is a pseudo-spectral numerical method used to solve nonlinear partial differential equations like the nonlinear Schrödinger equation. The name arises for two reasons. First, the method relies on computing the solution in small steps, and treating the linear and the nonlinear steps separately (see below). Second, it is necessary to Fourier transform back and forth because the linear step is made in the frequency domain while the nonlinear step is made in the time domain. An example of usage of this method is in the field of light pulse propagation in optical fibers, where the interaction of linear and nonlinear mechanisms makes it difficult to find general analytical solutions. However, the split-step method provides a numerical solution to the problem.

Description of the method

Consider, for example, the nonlinear Schrödinger equation **[111]**

$$i\frac{\partial A}{\partial x} - \frac{\beta}{2}\frac{\partial^2 A}{\partial t^2} + \gamma|A|^2 A = 0, \tag{2.37}$$

where $A(t,x)$ describes the pulse envelope in time t at the spatial position x. Rewriting this equation as

$$\frac{\partial A}{\partial x} = -i\frac{\beta}{2}\frac{\partial^2 A}{\partial t^2} + i\gamma|A|^2 A = [\hat{D} + \hat{N}]A. \tag{2.38}$$

The equation can be split into a linear part,

$$\frac{\partial A_D}{\partial x} = -i\frac{\beta}{2}\frac{\partial^2 A}{\partial t^2} = \hat{D}A. \tag{2.39}$$

and a nonlinear part,

$$\frac{\partial A_N}{\partial x} = i\gamma|A|^2 A = \hat{N}A. \tag{2.40}$$

Both the linear and the nonlinear parts have analytical solutions, but the nonlinear Schrödinger equation containing both parts does not have a general analytical solution.

However, if only a 'small' step h is taken along x, then the two parts can be treated separately with only a 'small' numerical error. One can therefore first take a small nonlinear step,

$$A_N(t, x+h) = \exp[i\gamma|A|^2 h]A(t, x), \tag{2.41}$$

using the analytical solution.

The dispersion step has an analytical solution in the frequency domain, so it is first necessary to Fourier transform A_D using

$$\tilde{A}_D(w, x) = \int_{-\infty}^{+\infty} A_D(t, x)\exp[i(w - w_0)t]dt, \tag{2.42}$$

where w_0 is the center frequency of the pulse. It can be shown that using the above definition of the Fourier transform, the analytical solution to the linear step is

$$\tilde{A}_D(w, x+h) = \exp\Big[i\frac{\beta}{2}(w - w_0)^2 h\Big]A_D(w, x), \tag{2.43}$$

By taking the inverse Fourier transform of $\tilde{A}_D(w, x+h)$ one obtains $A_D(t, x+h)$; the pulse has thus been propagated a small step h. By repeating the above N times, the pulse can be propagated over a length of Nh.

The above shows how to use the method to propagate a solution forward in space; however, many physics applications, such as studying the evolution of a wave packet describing a particle, require one to propagate the solution forward in time rather than in space. The non-linear Schrodinger equation, when used to govern the time evolution of a wave function, takes the form

$$i\hbar\frac{\partial\psi}{\partial t} = -\frac{\hbar^2}{2m}\frac{\partial^2\psi}{\partial x^2} + \gamma|\psi|^2\psi = [\hat{D} + \hat{N}]\psi, \tag{2.44}$$

where $\hat{D} = -\frac{\hbar^2}{2m}\frac{\partial^2\psi}{\partial x^2}$ and $\hat{N} = \gamma|\psi|^2$, and that m is the mass of the particle and $\hbar$ is Planck's constant.

The formal solution to this equation is a complex exponential

$$\psi(x, t) = e^{it(\hat{D}+\hat{N})}\psi(x, 0). \tag{2.45}$$

Since $\hat{D}$ and $\hat{N}$ are operators, they do not in general commute. However, the Baker-Hausdorff formula can be applied to show that the error from treating them as if they do will be of order dt^2 if we are taking a small but finite time step dt. We therefore can write

$$\psi(x, t + dt) \approx e^{idt\hat{D}} e^{idt\hat{N}} \psi(x, t). \tag{2.46}$$

The part of this equation involving $\hat{N}$ can be computed directly using the wave function at time t, but to compute the exponential involving $\hat{D}$ we use the fact that in frequency space, the partial derivative operator can be converted into a number by substituting ik for $\frac{\partial}{\partial x}$, where k is the frequency (or more properly, wave number, as we are dealing with a spatial variable and thus transforming to a space of spatial frequencies-i.e wave numbers) associated with the Fourier transform of whatever is being operated on. Thus, we take the Fourier transform of $e^{idt\hat{N}}\psi(x, t)$ recover the associated wave number, compute the quantity e^{-idtk^2} and use it to find the product of the complex exponentials involving and in frequency space as below:
$e^{-idtk^2} F\Big[e^{idt\hat{N}}\psi(x, t)\Big]$,
where F denotes a Fourier transform. We then inverse Fourier transform this expression to find the final result in physical space, yielding the final expression

$$\psi(x, t + dt) = F^{-1}\Big[e^{-idtk^2} F\Big[e^{idt\hat{N}}\psi(x, t)\Big]\Big] \tag{2.47}$$

A variation on this method is the symmetrized split-step Fourier method, which takes half a time step using one operator, then takes a full time step with only the other, and then takes a second half time step again with only the first. This method is an improvement upon the generic split-step Fourier method because its error is of order dt^3 for a time step dt. The Fourier transforms of this algorithm can be computed relatively fast using the fast Fourier transform (FFT). Compared to the typical finite difference methods **[122]**, the split-step Fourier method can therefore be much faster.

Conclusion

This chapter was devoted to present the protein dynamics models taking into account inhomogeneity and LRI effects. We have presented the analytical and numerical methods used in the study of the dynamics of solitary waves in protein molecules. The numerical methods are used to consolidate the analytical results. The methods could have different

schemes from the same differential equation, but they have the same aim; that the dynamics of the system should correspond closely to the dynamics of the differential equation. In the next chapter, we will present our results together with discussions.

Chapter 3

Results and Discussions

Introduction

In previous chapters we have given generalities on protein molecules, soliton theory and Davydov's model. The different methods used to achieve our objectives were also highlighted. The mathematical methods were based on MI, perturbation soliton theory and Jacobian elliptic functions. To confirm the analytical methods and plot the different curves, we use the Runge-Kutta algorithm of the fourth order and the Fourier method in several steps. This chapter is based on our results. There is a lot of work on Davydov's model; but this thesis focuses on the effects of the long-range. We also investigate the generation of solitons and localized structures through the activation of MI in the particular case of long-range.

3.1 Long-range effects

Many biological processes such as muscle contraction, active transport and enzyme catalysis rely on energy. This energy, which is released through the hydrolysis of adenosine triphosphate (ATP), is mainly transported and stored by proteins. Understanding the subsequent phenomena, those related to the management of energy by proteins, have been an active research topic since the pioneering work by Davydov **[8]**. Based on a simple formulation of the problem Davydov showed that energy is carried by solitonic structures, therefore establishing the relationship between such entities and lattice distortions. Namely, considering the structure of $\alpha-$helix proteins Davydov and Kislukha **[6, 7]**

used the exciton formalism to explain the self-trapping of the amide-I oscillations, as the consequence of the interaction between the vibrational exciton and the distortion in the protein structure resulting from the presence of the exciton. They established that as a result of the interplay between nonlinearity and dispersion, the self-trapped vibrational amide-I energy coupled to the protein structure deformation may travel as a soliton in the protein strand **[4, 5]**.

Earlier models on the issue of energy transport and storage in protein chains were focused on a structure with only one strand of hydrogen-bonded peptide units, both in the discrete and continuum regimes **[6–8]**. These models have been the subject of great controversy, owing to their formulation involving inconsistencies in predictions on the Davydov soliton lifetime, and more importantly its stability at the biological temperature of $300K$ **[9–16]**. Nevertheless, numerical simulations have revealed that such solitons may be stable at 300 K, but these studies were carried out from a purely classical point of view with no consistent argument to prove their stability **[4, 5, 17–22]**. In order to solve this issue, adopting a description of the $\alpha-$helix protein in terms of a biological system stabilized by three quasi-linear strands, turned out to be a suitable picture. Most of the pioneering analytical and numerical contributions in that direction can be found in Refs. **[5, 23, 24]**. In the same direction slightly modified Davydov models of $\alpha-$helix proteins were addressed by Daniel and Latha **[25]**, in which both discrete and continuum regimes were studied with a particular interest in the influence of the inter-spine coupling and its consequences on the process of energy transport and storage among the spines. Based on the fact that the process of modulational instability (MI) is a direct mechanism leading to solitons and the formation of nonlinear structures **[26–30]**, Tabi and co-workers **[31–33]** showed that the process may also be envisaged in the context of three-stranded molecular structures. More recently, a generalized model of $\alpha-$helix protein chains including the competition between diagonal and off-diagonal couplings was proposed **[34]**. The subsequent modes of energy were found to be very sensitive to the nonlinear effects introduced by the two types of couplings. In Ref. **[33]**, using the model by Hennig **[35]**, Tabi et al. showed that during the process of energy transport covalent bonds may be compressed, while hydrogen bonds display regular oscillating behaviors leading to favourable condition for energy transport and storage in the coupled spines via polaronic structures. Relying on data from X-ray analysis on proteins **[36–38]** it was also shown that the tridimensional structure is favorable to energy and particle trans-

fer in proteins, because of the significant presence of hidrogen (H) bridges between the spines **[39]**. In other words the polarons that arise in protein dynamics may correspond to the energy related to the electron transport, depending on the coupling strength to vibrational motions **[33, 35, 133]**. Moreover, in recent investigations it was suggested that long-range (LR) dispersive interactions may be responsible for interesting dynamical behaviors, especially in molecular systems like DNA and proteins **[40–42]**, neural **[43,44]** and cell **[45]** networks.

Our main objective in this part is to show that LR dispersive interactions may enhance the efficiency of energy transport and storage in three-stranded molecules with inter-spine coupling. In this goal we shall use the theory of MI both analytically and numerically, with emphasis on the importance of the competing effects between the LR interactions among polypeptides units in individual protein helices and nonlinearity. The paper is outlined as follows: in Section 3.2.3 we introduce the model Hamiltonian, and derive the dynamical equations which are modified coupled discrete nonlinear Schrödinger (DNLS) equations. In Section 3.2.3 the theory of MI is applied to the model starting with the linear stability analysis for plane wave solutions, followed by full numerical simulations to confirm pedictions of the linear stability analysis and the emergence of nonlinear wave patterns with soliton features. The last section is devoted to concluding remarks.

3.1.1 Hamiltonian Model and dynamical equations

The generalized Hamiltonian for linked polypeptide chains arranged in three-dimensional helix has been proposed using Davydov's formulation **[6,8]**. It considers the coupling between amide-I vibration, and displacements of amino-acid residues. Its tridimensional version, as proposed in Refs. **[33–35]**, is given by:

$$H = H_{exc} + H_{vib} + H_{int}, \tag{3.1}$$

where H_{exc} is the energy associated with intramolecular excitations, H_{vib} is the contribution from the displacements of peptide groups also known as lattice vibrations; H_{int} is the interaction energy between the amide-I excitations and the displacements of peptide groups. The energy H_{exc} is defined as:

$$H_{exc} = \sum_{n,\alpha} \left[E_0 \beta^{\dagger}_{n,\alpha} \beta_{n,\alpha} - \sum_{m \neq n} J_{n-m} \beta^{\dagger}_{n,\alpha} \beta_{m,\alpha} + L \left(\beta_{n,\alpha+1} + \beta_{n,\alpha-1} \right) \beta^{\dagger}_{n,\alpha} \right], \tag{3.2}$$

with the subscript n referring to the lattice index along a strand (or chain) α, where $\alpha = 1, 2, 3$. The expression of H_{exc} suggests that an individual amino acid will be identified by the index pair (n, α), such that $\beta_{n,\alpha}$ ($\beta^{\dagger}_{n,\alpha}$) are boson creation (annihilation) operators associated with intramolecular vibrations of the nth peptide group in the strand α. These operators satisfy the usual commutation relations for bosons i.e. $[\beta_{n,\alpha}, \beta^{\dagger}_{m,\alpha}] = \delta_{m,n}$ and $[\beta_{n,\alpha}, \beta_{m,\alpha}] = 0$. E_0 is the local amide-I vibrational energy, in this context the term $E_0\beta^{\dagger}_{n,\alpha}\beta_{n,\alpha}$ is the vibrational energy at the site (n, α). The term $\sum_{m\neq n} J_{n-m}\beta^{\dagger}_{n,\alpha}\beta_{m,\alpha}$ is the energy related to the LR interactions between molecular excitations on sites n and m, belonging to the same chain. The coupling parameter J_{n-m} is the LR transfer integral between sites n and m, here considered of the form:

$$J_{n-m} = J_0|n-m|^{-r}, \tag{3.3}$$

with J_0 the strength of the transfer integral and r a parameter range whose values are in the interval $[1, +\infty[$. However r covers different physical contexts, depending on its value. For example if $r \to \infty$ the LR interaction reduces to nearest-neighbor couplings, a case corresponding to the models studied in Refs. **[33,35]**. For $r = 5$ the LR interaction is of a dipole-dipole type, while for $r = 3$ the LR interaction is of the Coulomb type. We should stress that the strongest interaction effects are due to smaller values of r. Therefore, the case $r = 1$ is a particular one that implies strong LR forces among the peptide groups that constitute the protein lattice. This may have some direct biological consequences on the structural dynamics of the molecule and on the localization of energy. Some other contributions have recently considered the finite range interaction using the Kac-Baker potential to model intermolecular interactions, an proposed strong LR coupling to be responsible for stabilizing the protein chain structure **[90]**.

The parameter L in formula (3.22) is the linear coupling energy between covalently bonded peptide groups between different strands. H_{vib} describes the vibronic dynamics of the molecular system, and includes both the radial and longitudinal displacements of the peptide units from their equilibrium positions. Note that radial and longitudinal displacements are related to the changes in radius $R \to R + v_{n,\sigma}$ and the pitch $b \to b + u_{n,\sigma}$, and feature the distortions of the covalent and hydrogen bonds respectively. This contribution to the total Hamiltonian is written as:

$$H_{vib} = \frac{1}{2}\sum_{n,\alpha}\left\{\frac{\left(P^{u}_{n,\alpha}\right)^2}{M} + \frac{\left(P^{v}_{n,\alpha}\right)^2}{M} + \kappa\left(u_{n,\alpha} - u_{n-1,\alpha}\right)^2 + \frac{1}{4}\varpi\left(v_{n,\alpha} - v_{n,\alpha-1}\right)^2\right\}. \tag{3.4}$$

M is the mass of a peptide group, κ and ω are the elasticity coefficients of the hydrogen and covalent bonds, respectively. $u_{n,\alpha}$ is the longitudinal displacement of the molecule parallel to the helical axis, and $v_{n,\alpha}$ the displacements along the helix radius. The quantities $P^u_{n,\alpha}$ and $P^v_{n,\alpha}$ are the momentum conjugate to $u_{n,\alpha}$ and $v_{n,\alpha}$ respectively. The vibrational and excitonic parts interact through the Hamiltonian

$$H_{int} = \sum_{n,\alpha} \left[\chi(u_{n+1,\alpha} - u_{n,\alpha}) + \frac{1}{2}\eta(v_{n,\alpha+1} - 2v_{n,\alpha} + v_{n,\alpha-1}) \right] \beta^+_{n,\alpha}\beta_{n,\alpha}. \tag{3.5}$$

In Eq.(3.25), the terms associated with the parameters χ and η represent the diagonal coupling between the excitonic amplitude and the displacement of the peptide groups in the longitudinal and radial directions, respectively. Otherwise, the adjacent bonds oscillations are affected by the dynamics of the exciton as discussed in Refs. **[33–35]**.

The following quantum state vector can be used to understand the collective excitation of the system

$$|\psi(t)\rangle = \sum_{n,\alpha} A_{n,\alpha}(t)\beta^\dagger_{n,\alpha} \left\{ \exp\left[-\frac{i}{\hbar} \sum_{n,\alpha} \left[b_{n,\alpha}(t)P^u_{n,\alpha} - \phi_{n,\alpha}(t)u_{n,\alpha} \right] + \left[c_{n,\alpha}(t)P^v_{n,\alpha} - \pi_{n,\alpha}(t)v_{n,\alpha} \right] \right] \right\} |0\rangle, \tag{3.6}$$

where $\hbar$ is the PlanckŠs constant and $|0\rangle$ is the ground-state vector. $A_{n,\alpha}(A^*_{n,\alpha})$ is the coherent state representation of the operators $\beta_{n,\alpha}$ $(\beta^\dagger_{n,\alpha})$. We have introduced $b_{n,\alpha}$ and $c_{n,\alpha}$ as the coherent state representations of $u_{n,\alpha}$ and $v_{n,\alpha}$ respectively, and $\phi_{n,\alpha}$ and $\pi_{n,\alpha}$ for their conjugate momenta $P^u_{n,\alpha}$ and $P^v_{n,\alpha}$. Moreover, the coherent state representations of the operators for $\beta_{n,\alpha}$, $\beta^\dagger_{n,\alpha}$, $u_{n,\alpha}$, $v_{n,\alpha}$, $P^u_{n,\alpha}$ and $P^v_{n,\alpha}$ are written as

$$\begin{aligned} A_{n,\alpha}(t) &= \langle\psi(t)|\beta_{n,\alpha}|\psi(t)\rangle, \quad A^*_{n,\alpha}(t) = \langle\psi(t)|\beta^\dagger_{n,\alpha}|\psi(t)\rangle, \\ b_{n,\alpha}(t) &= \langle\psi(t)|u_{n,\alpha}|\psi(t)\rangle, \quad c_{n,\alpha}(t) = \langle\psi(t)|v_{n,\alpha}|\psi(t)\rangle, \\ \phi_{n,\alpha}(t) &= \langle\psi(t)|P^u_{n,\alpha}|\psi(t)\rangle, \quad \pi_{n,\alpha}(t) = \langle\psi(t)|P^v_{n,\alpha}|\psi(t)\rangle. \end{aligned} \tag{3.7}$$

Ansatz Eq. (3.27) satisfies the normalization condition $\langle\psi(t)|\psi(t)\rangle = \sum_{n,\alpha} |A_{n,\alpha}|^2 = N$, where $|A_{n,\alpha}|^2$ characterizes the probability amplitude for finding a quantum of Amide-I energy in a particular amino acid. The Hamiltonian that gives the coherent states is written in the form

$$\langle H\rangle = \langle\psi(t)|H|\psi(t)\rangle, \tag{3.8}$$

which is written in the more expanded form

$$\begin{aligned}\langle H\rangle = \sum_{n,\alpha}\Bigg\{ A^*_{n,\alpha}\Bigg[(E_0+W)A_{n,\alpha} - \sum_{m\neq n} J_{n-m}A_{m,\alpha} - L(A_{n,\alpha+1}+A_{n,\alpha-1})\Bigg] \\ + \chi(b_{n+1,\alpha}-b_{n-1,\alpha})A^*_{n,\alpha}A_{n,\alpha} + \frac{1}{2}(c_{n,\alpha+1}-2c_{n,\alpha}+c_{n,\alpha-1})A^*_{n,\alpha}A_{n,\alpha}\Bigg\},\end{aligned} \tag{3.9}$$

with

$$W = \frac{1}{2}\sum_{n,\alpha}\left\{\frac{(\phi_{n,\alpha})^2}{M} + \frac{(\pi_{n,\alpha})^2}{M} + \kappa\left(b_{n,\alpha}-b_{n-1,\alpha}\right)^2 + \frac{1}{4}\varpi\left(c_{n,\alpha}-c_{n,\alpha-1}\right)^2\right\}. \tag{3.10}$$

The dynamics of the system is easily understood by constructing the Heisenberg's equation of motion, i.e.,

$$i\hbar\frac{\partial}{\partial t}\langle X_{n,\alpha}\rangle = \langle[X_{n,\alpha},H]\rangle, \tag{3.11}$$

where X stands for the dynamic variables $A_{n,\alpha}$, $b_{n,\alpha}$, $c_{n,\alpha}$, $\phi_{n,\alpha}$ and $\pi_{n,\alpha}$ satisfying the commutation relations $[X,X^*]=1$ and $[\beta_{n,\alpha,P_{n,\alpha}}] = [b_{n,\alpha},\phi_{n,\alpha}] = [\gamma_{n,\alpha},P_{n,\alpha}] = [c_{n,\alpha},\pi_{n,\alpha}] = i\hbar$. This leads to the following set of coupled equations:

$$\begin{aligned} i\hbar\frac{d}{dt}A_{n,\alpha}(t) &= \chi(b_{n+1,\alpha}-b_{n-1,\alpha})A_{n,\alpha} + \frac{\eta}{2}(c_{n,\alpha+1}+2c_{n,\alpha}+c_{n,\alpha-1})A_{n,\alpha} \\ &- L(A_{n,\alpha+1}+A_{n,\alpha-1}) - \sum_{m\neq n} J_{n-m}A_{m,\alpha} \end{aligned} \tag{3.12}$$

$$\frac{d^2}{dt^2}b_{n,\alpha}(t) = -\kappa(b_{n+1,\alpha}-2b_{n,\alpha}+b_{n-1,\alpha}) + \chi(|A_{n+1,\alpha}|^2 - |A_{n-1,\alpha}|^2) \tag{3.13}$$

$$\frac{d^2}{dt^2}c_{n,\alpha}(t) = -\frac{\varpi}{4}\left(c_{n,\alpha+1}+c_{n,\alpha-1}-2c_{n,\alpha}\right) - \frac{\eta}{2}\left(|A_{n,\alpha+1}|^2 + |A_{n,\alpha-1}|^2 + 2\,|A_{n,\alpha}|^2\right) \tag{3.14}$$

Another fact that is not negligible in the present model is that the velocity of the intermolecular transport of excitonic energy is much lower than the velocity of sound of the acoustic bond oscillations. This causes the terms of inertia to be negligible, leading to the following adiabatic approximations:

$$\begin{aligned} b_{n,\alpha}-b_{n-1,\alpha} &= -\frac{\alpha}{\kappa}\left(A^*_{n,\alpha}A_{n-1,\alpha} + A^*_{n-1,\alpha}A_{n,\alpha}\right) + \frac{\chi}{\kappa}\left(|A_{n-1,\alpha}|^2 + |A_{n,\alpha}|^2\right) \\ b_{n+1,\alpha}-b_{n,\alpha} &= -\frac{\alpha}{\kappa}\left(A^*_{n,\alpha}A_{n+1,\alpha} + A^*_{n+1,\alpha}A_{n,\alpha}\right) + \frac{\chi}{\kappa}\left(|A_{n+1,\alpha}|^2 + |A_{n,\alpha}|^2\right) \\ c_{n,\alpha+1}+c_{n,\alpha-1}-2c_{n,\alpha} &= \frac{2\eta}{\varpi}\left(|A_{n,\alpha+1}|^2 + |A_{n,\alpha-1}|^2 + 2\,|A_{n,\alpha}|^2\right), \quad \alpha=1,2,3, \end{aligned} \tag{3.15}$$

upon which the following set of coupled equation is obtained

$$\begin{aligned} i\frac{\partial A_{n,\alpha}}{\partial t} = &-\frac{\chi^2}{\kappa}\left[|A_{n+1,\alpha}|^2 + |A_{n-1,\alpha}|^2 + 2|A_{n,\alpha}|^2\right]A_{n,\alpha} - \frac{2\eta^2}{\kappa}\left[|A_{n,\alpha-1}|^2 + |A_{n,\alpha+1}|^2 + 2|A_{n,\alpha}|^2\right]A_{n,\alpha} \\ &- \sum_{l=1}^{\infty} J'_l(A_{n+l,\alpha}+A_{n-l,\alpha}) + L(A_{n,\alpha+1}+A_{n,\alpha-1}), \quad \alpha=1,2,3, \end{aligned} \tag{3.16}$$

which has been obtained after introducing the scaled quantities $\chi \longrightarrow \frac{\hbar}{\sqrt{M}J_0^{3/2}}\chi$, $\varpi \longrightarrow \frac{\hbar^2}{MJ_0^2}\varpi$, $\kappa \longrightarrow \frac{\hbar^2}{MJ_0^2}\kappa, \eta \longrightarrow \frac{\hbar^2}{MJ_0^2}\eta, L \longrightarrow \frac{L}{J_0}, t \longrightarrow \frac{J_0}{\hbar}t$. In Eqs.(3.36), we have simplified the LR term by considering $l = n-m$ so that the dispersion term becomes $\sum_{l=1}^{\infty} J_l'(A_{n+l,\alpha} + A_{n-l,\alpha})$, with $J_l' = |l|^{-r}$. Eqs.(3.36) are an ensemble of three CDNLS equations. In the same chain, there are in fact two types of couplings, i.e., the nonlinear coupling term $\frac{\chi^2}{\kappa}\left[|A_{n+1,\alpha}|^2 + |A_{n-1,\alpha}|^2 + 2|A_{n,\alpha}|^2\right]A_{n,\alpha}$ and the linear or LR coupling term $\sum_{l=1}^{\infty} J_l'(A_{n+l,\alpha} + A_{n-l,\alpha})$. Obviously, the nonlinear coupling term is restricted to nearest-neighbor peptide groups. Interestingly, interaction among adjacent spine is insured by a linear term, $L(A_{n,\alpha+1}+A_{n,\alpha-1})$, and the nonlinear term $\frac{2\eta^2}{\kappa}\left[|A_{n,\alpha-1}|^2 + |A_{n,\alpha+1}|^2 + 2|A_{n,\alpha}|^2\right]A_{n,\alpha}$. Based on this, there is indeed a competition between nonlinear and dispersive terms. However, this is not enough to confirm the emergence of solitonic structures in the proposed model. This requires more investigation related to the MI as done in the next section. For the rest of the calculations, the following set of parameter values will be used **[4, 33, 34]**: $E_0 = 0,205\text{eV}=1,55\times10^{-22}$ Nm, $\kappa = 19.36$N, $L = 2.46\times10^{-22}$N.m, $\varpi = [91.0-155.5]\text{Nm}^{-1}$ $J = 15.47\times10^{-23}$J, $I = [91.0-155.5]\text{N.m}^{-1}$, $M = 1.9\times10^{-25}$ Kg, $\chi = [2-6]\times10^{-11}$N, $\eta = [0.7-1.2]\times10^{-11}$ N.

3.1.2 Unstable energy patterns

The direct way to predict the emergence of nonlinear structures in physical systems is the through the activation of MI, i.e., the study of the stability of plane wave solutions. Such waves solutions are generally considered to be of the form $A_{n,\alpha} = A_{0,\alpha}e^{i(q_\alpha n-\omega_\alpha t)}$ $(\alpha = 1,2,3)$ where q_α and ω_α are the wavenumbers and the frequencies, respectively. The amplitudes $A_{0,\alpha}$ are assumed to be real. The solutions verify the linear dispersion relations

$$\omega_\alpha = -\frac{-4\chi^2}{\kappa}|A_{0,\alpha}|^2 - \frac{2\eta^2}{\kappa}\left[|A_{0,\alpha-1}|^2 + 2|A_{0,\alpha}|^2 + 2|A_{0,\alpha+1}|^2\right] - 2\sum_{l=1}^{\infty} J_l'\cos q_\alpha l \quad (3.17)$$

In order to study the stability of the plane wave solutions, we introduce small perturbations into their amplitudes in the form $A_{n,\alpha} = A_{0,\alpha}(1+B_{n,\alpha}(t))e^{i(q_\alpha n-\omega_\alpha t)}$ $(\alpha = 1,2,3)$, where $B_{n,\alpha}(t)$ are the small perturbations, which, after linearizing around the unperturbed plane

waves, are governed by the set of coupled equations

$$\begin{aligned} i\frac{\partial B_{n,\alpha}}{\partial t} &= -\frac{\chi^2}{\kappa}[(B_{n+1,\alpha}+B^+_{n+1,\alpha})+(B_{n-1,\alpha}+B^+_{n-1,\alpha})+2(B_{n,\alpha}+B^+_{n,\alpha})]|A_{0,\alpha}|^2 \\ &- \frac{2\eta^2}{\kappa}[(B_{n,\alpha-1}+B^+_{n,\alpha-1})|A_{0,\alpha-1}|^2+(B_{n,\alpha+1}+B^+_{n,\alpha+1})|A_{0,\alpha+1}|^2+2(B_{n,\alpha}+B^+_{n,\alpha})|A_{0,\alpha}|^2] \\ &- \sum_{l=1}^{\infty} J'_l[(B_{n+l,\alpha}+B_{n-l,\alpha}-2B_{n,\alpha})\cos q_\alpha l - i(B_{n+l,\alpha}-B_{n-l,\alpha})\sin q_\alpha l]. \end{aligned} \tag{3.18}$$

Moreover, solutions for Eqs. (3.38) are assumed in the form $B_{n,\alpha} = a_{0,\alpha}e^{i(Qn-\Omega t)} + b^*_{0,\alpha}e^{-i(Qn-\Omega^* t)}$, with Q and Ω being the wavenumber and complex frequency of perturbation. On introducing those solutions into (3.38), one finds the following linear homogeneous system for $a_{0,1}$, $b_{0,1}$, $a_{0,2}$, $b_{0,2}$, $a_{0,3}$, $b_{0,3}$:

$$\begin{pmatrix} \Omega-m_{11} & m_{12} & m_{13} & m_{14} & m_{15} & m_{16} \\ m_{21} & -\Omega+m_{22} & m_{23} & m_{24} & m_{25} & m_{26} \\ m_{31} & m_{32} & \Omega+m_{33} & m_{34} & m_{35} & m_{36} \\ m_{41} & m_{42} & m_{43} & -\Omega+m_{44} & m_{45} & m_{46} \\ m_{51} & m_{52} & m_{53} & m_{54} & \Omega+m_{55} & m_{56} \\ m_{61} & m_{62} & m_{63} & m_{64} & m_{65} & -\Omega+m_{66} \end{pmatrix} \begin{pmatrix} a_{0,1} \\ b_{0,1} \\ a_{0,2} \\ b_{0,2} \\ a_{0,3} \\ b_{0,3} \end{pmatrix} = \begin{pmatrix} 0 \\ 0 \\ 0 \\ 0 \\ 0 \\ 0 \end{pmatrix}, \tag{3.19}$$

with the matrix elements $m_{i,j}$ being given by

$$m_{11} = -\frac{4\chi^2}{\kappa}|A_{0,1}|^2\sin^2\left(\frac{Q}{2}\right) - \frac{4\eta^2}{\kappa}|A_{0,1}|^2 - 2\sum_{l=1}^{\infty} J'_l\left\{2\sin^2\left(\frac{Ql}{2}\right)\cos q_1 l - \sin Ql\sin q_1 l\right\},$$

$$m_{12} = -\frac{4\chi^2}{\kappa}|A_{0,1}|^2\sin^2\left(\frac{Q}{2}\right) - \frac{4\eta^2}{\kappa}|A_{0,1}|^2, \quad m_{21} = \frac{2\chi^2}{\kappa}|A_{0,1}|^2\cos Q + \frac{6\eta^2}{\kappa}|A_{0,1}|^2,$$

$$m_{13} = m_{14} = m_{23} = m_{24} = m_{53} = m_{54} = m_{63} = m_{64} = \frac{2\eta^2}{\kappa}|A_{0,2}|^2,$$

$$m_{15} = m_{16} = m_{25} = m_{26} = m_{35} = m_{36} = m_{45} = m_{46} = \frac{2\eta^2}{\kappa}|A_{0,3}|^2,$$

$$m_{22} = \frac{2\chi^2}{\kappa}|A_{0,1}|^2\cos Q + \frac{6\eta^2}{\kappa}|A_{0,1}|^2 - 2\sum_{l=1}^{\infty} J'_l\left\{2\sin^2\left(\frac{Ql}{2}\right)\cos q_1 l + \sin Ql\sin q_1 l\right\},$$

$$m_{31}=m_{32}=m_{41}=m_{42}=m_{51}=m_{52}=m_{61}=m_{62}=\frac{2\eta^2}{\kappa}|A_{0,1}|^2,$$

$$m_{33}=m_{44}=-\frac{4\chi^2}{\kappa}|A_{0,2}|^2\sin^2\left(\frac{Q}{2}\right)+\frac{4\eta^2}{\kappa}|A_{0,2}|^2-2\sum_{l=1}^{\infty}J_l'\left\{2\sin^2\left(\frac{Ql}{2}\right)\cos q_2 l-\sin Ql\sin q_2 l\right\},$$

$$m_{34}=m_{43}=-\frac{4\chi^2}{\kappa}|A_{0,2}|^2\sin^2\left(\frac{Q}{2}\right)+\frac{4\eta^2}{\kappa}|A_{0,2}|^2,\ \ m_{65}=-\frac{4\chi^2}{\kappa}|A_{0,3}|^2\sin^2\left(\frac{Q}{2}\right)+\frac{4\eta^2}{\kappa}|A_{0,3}|^2,$$

$$m_{55}=-\frac{4\chi^2}{\kappa}|A_{0,3}|^2\sin^2\left(\frac{Q}{2}\right)+\frac{4\eta^2}{\kappa}|A_{0,3}|^2-2\sum_{l=1}^{\infty}J_l'\left\{2\sin^2\left(\frac{Ql}{2}\right)\cos q_3 l-\sin Ql\sin q_3 l\right\},$$

$$m_{56}=-\frac{4\chi^2}{\kappa}|A_{0,3}|^2\sin^2\left(\frac{Q}{2}\right)+\frac{4\eta^2}{\kappa}|A_{0,3}|^2-2\sum_{l=1}^{\infty}J_l'\sin Ql\sin q_3 l,$$

$$m_{66}=-\frac{4\chi^2}{\kappa}|A_{0,3}|^2\sin^2\left(\frac{Q}{2}\right)+\frac{4\eta^2}{\kappa}|A_{0,3}|^2-2\sum_{l=1}^{\infty}J_l'\left\{2\sin^2\left(\frac{Ql}{2}\right)\cos q_3 l+\sin Ql\sin q_3 l\right\}.$$

The condition for the above system to admit non-trivial solutions is obtained by setting its determinant to zero. One therefore finds a sixth-order polynomials

$$\Omega^6+P_5\Omega^5+P_4\Omega^4+P_3\Omega^3+P_2\Omega^2+P_1\Omega+P_0=0 \tag{3.20}$$

whose solutions may easily be found via symbolic computation, with the coefficients P_j being given in the Appendix. Solutions for Eq.(3.40) can be found analytically, using symbolic computation, but this is cumbersome are requires more simplifications and the study of some few cases. A more complete investigation of the solutions requires the use of numerical schemes, which give all the possible solutions. In that respect, such solutions may be real or complex depending on the values of parameters and most of the features related to MI are due to complex solutions. For example, solutions for Ω are generally in the form $\Omega=\Omega_r+i\Omega_i$, which modifies the perturbations as $B_{n,\alpha}(t)=e^{\Omega_i t}\left[a_{0,\alpha}e^{i(Qn-\Omega_r t)}+b_{0,\alpha}e^{-i(Qn-\Omega_r t)}\right]$. Therefore, one clearly sees that the imaginary part controls the stability/instability of the plane wave solutions. The rate of instability is in general evaluated in terms of the instability gain $G(q,Q)=|\mathrm{Im}(\Omega)|$, from which the onset of MI can be detected. As already indicated while presenting the model, one should stress that the coupling among adjacent peptides is of two competitive types, i.e., the LR and the nonlinear coupling. Previous works devoted to nearest-neighbor interactions have proven that the two types of coupling indeed affect the process of energy transport and storage in the three-stranded model **[33, 34]**. In the rest of this particular work, we insist on the concomitant effects of LR interactions and nonlinear coupling. To proceed, we first of all consider $q_1=q_2=q_3=q$ and $A_{10}=A_{20}=A_{30}=0.1$. For weak values of the nonlinear coupling parameter, i.e., $\chi=2$, we have the features of

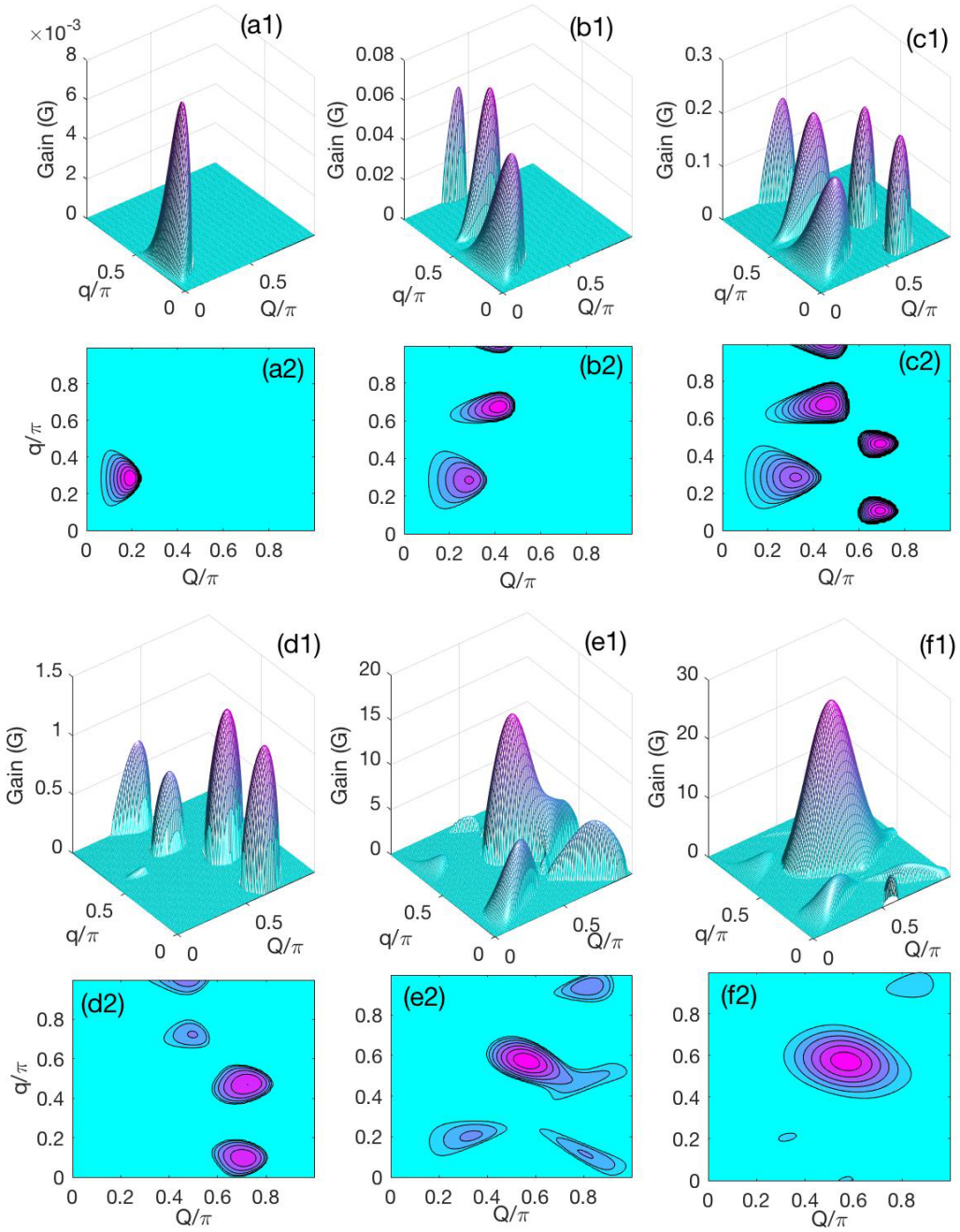

Figure 3.1: The panels show plots of the MI gain, and the corresponding stability/instability diagram, versus the wavenumbers Q and q, with changing χ and the range parameter r. For $\chi = 2$, $r = 1.5$ corresponds to panels (a1) and (a2), where there is only one region of instability. For $r = 1.2$, additional instability sidebands appear for $r = 1.2$ (panels 3.6(b1)-(b2)), and persist for $r = 1.1$ (panels 3.6(c1)-(c2)). Panels (d1)-(d2), (e1)-(e2) and (f1)-(f2) corresponds to $\chi = 8$, where r takes the respective values as in the previous case. Here, under strong LR effects, the numerous number of instability regions tend to merge into one one instability zone.

stability/instability given in Fig. 3.6. High values of the range parameter correspond to weak LR interactions and, when $r \to \infty$, the system behaves as restricted to nearest-neighbor interactions. In that respect, for $r = 1.5$, we have the gain of Fig. 3.6(a1) and its corresponding stability/instability diagram plotted in Fig. 3.6(a2), where there is only one region of instability. With decreasing r, i.e., increasing the LRI effect, additional instability sidebands appear for $r = 1.2$ (Figs. 3.6(b1)-(b2)), and persist for $r = 1.1$ (Figs. 3.6(c1)-(c2)). This shows that under weak nonlinear intra-spine interaction, LR interactions may be responsible for the explosion of the instability domain, leading to the emergence of other regions of instability. However, under strong nonlinear intra-strand coupling, the comportment is found to be different as depicted in Figs. 3.6(d1)-(d2), (e1)-(e2) and (f1)-(f2), where we have fixed $\chi = 8$. Panels (d1)-(d2) correspond to $r = 1.5$, value of the range parameter that gives rise to several regions of instability. Their number drops progressively with decreasing r, as shown in panels (e1)-(e2) and (f1)-(f2), for which r takes respectively the values 1.2 and 1.1. In the meantime, one should be aware that when values of parameters are picked from one of the regions of instability, the plane waves will be said to be unstable under modulation and will therefore be expected to break-up into solitonic structures. Otherwise, they will propagate with their properties not being changed, and will be said to be stable under modulation.

Beyond these information on the onset of MI, the linear stability analysis fails to predict the behaviors of solitons and nonlinear structures at long timescale. Therefore, in order to verify the accuracy of the linear stability analysis, we propose to integrate directly the set of Eqs.(3.36) using the fourth-order Runge-Kutta computational scheme, with periodic boundary conditions and timescale $\Delta t = 10^{-3}$. We consider the initial condition $A_{n,\alpha} = A_{0,\alpha}\,(1 + 0.01e^{iqn})\,e^{iQn} \quad (\alpha = 1, 2, 3)$ and to start, we fix $A_{10} = 0.1$ and $A_{20} = A_{30} = 0$, with the wavenumbers q and Q taking respectively the values 0.35π and 0.28π and $\chi = 2$. Particularly, we have excited only one strand in order to observe the dynamical response of the other two strands and the effectiveness of the inter-spine coupling. The chosen values of the wavenumbers fall well inside the regions of instability depicted in Fig. 3.6(a1)-(a2), and are to this fact expected to support nonlinear pattern formation. This is for example confirmed by the structures obtained in Fig. 3.7, whose shape and characteristics are influenced by the change in the range parameter r. In general, over longtime simulation they appear and have the shape of soliton-like patterns. This is a direct proof of the accuracy between our analytical predictions and direct nu-

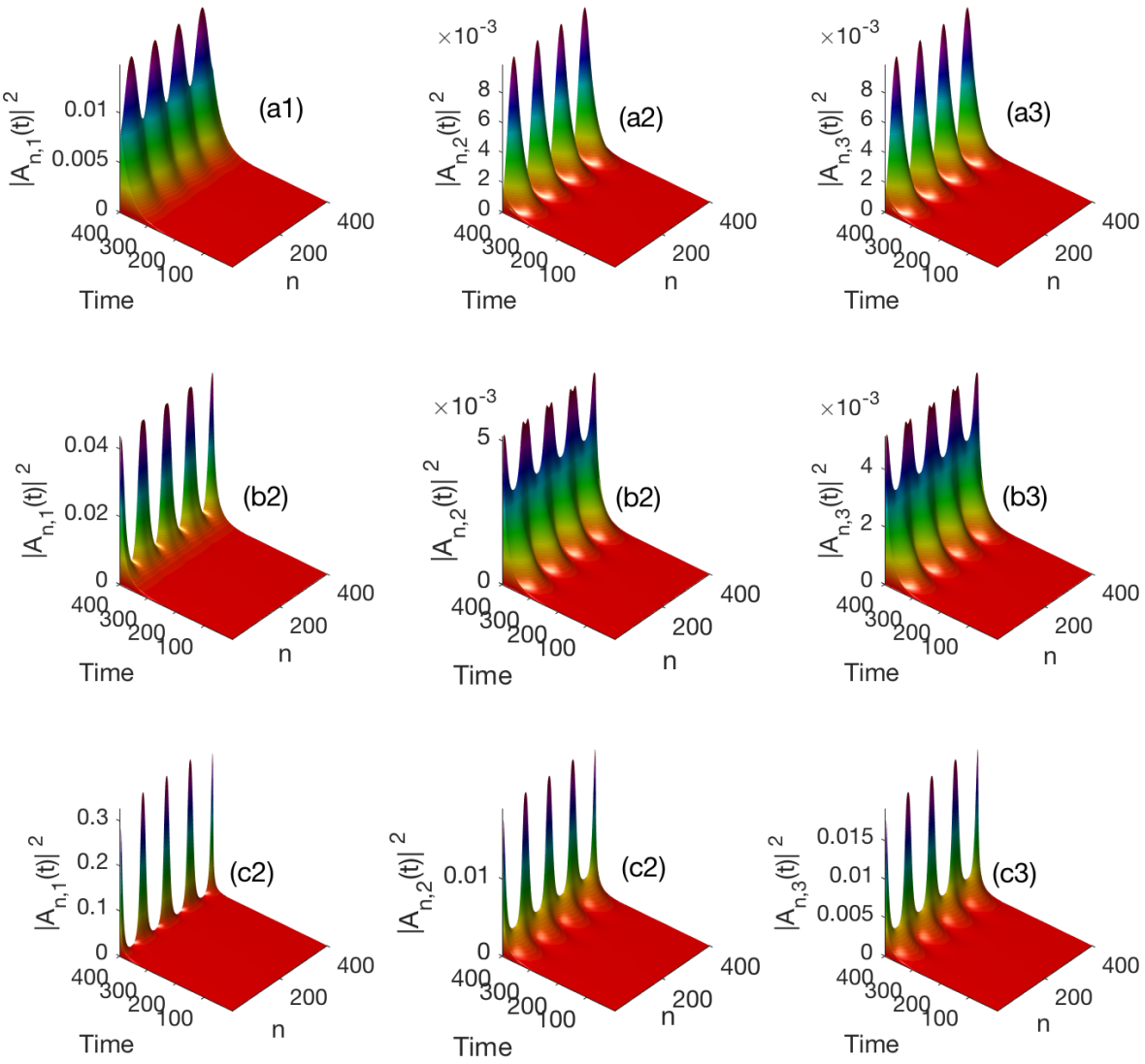

Figure 3.2: Numerical energy patterns obtained for $\chi = 2$ and: $(\mathrm{aj})_{j=1,2,3}$ $r = 1.5$, $(\mathrm{bj})_{j=1,2,3}$ $r = 1.2$ and $(\mathrm{cj})_{j=1,2,3}$ $r = 1.1$, with $A_{10} = 0.1$, $A_{20} = A_{30} = 0$, $\kappa = 11$ and $\omega = 100$.

merical calculations on the generic model. As only one of the spines has been excited, one notices the response from the other two strands, which obviously have the same amplitude of excitation. This has been reported in a number of recent contributions, but in the absence of LRI **[32–35]**. Nevertheless, they are the consequence of the interplay between nonlinear and dispersive effects. More precisely, the trains of waves obtained

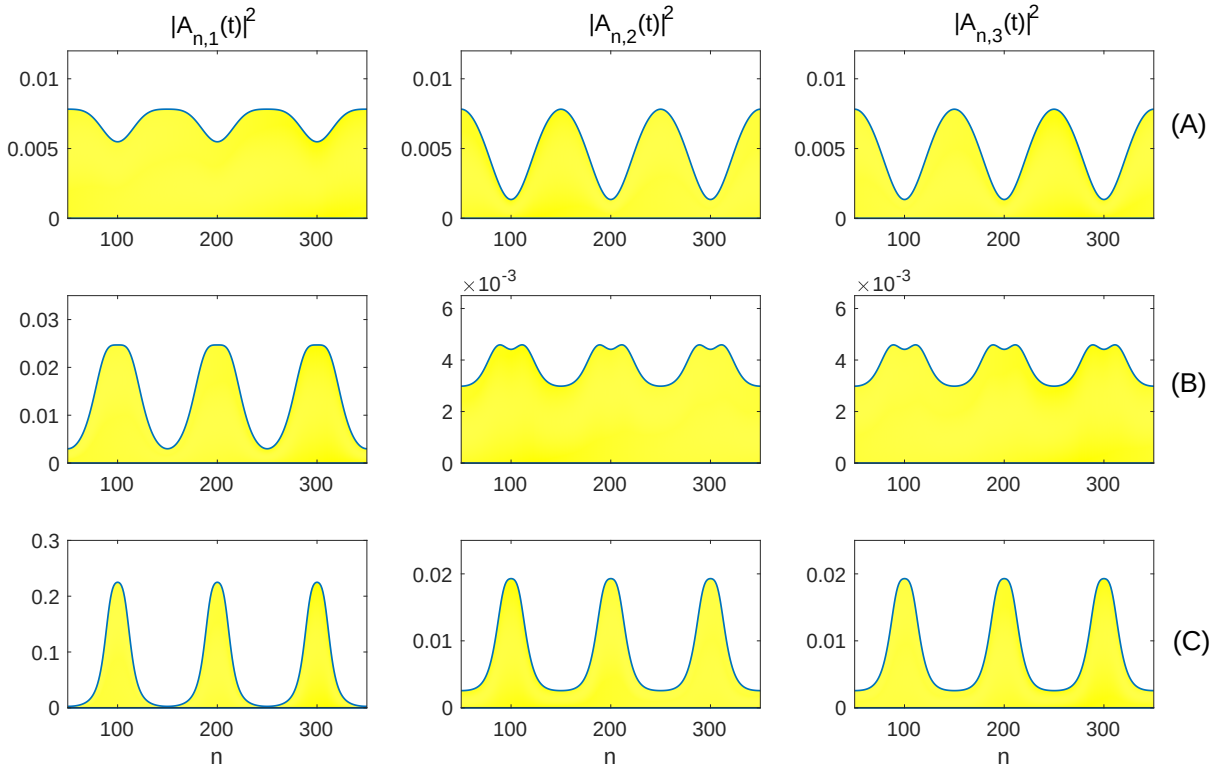

Figure 3.3: Spatial energy modes corresponding to Fig. 3.8 at time $t = 400$, in the lattice sequence $50 \leq n \leq 350$. Line (A) is plotted for $r = 1.5$, line (B) for $r = 1.2$ and line (C) for $r = 1.1$. The other parameters are $\chi = 2$, $A_{10} = 0.1$, $A_{20} = A_{30} = 0$, $\kappa = 11$ and $\omega = 100$.

have features of pulse solitons, but while comparing Fig. 3.7(a1) to Figs. 3.7(a2) and (a3), the presence of extended waves for $|A_{n,1}|$ is a fact, while $|A_{n,2}|$ and $|A_{n,3}|$ display patterns with periodic background. Figs. 3.7(aj)$_{j=1,2,3}$ have been recorded for $r = 1.5$. For $r = 1.2$, the manifestations of MI are shown in Figs. 3.7(bj)$_{j=1,2,3}$, where the number of breathing patterns has increased. Moreover, $|A_{n,2}|$ and $|A_{n,3}|$ display some initiation of two-humped solitonic structures with filled profile, while for $|A_{n,1}|$, individual pulses of energy are visible. In Fig. 3.8, the calculations of Fig. 3.7 have been repeated, where line (A) corresponds to Figs. 3.7(aj)$_{j=1,2,3}$, line (B) to Figs. 3.7(bj)$_{j=1,2,3}$ and line (C) to Figs. 3.7(cj)$_{j=1,2,3}$. There, the energy density has been recorded versus space and one clearly confirms the profile depicted in Fig. 3.7 with changing the value of the range parameter. For small values of the later, energy is distributed among lattice sites and remains available for intrinsic lattice dynamics. Interestingly, although there is still intrinsic energy, sequences of high energy patterns emerge in the form of impulses as confirmed

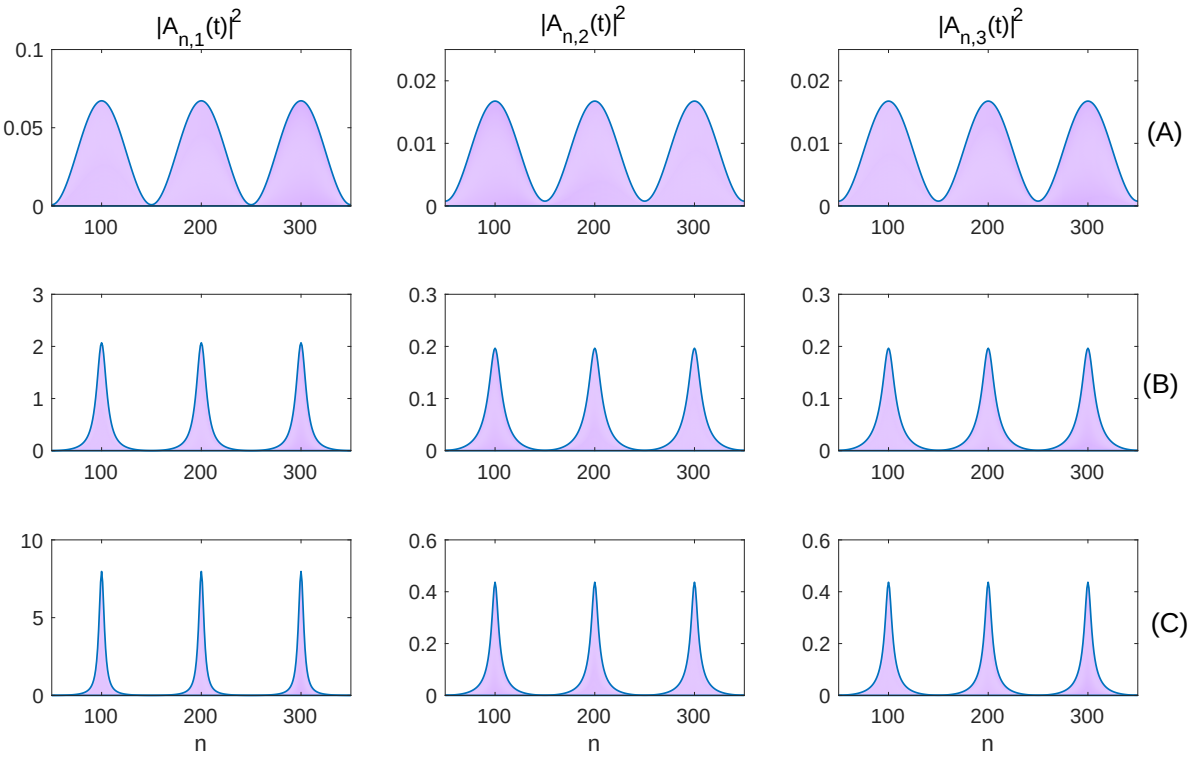

Figure 3.4: Spatial energy patterns related to strong intra-spine interaction, i.e., $\chi = 8$, in the lattice sequence $50 \leq n \leq 350$ at time $t = 400$. Line (A) is plotted for $r = 1.5$, line (B) for $r = 1.2$ and line (C) for $r = 1.1$. The other parameters are $A_{10} = 0.1$, $A_{20} = A_{30} = 0$, $\kappa = 11$ and $\omega = 100$.

by line (C) of Fig. 3.8. The result of line (C), however, shows the robustness of energy localization in molecular models, especially monitored by solitonic structures under the influence of any factor that may modify both the intrinsic nonlinearity and the dispersion inherent to such systems. Like in DNA, the stored and transported energy is supposed to adopt a specific profile for the process of its transport to be initiated **[124]**. That is indeed why, when all the conditions are gathered, under the activation of MI, trains of solitons as those observed in Fig. 3.8, line (C), may be observed. To remind, the results of Fig. 3.7 and 3.8 have been recorded for weak nonlinear intra-spine coupling χ. In Fig. 3.9, we have therefore increased its value as $\chi = 8$. The obtained results suggest that for $r = 1.5$, energy patterns display periodic profiles, with the excitonic patterns $|A_{n,2}|$ and $|A_{n,3}|$ still having the same characteristics. For $r = 1.2$, the localized states described in Ref. **[35]** appear, due to strong coupling χ and mainly because of the strength of the LR coupling that increases. Remarkably, the spatial expansion of the obtained patterns

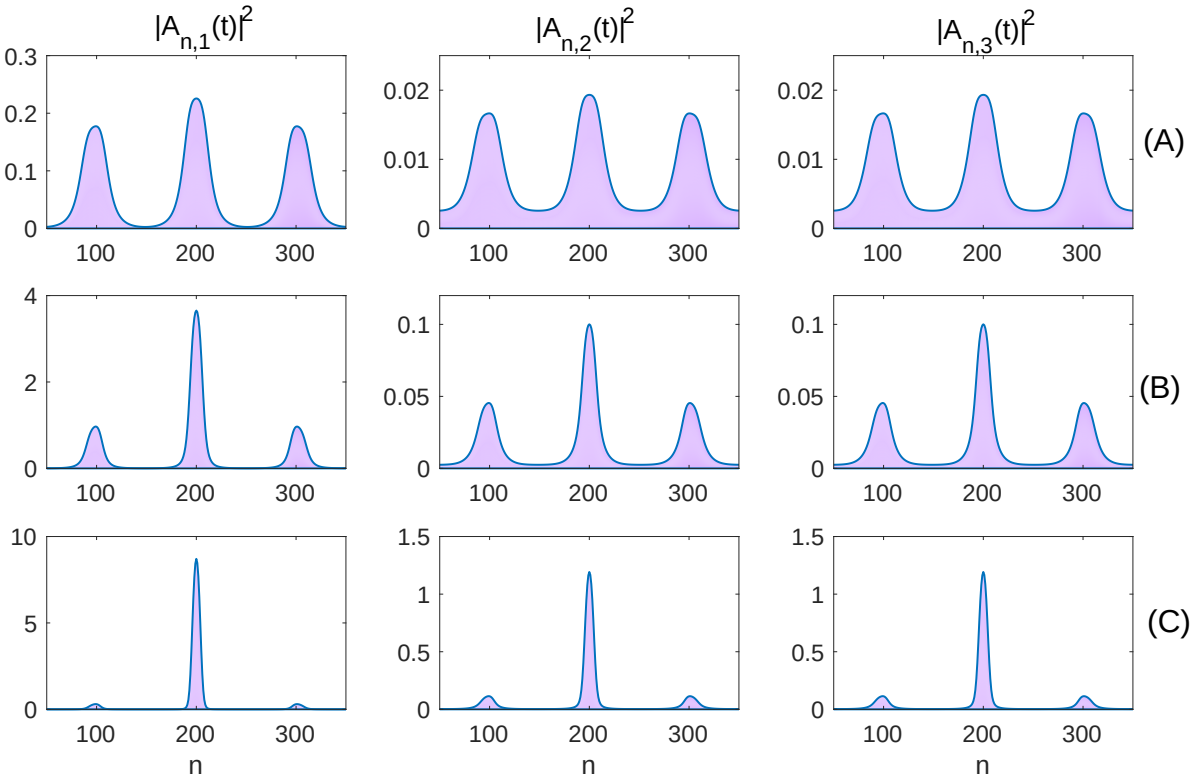

Figure 3.5: Spatial energy patterns related to strong intra-spine interaction, i.e., $\chi = 14$, in the lattice sequence $50 \leq n \leq 350$ at time $t = 400$. Line (A) is plotted for $r = 1.5$, line (B) for $r = 1.2$ and line (C) for $r = 1.1$. The other parameters are $A_{10} = 0.1$, $A_{20} = A_{30} = 0$, $\kappa = 11$ and $\omega = 100$.

gets restrained, compared to the case of line (A). This persists when $r = 1.1$, where the wave spatial expansion of $|A_{n,1}|$ gets more narrower, therefore involving few sequences of lattice sites. This phenomenon is ubiquitous to many molecular systems due to the strong competition between nonlinearity and dispersion. Multi-humped solitonic structures were already reported in a three-stranded model of $\alpha-$helix proteins, but were shown to merge into a single structure with increasing χ. The same behavior is obvious in Fig. 3.5, where the value of χ has been increased to 14. In fact, the observed spectrum of behaviors is a consequence of the coupled effects of nonlinear coupling and LRI, leading to an effective transition from extended trains of waves to asymmetric solitonic humps when r becomes small, i.e., under strong LRI. Line (A) of Fig. 3.5 has been plotted for $r = 1.5$, line (B) for $r = 1.2$ and line (C) for $r = 1.1$. The existence of such waves in proteins was already suggested by Brown et al. **[20–22]** and Ivic et al. **[123, 125, 126]**. That was to demonstrate that due to the structural modification taking place in real proteins during

energy transport, the observed structures were suitable. Falvo and Pouthier **[127, 128]**, considering a three-spine model showed that the vibron dynamics was the consequence of the competitive effects between inter-spine vibron hops, leading to some dressing effects, capable of reducing vibrational exchange between spines, the direct consequence being the emergence of energy patterns that move along a single spine, therefore reducing the system to a one-dimensional Davydov model. In contrast, the nonlinear effects present in the proposed model enhance the emergence of solitonic waves that, under appropriate LR dispersive contribution in all the spines, reinforce inter-based energy storage and distribution. Indeed, the model Eqs.(3.36) include coupling parameters to vibrational dynamics, especially H-bonds among spines, which were already revealed to be vital for mediating electronic transport in proteins **[35,39,133]**. They are indeed the driving force in such a process, which to some extent is common to most of biological molecules. Due to the presence of H-bonds, charge transport in DNA may be controlled and give rise to important dynamical spectrum with appropriate biological implications **[30, 129–132]**.

3.1.3 Conclusion

This investigation considered a three-stranded $\alpha-$helix protein model with LR dispersive interactions and inter-spine coupling. The improved quantum model for exciton-phonon dynamics has been reduced to a set of three coupled modified DNLS equations with LR interactions. The MI analysis has therefater been conducted, and regions of instability detected. Those regions, where the plane wave solutions are supposed to disintegrate into trains of soliton-like objects, have been found to be very sensitive to the LR and nonlinear coupling parameters, r and χ respectively. For small values of χ, strong LR interaction, i.e., small r, tends to induce additional instability sidebands which reduce to only one region when r decreases. Contrarily, for high values of χ, the spectrum of instability displays many regions of instability that are annihilated by strong LR effects. This has been confirmed numerically, using instability parameters. In that respect, it has been confirmed that when parameters fall well inside instability zones, there appear trains of solitonic entities due to the balanced effect of nonlinearity and dispersion. More importantly, for small χ, ordinary extended waves transform progressively into trains of pulses with decreasing r. Although this remains obvious for big χ and high r, more spatially restrained structures emerge under strong LR effects. This gets more pronounced when χ increases. In view of the above, solitonic structures are robust in H-bonded molecules,

especially in proteins and DNA. In that respect, they may be of different significance, depending on the backbone structure of the studied biomolecule. However, most of the cases rely on the strong relationship between vibrational and excitonic dynamics. In DNA for example, solitonic energy patterns have been found to be more effective when the H-bonds linking the bases in pairs are compressed, leading to slight breathing oscillations of the strand under the activation of MI **[30, 129, 131, 132]**, and the same seems to be effective in proteins. Understanding the various mechanisms and factors related to such processes is of paramount importance both in biology and nanobioelectronic. This requires the elaboration of more suitable models, that may bring together as many interactions as possible, including those related to the direct molecular environment of the protein such as thermal fluctuations, dissipation and LR coupling among peptide groups. Investigations in those directions are ongoing.

3.2 Fractional dynamic effects

3.2.1 Introduction

In the last decades, the understanding of energy transport and storage in biomolecules has received a remarkable development mainly based on the seminal contribution of Davydov **[8]**. It has been well-established that the energy which is transported via proteins originates from the hydrolysis of adenosine triphosphate (ATP) **[8]**. Namely, considering the structure of $\alpha-$helix proteins, Davydov and Kislukha **[6,7]** used the exciton formalism to explain the self-trapping of the amide-I oscillations as the consequence of the interaction between the vibrational exciton and the distortion in the protein structure, resulting from the presence of the exciton. They established that the interplay between nonlinearity and dispersion may favor solitons to travel in the protein strand and carry the self-trapped vibrational amide-I energy. Many of the contributions that followed focussed on the existence of only one exciton state **[4, 5, 31–33, 42, 77, 134–136]**. Works by Pouthier and Falvo **[127, 128, 137]** however insisted on the existence of at least two excited states as a way of stabilizing the self-trapped energy. Merlin and Latha **[138,139]**also addressed such aspects and rather showed, based on a paper from Ekobena et al. **[31]**, that anharmonicity may play an important role when more that one excitations are considered. The soliton that are usually obtained in this context are solutions of coupled nonlinear Schrödinger

(NLS) equations, each describing a specific excitonic state **[32,33,41,77,135]**. Attention has been given recently to protein structures with long-range (LR) intermolecular interactions, leading to space-fractional NLS equations **[41,140]**. In this framework, Tarasov and Zaslavsky **[141,142]** have shown that in the presence of power-law LR interactions, it was possible to reduce a purely discrete problem to its space-fractional formulation. A three-stranded model of $\alpha-$helix proteins was used recently as an example by Mvogo et al. **[41]**, but further approximations were made to recover a classical set of coupled NLS equations, therefore avoiding the complexity imposed by the fractional terms. More recently, the modulational instability (MI) of a fractional NLS equation was addressed, where Zhang et al. **[143]** showed that the fractional-order parameter may have important influence on the onset and long-time evolution of nonlinear modulated patterns. Tabi **[140]** also studied the MI of plane wave in an $\alpha-$helix model and brought out the effect of the fractional derivative on the process of energy transport and storage along a single protein strand. This work is a generalization of such a model, i.e., when more that one excitonic degree of freedom is considered. We show that for a two-exciton model, transport and storage of energy can fully be described by a set of nonlinearly coupled space-fractional NLS equations. The linear stability analysis of their plane wave solutions is then performed with emphasis on the effect of changing both the fractional-order parameters and the coefficient of nonlinearity. Numerical experiments are used to confirm the analytical predictions through the long-time behaviors of the subsequent modulated trains of waves. Concluding remarks end the paper.

3.2.2 Model and dynamical equation

3.2.2.1 Model

The generalized Hamiltonian corresponding to the dynamics of two excitons in a protein lattice has been proposed in some recent works as an improvement of the Davydov model **[6,8]**. In the presence of LR intrachain molecular interaction between molecular excitations, the Hamiltonian writes

$$H=\sum_{n}\Big[\hbar\omega_0(A_n^{\dagger}A_n+B_n^{\dagger}B_n)-\sum_{m\neq n}J_{n-m}^{(1)}(A_n^{\dagger}A_m+A_nA_m^{\dagger})-\sum_{m\neq n}J_{n-m}^{(1)}(B_n^{\dagger}B_m+B_nB_m^{\dagger})$$
$$+\frac{g_1}{2}(A_n^{\dagger}A_n^{\dagger}A_nA_n+B_n^{\dagger}B_n^{\dagger}B_nB_n)+g_2A_n^{\dagger}A_nB_n^{\dagger}B_n\Big], \tag{3.21}$$

with the subscript n referring to the lattice index along the strand (or chain). The expression of H suggests that an individual amino acid will be identified by the index pair n, such that A_n ($A_n^\dagger$) and B_n ($B_n^\dagger$) are boson creation (annihilation) operators associated with intramolecular vibrations of the nth peptide group. These operators satisfy the usual commutation relations for bosons, i.e., $[A_n, A_m^\dagger] = \delta_{m,n}$, $[A_n, A_m] = 0$, $[B_n, B_m^\dagger] = \delta_{m,n}$ and $[B_n, B_m] = 0$. $\hbar\omega_0$ is the local amide-I vibrational energy, and the terms $\hbar\omega_0 A_n^\dagger A_n$ and $\hbar\omega_0 B_n^\dagger B_n$ are the vibrational energies at the site n from the two exciton bound states. The terms $\sum_{m\neq n} J_{n-m}^{(1)}(A_n^\dagger A_m + A_n A_m^\dagger)$ and $\sum_{m\neq n} J_{n-m}^{(2)}(B_n^\dagger B_m + B_n B_m^\dagger)$ are the energies related to the LR interactions between molecular excitations on sites n and m. The coupling parameters $J_{n-m}^{(1)}$ and $J_{n-m}^{(2)}$ are the LR transfer integrals between sites n and m, here considered of the form **[43–45, 144]**:

$$J_{n-m}^{(1)} = J_1|n-m|^{-s_1} \quad \text{and} \quad J_{n-m}^{(2)} = J_2|n-m|^{-s_2}, \tag{3.22}$$

with J_1 and J_2 being the strengths of the transfer integral between the chain and each of the excitations. s_i ($i = 1, 2$) are range parameters whose values belong to the interval $[1, +\infty[$. However s_i cover different physical contexts, depending on its value. For example if $s_i \to \infty$, the LR interaction reduces to nearest-neighbor couplings. For $s_i = 5$, the LR interaction is of a dipole-dipole type, while for $s_i = 3$, the LR interaction is of the Coulomb type. We should stress that the strongest interaction effects are due to smaller values of s_i.

We make use of the Heisenberg formulation and obtain the following exciton equations:

$$i\hbar\frac{\partial A_n}{\partial t} = \hbar\omega_0 A_n - \sum_{m\neq n} J_{n-m}^{(1)} A_m + (g_1 A_n A_n^\dagger + g_2 B_n B_n^\dagger)A_n, \tag{3.23a}$$

$$i\hbar\frac{\partial B_n}{\partial t} = \hbar\omega_0 B_n - \sum_{m\neq n} J_{n-m}^{(2)} B_m + (g_1 B_n B_n^\dagger + g_2 A_n A_n^\dagger)B_n. \tag{3.23b}$$

In order to study coherent states, it will be useful to rewrite Eq.(3.23) in terms of eigenfunctions of the operators A_n, $A_n^\dagger$, B_n and $B_n^\dagger$ so that, if the Glauber coherent states $|\{\alpha_n\}\rangle = \prod_n |\alpha_n\rangle$, $A_n|\alpha_n\rangle = \alpha_n|\alpha_n\rangle$, $|\{\beta_n\}\rangle = \prod_n |\beta_n\rangle$ and $B_n|\beta_n\rangle = \beta_n|\beta_n\rangle$ are introduced **[?]**, the set of Eqs.(3.23) becomes

$$i\hbar\frac{\partial \alpha_n}{\partial t} = \hbar\omega_0 \alpha_n - \sum_{m\neq n} J_{n-m}^{(1)} \alpha_m + (g_1|\alpha_n|^2 + g_2|\beta_n|^2)\alpha_n, \tag{3.24a}$$

$$i\hbar\frac{\partial \beta_n}{\partial t} = \hbar\omega_0 \beta_n - \sum_{m\neq n} J_{n-m}^{(2)} \beta_m + (g_2|\alpha_n|^2 + g_1|\beta_n|^2)\beta_n. \tag{3.24b}$$

Eqs.(3.24) are a set of nonlinearly coupled NLS equations with LR dispersive interactions. When $g_2 = 0$, the two equations will be completely decoupled and will reduce to individual discrete NLS equations. For instance, we can get rid of the terms $\hbar\omega_0\alpha_n$ and $\hbar\omega_0\beta_n$ via the gauge transformations $\alpha_n(t) = u_n(t)e^{-i\omega_0 t}$ and $\beta_n(t) = v_n(t)e^{-i\omega_0 t}$. This yields

$$i\frac{\partial u_n}{\partial t} = -\sum_{m\neq n} J^{(1)}_{n-m}u_m + (g_1|u_n|^2 + g_2|v_n|^2)u_n, \tag{3.25a}$$

$$i\frac{\partial v_n}{\partial t} = -\sum_{m\neq n} J^{(2)}_{n-m}v_m + (g_2|u_n|^2 + g_1|v_n|^2)v_n, \tag{3.25b}$$

where we have further made the change of variable $t \to t/\hbar$.

3.2.2.2 The coupled NLS equation with fractional derivative

In order to obtain the fractional-derivative formulation of Eqs.(3.25), we introduce the functions **[41, 141, 142]**

$$\phi(k,t) = \sum_{m=-\infty}^{+\infty} e^{-iknd}u_n(t), \;\; \psi(k,t) = \sum_{m=-\infty}^{+\infty} e^{-iknd}v_n(t) \;\text{ and }\; J(k) = \sum_{m=-\infty}^{+\infty} e^{-iknd}J_n, \tag{3.26}$$

where the parameter k is a wavenumber, d is the lattice spacing and J_n is given by Eq. (3.22). Inversely, the functions $u_n(t)$ and $u_n(t)$ are respectively related to $\phi(k,t)$ and $\psi(k,t)$ through the relations

$$u_n(t) = \int_{-\pi}^{\pi} e^{iknd}\phi(k,t)dk \;\text{ and }\; v_n(t) = \int_{-\pi}^{\pi} e^{iknd}\psi(k,t)dk. \tag{3.27}$$

In the continuum approximation, i.e., $u_n(t) \to u(x,t)$ and $v_n(t) \to v(x,t)$, with $x = nd$, when $k \to 0$, relations (3.26) and (3.27) become

$$\begin{aligned} \phi(k,t) &= \int_{-\infty}^{+\infty} e^{-ikx}u(x,t)dx, \;\; \psi(k,t) = \int_{-\infty}^{+\infty} e^{-ikx}v(x,t)dx, \\ u(x,t) &= \frac{1}{2\pi}\int_{-\infty}^{+\infty} e^{ikx}\phi(k,t)dk, \;\; v(x,t) = \frac{1}{2\pi}\int_{-\infty}^{+\infty} e^{ikx}\psi(k,t)dk. \end{aligned} \tag{3.28}$$

Applying all the above to Eq.(3.25) in the continuum approximation leads to

$$i\frac{\partial u(x,t)}{\partial t} = -J_1(0)u(x,t) - \int_{-\infty}^{+\infty} dydxK_1(x-y)\frac{\partial u(x,t)}{\partial x} + \left(g_1|u(x,t)|^2 + g_2|v(x,t)|^2\right)u(x,t) \tag{3.29a}$$

$$i\frac{\partial v(x,t)}{\partial t} = -J_2(0)v(x,t) - \int_{-\infty}^{+\infty} dydxK_2(x-y)\frac{\partial v(x,t)}{\partial x} + \left(g_2|u(x,t)|^2 + g_1|v(x,t)|^2\right)v(x,t), \tag{3.29b}$$

where the Kernels $K_i(x)$ $(i = 1, 2)$ are given by

$$K_i(x) = \frac{1}{\pi}\int_{-\infty}^{+\infty} e^{ikx}\frac{G_i(k)}{k^2}dk, \quad i = 1, 2, \tag{3.30}$$

with $G_i(k) = J_i(0) - J_i(k)$, $J_i = \zeta(s_i)^{-1}$, with the $\zeta-$function being given by $\zeta = \sum_{1=1}^{\infty} n^{-s}$. For the specific case where $2 \leq s_i < 3$, the function $G(k)$ is in the form

$$G_i(k) = \frac{\pi J_i}{\Gamma(\sigma_i + 1)\sin\left(\frac{\pi\sigma_i}{2}\right)}|k|^{\sigma_i}, \tag{3.31}$$

where where $\Gamma(\sigma)$ is the $\Gamma-$function, with $\sigma = s - 1$ and $\Gamma(\sigma + 1) = \sigma\Gamma(\sigma)$. Therefore, given the possible values of s, the values of σ will be found between 1 and 2. Under such considerations, the continuum equations (3.29) become

$$i\frac{\partial u(x,t)}{\partial t} = -J_1(0)u(x,t) - P_1\frac{\partial^{\sigma_1}}{\partial|x|^{\sigma_1}}u(x,t) + \left(g_1|u(x,t)|^2 + g_2|v(x,t)|^2\right)u(x,t), \tag{3.32a}$$

$$i\frac{\partial v(x,t)}{\partial t} = -J_2(0)v(x,t) - P_2\frac{\partial^{\sigma_2}}{\partial|x|^{\sigma_2}}v(x,t) + \left(g_2|u(x,t)|^2 + g_1|v(x,t)|^2\right)v(x,t), \tag{3.32b}$$

where the coefficients P_i $(i = 1, 2)$ are given by

$$P_1 = \frac{\pi J_1}{\Gamma(\sigma_1 + 1)\sin\left(\frac{\pi\sigma_1}{2}\right)} \text{ and } P_2 = \frac{\pi J_2}{\Gamma(\sigma_2 + 1)\sin\left(\frac{\pi\sigma_2}{2}\right)}. \tag{3.33}$$

The Riesz fractional derivatives are given by **[146, 147]**

$$\frac{\partial^{\sigma_1}}{\partial|x|^{\sigma_1}}u(x,t) = -\frac{1}{2\pi}\int_{-\infty}^{+\infty}|k|^{\sigma_1}\phi(k,t)dk \text{ and } \frac{\partial^{\sigma_2}}{\partial|x|^{\sigma_2}}v(x,t) = -\frac{1}{2\pi}\int_{-\infty}^{+\infty}|k|^{\sigma_2}\psi(k,t)dk. \tag{3.34}$$

By making use of the gauge transfomations $u(x,t) \to u(x,t)e^{iJ_1t}$ and $v(x,t) \to v(x,t)e^{iJ_2t}$, we finally obtain

$$i\frac{\partial u(x,t)}{\partial t} = -P_1\frac{\partial^{\sigma_1}}{\partial|x|^{\sigma_2}}u(x,t) + \left(g_1|u(x,t)|^2 + g_2|v(x,t)|^2\right)u(x,t), \tag{3.35a}$$

$$i\frac{\partial v(x,t)}{\partial t} = -P_2\frac{\partial^{\sigma_2}}{\partial|x|^{\sigma_2}}v(x,t) + \left(g_2|u(x,t)|^2 + g_1|v(x,t)|^2\right)v(x,t), \tag{3.35b}$$

which is a set of coupled NLS equations with space-fractional derivatives. Obviously, the dispersion terms P_i are functions of the fractional-order parameters σ_i. However, the Riesz fractional derivative is also expressed as **[146, 147]**

$$\frac{\partial^{2\sigma}}{\partial|x|^{\sigma}}f(x,t) = -\left(-\frac{\partial^2}{\partial|x|^2}\right)^{\sigma/2}f(x,t) = -\frac{1}{2\cos\left(\frac{\pi\sigma}{2}\right)}\left[{}_{-\infty}\mathcal{D}_x^{\sigma}f(x,t) + {}_x\mathcal{D}_{+\infty}^{\sigma}f(x,t)\right], \tag{3.36}$$

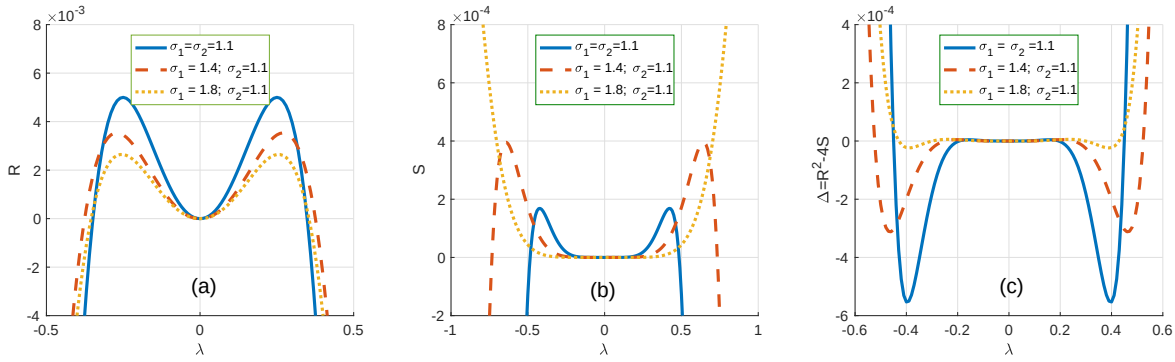

Figure 3.6: The panels show plots of the of the coefficients R and S of Eq. (3.42) and its discriminant $\Delta = R^2 - 4S$, versus the perturbation wavenumber λ. The fractional-order parameters change as shown in the legends, with $g_1 = g_2 = -0.05$ and $J_1 = J_2 = 0.08$.

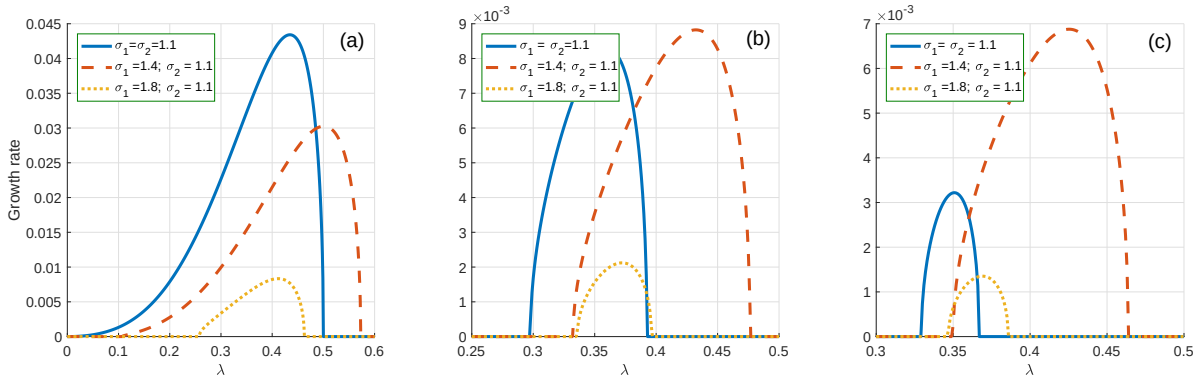

Figure 3.7: The panels show plots of the MI growth rate (3.45) versus the perturbation wavenumber λ. (a) corresponds to $g_1 = -0.5$, (b) to $g_1 = -0.1$ and (c) to $g_1 = -0.08$. We have fixed $g_2 = -0.05$, while the fractional-order parameters change as displayed by the legends, with $J_1 = J_2 = 0.08$.

where ${}_{-\infty}\mathcal{D}_x^{\sigma} f(x,t)$ and ${}_{x}\mathcal{D}_{+\infty}^{\sigma} f(x,t)$, are the left- and right-side Riemann-Liouville fractional derivatives of order σ, that are respectively given by **[146, 147]**

$$
\begin{aligned}
{}_{x}\mathcal{D}_{+\infty}^{\sigma} f(x,t) &= \frac{1}{\Gamma(n-\sigma)} \frac{\partial^n}{\partial x^n} \int_{-\infty}^{x} \frac{f(\xi,t)d\xi}{(x-\xi)^{\sigma-x+1}}, \\
{}_{-\infty}\mathcal{D}_x^{\sigma} f(x,t) &= \frac{(-1)^n}{\Gamma(n-\sigma)} \frac{\partial^n}{\partial x^n} \int_{-\infty}^{x} \frac{f(\xi,t)d\xi}{(\xi-x)^{\sigma-x+1}}.
\end{aligned}
\tag{3.37}
$$

3.2.3 Modulational instability analysis

The set of Eqs.(3.35) admits the plane waves $u(x,t) = u_0 e^{i\omega_1 t}$ and $v(x,t) = v_0 e^{i\omega_2 t}$ as solutions, with the frequencies and amplitudes u_0 and v_0 being related by

$$\omega_1 = -(g_1|u_0|^2 + g_2|v_0|^2) \text{ and } \omega_2 = -(g_1|v_0|^2 + g_2|u_0|^2). \tag{3.38}$$

We consider small perturbations χ_1 and χ_2 into the above solutions, i.e., $u(x,t) = u_0(1 + \chi_1(x,t))e^{i\omega_1 t}$ and $v(x,t) = v_0(1 + \chi_2(x,t))e^{i\omega_2 t}$. This leads, after linearizing around the unperturbed plane waves, to the set of equations

$$i\frac{\partial}{\partial t}\chi_1(x,t) = -P_1\frac{\partial^{\sigma_1}}{\partial|x|^{\sigma_1}}\chi_1(x,t) + g_1|u_0|^2(\chi_1 + \chi_1^*) + g_2|v_0|^2(\chi_2 + \chi_2^*), \tag{3.39a}$$

$$i\frac{\partial}{\partial t}\chi_2(x,t) = -P_2\frac{\partial^{\sigma_2}}{\partial|x|^{\sigma_2}}\chi_2(x,t) + g_1|v_0|^2(\chi_2 + \chi_2^*) + g_2|u_0|^2(\chi_1 + \chi_1^*) \tag{3.39b}$$

for the perturbations. Moreover, the problem can be efficiently solved by separating real from imaginary parts, i.e., $\chi_1 = a_1 + ib_1$ and $\chi_2 = a_2 + ib_2$, leading to the equations

$$\begin{aligned}
\frac{\partial}{\partial t}a_1(x,t) &= -P_1\frac{\partial^{\sigma_1}}{\partial|x|^{\sigma_1}}b_1(x,t),\\
\frac{\partial}{\partial t}b_1(x,t) &= P_1\frac{\partial^{\sigma_1}}{\partial|x|^{\sigma_1}}a_1(x,t) - 2g_1|u_0|^2a_1(x,t) - 2g_2|v_0|^2a_2(x,t),\\
\frac{\partial}{\partial t}a_2(x,t) &= -P_2\frac{\partial^{\sigma_2}}{\partial|x|^{\sigma_2}}b_2(x,t),\\
\frac{\partial}{\partial t}b_2(x,t) &= P_2\frac{\partial^{\sigma_2}}{\partial|x|^{\sigma_2}}a_2(x,t) - 2g_1|v_0|^2a_2(x,t) + 2g_2|u_0|^2a_1(x,t).
\end{aligned} \tag{3.40}$$

Solutions for Eqs.(3.40) can be considered in the form of the following Fourier transfroms:

$$\begin{aligned}
\tilde{a}_1(\lambda,\Omega) &= \int\int_{-\infty}^{+\infty} a_1(x,t)e^{i(\lambda x+\Omega t)}dxdt,\\
\tilde{a}_2(\lambda,\Omega) &= \int\int_{-\infty}^{+\infty} a_2(x,t)e^{i(\lambda x+\Omega t)}dxdt,\\
\tilde{b}_1(\lambda,\Omega) &= \int\int_{-\infty}^{+\infty} b_1(x,t)e^{i(\lambda x+\Omega t)}dxdt,\\
\tilde{b}_2(\lambda,\Omega) &= \int\int_{-\infty}^{+\infty} b_2(x,t)e^{i(\lambda x+\Omega t)}dxdt.
\end{aligned} \tag{3.41}$$

Replacing the above solutions into Eqs.(3.40) leads to a homogeneous system for $\tilde{a}_1$, $\tilde{b}_1$, $\tilde{a}_2$ and $\tilde{b}_2$. The condition for such a system to admit non-trivial solutions is obtained by setting its determinant to zero, which leads to the nonlinear dispersion relation

$$\Omega^4 - R\Omega^2 + S = 0, \tag{3.42}$$

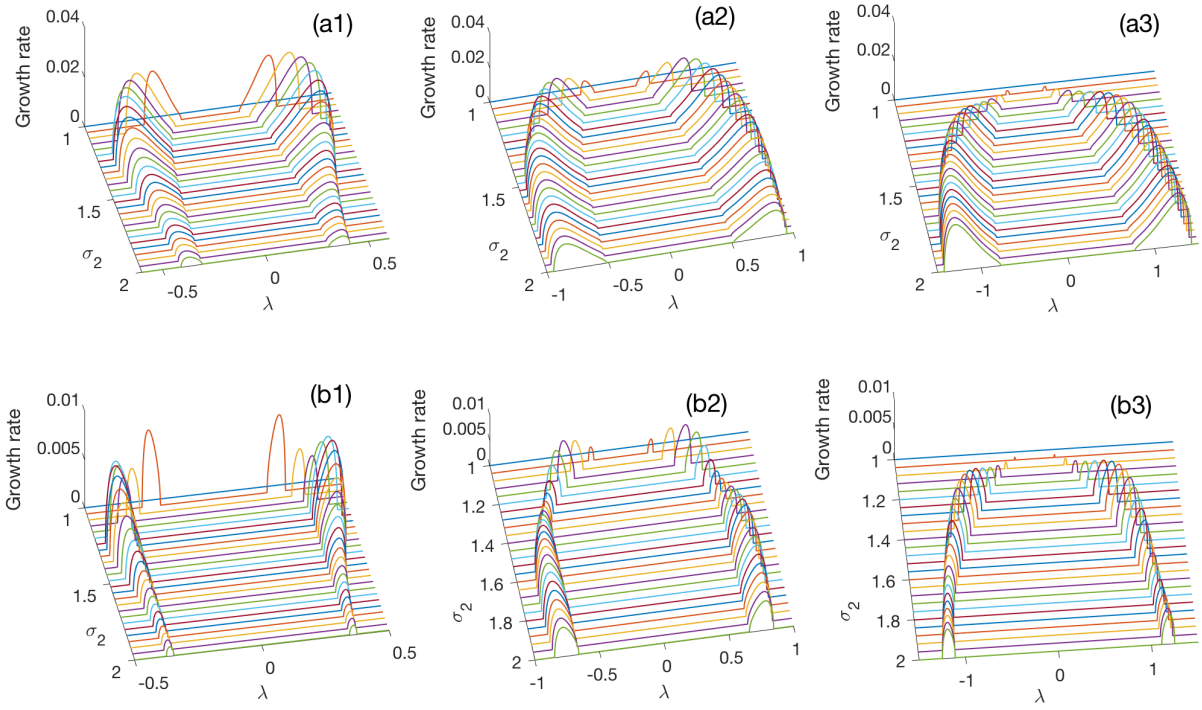

Figure 3.8: Plots of the MI growth rate versus the perturbation wavenumber λ and the fractional-order parameter σ_2. Panels $(\text{aj})_{j=1,2,3}$ correspond to $g_1 = -0.5$ and $g_2 = -0.05$, and panels $(\text{bj})_{j=1,2,3}$ gives Γ for $g_1 = -0.08$ and $g_2 = -0.05$. Columns (a1)-(b1) are obtained for $\sigma_1 = 1.1$, (a2)-(b2) for $\sigma_1 = 1.4$ and (a3)-(b3) for $\sigma_1 = 1.8$, with $J_1 = J_2 = 0.08$.

where

$$\begin{aligned} R &= P_2|\lambda|^{\sigma_2}(2g_1|v_0|^2 - P_2|\lambda|^{\sigma_2}) + P_1|\lambda|^{\sigma_1}(2g_1|u_0|^2 - P_1|\lambda|^{\sigma_1}), \\ S &= P_1P_2|\lambda|^{\sigma_1+\sigma_2}\left[4g_2^2|u_0|^2|v_0|^2 - (P_1|\lambda|^{\sigma_1} - 2g_1|u_0|^2)(P_2|\lambda|^{\sigma_2} - 2g_1|v_0|^2)\right]. \end{aligned} \tag{3.43}$$

Obviously, the coefficients of the dispersion relation (3.42) depend on the fractional-order parameters σ_1 and σ_2. However, the plane wave solutions will remain stable if the conditions $R > 0$, $S > 0$ and $\Delta = R^2 - 4S > 0$ are simultaneously satisfied. In order to find the intervals of parameters where such condition can be satisfied, we have plotted R, S and Δ in Fig. 3.6 versus the perturbation wavenumber λ.

The condition $R > 0$ is studied in Fig. 3.6(a), where the stability region is found in the interval $0 < \lambda < \lambda_+$. However, depending on the value of the fractional-order parameters σ_1 and σ_2, that interval can get expanded or reduced. It gets expanded for $\sigma_1 = 1.4$ and

$\sigma_2 = 1.1$, and drops for $\sigma_1 = 1.8$ and $\sigma_2 = 1.1$.

The condition $S > 0$ is addressed in Fig. 3.6(b). For $\{\sigma_1 = \sigma_2 = 1.1\}$ and $\{\sigma_1 = 1.4; \sigma_2 = 1.1\}$, there is an interval $\lambda_- < \lambda < \lambda_+$ (with $\lambda_- > 0$) where wave stability is expected. However, there is a change of behavior for $\{\sigma_1 = 1.8; \sigma_2 = 1.1\}$, where stable plane wave are possible in the interval $\lambda_- < \lambda < \infty$.

The discriminant Δ has been plotted in Fig. 3.6(c). The plane wave will remain stable where Δ is positive. Its sign changes with the fractional-order parameters. Under such a condition, Eq. (3.42) admits two solutions given by

$$\Omega_+^2 = \frac{1}{2}\left(R + \sqrt{R^2 - 4S}\right), \quad \Omega_-^2 = \frac{1}{2}\left(R - \sqrt{R^2 - 4S}\right). \tag{3.44}$$

On the other hand, if $\Delta = R^2 - 4S < 0$, there exists a domain of the wavenumber λ for which Ω^2 is negative. In this range, the solution of (3.42) are complex so that Ω^2 has a nonvanishing imaginary part. The plane waves will be unstable if this imaginary part of Ω is positive, causing the perturbation to grow exponentially. Then, the plane wave tends to self-modulate with a wavenumber λ corresponding to the growth rate

$$\Gamma = \mathrm{Im}\left(\Omega_\pm^2\right) = \pm\frac{1}{2}\sqrt{4S - R^2}. \tag{3.45}$$

The above growth rate of instability implies that the condition $\sqrt{4S - R^2} > 0$ should be satisfied for wave instability to take place. The growth rate of instability (3.45) is plotted in Fig. 3.7, versus the wavenumber λ, where the effect of the fractional-order parameters is obvious. To plot Fig. 3.7(a), we have fixed $g_2 = -0.5$ and $\sigma_2 = 1.1$. For $\sigma_1 = \sigma_2 = 1.1$, the plane wave is unstable in the region $0 < \lambda < 0.5$ which gets extended to $0 < \lambda < 0.58$ for $\sigma_1 = 1.4$. For $\sigma_1 = 1.8$, the region of instability gets reduced and restricted to the interval $0.26 < \lambda < 0.48$. The same behavior is obvious in all the other cases, where $g_2 = -0.1$ (Fig. 3.7(b)) and $g_2 = -0.05$ (Fig. 3.7(c)), but with a delocalization phenomenon of the instability domain. To remind, g_2 is the nonlinear coupling parameter between Eqs. (3.35a) and (3.35b), which when set to zero reduces the system to ordinary fractional NLS equations. Its interplay with space-fractional terms (or fractional dispersion) is responsible for the emergence of regions of instability as further confirmed by the growth rate diagrams plotted in Fig. 3.8, where the upper line corresponds to $g_2 = -0.5$ and the lower line to $g_2 = -0.08$. Therefore, when parameters fall inside regions of instability, the plane wave solutions will be said to be unstable under modulation. Otherwise, the plane wave solutions will be expected to remain stable, keeping their initial characteristics.

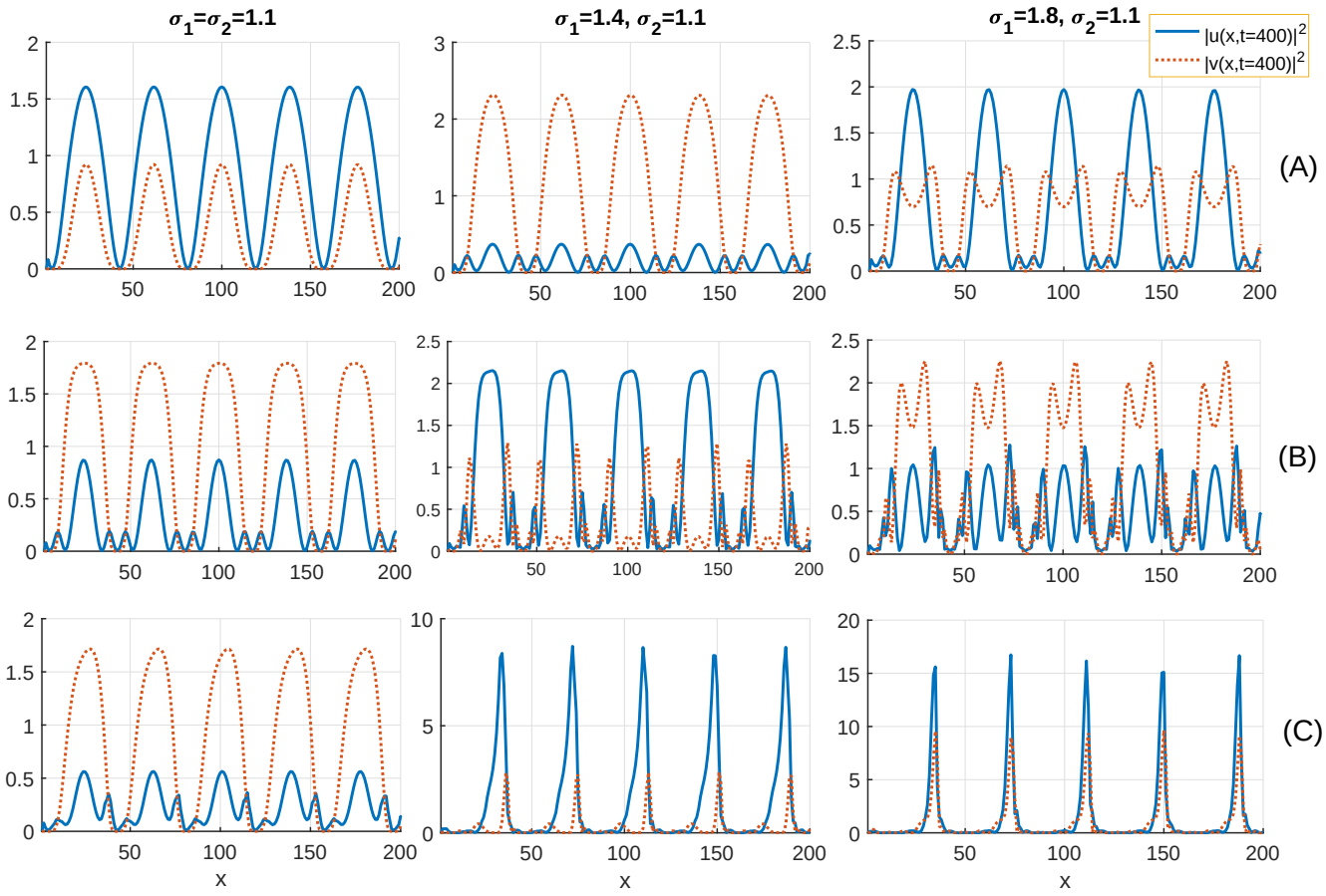

Figure 3.9: Plane wave modulation in the two-exciton chain for: Line (A) $g_1 = g_2 = -0.05$, Line (B) $g_1 = -0.08$ and $g_2 = -0.05$, and Line (C) $g_1 = -0.1$ and $g_2 = -0.05$. The first column on the left correspond to $\sigma_1 = \sigma_2 = 1.1$. The middle column corresponds to $\sigma_1 = 1.4$ and $\sigma_2 = 1.1$, and the right column corresponds to $\sigma_1 = 1.8$ and $\sigma_2 = 1.1$. We have fixed $\lambda = 0.3$ and $J_1 = J_2 = 0.08$.

Further details on the instability features of the plane wave solutions are given in Fig. 3.9, where the fractional CNLS Eqs.(3.35) have been solved numerically using the standard split-step Fourier method **[145]**. In order to verify both the dispersive and nonlinear coupling effects, we have assumed $v_0 = 0$ as initial condition of Eq. (3.35b), while the initial condition for Eq. (3.35a) is considered to be a perturbed plane wave solution with the perturbation wavenumber $\lambda = 0.3$. Lines (A) of Fig. 3.9 correspond to the case $g_1 = g_2 = -0.05$, where g_2 is the nonlinear coupling coefficient between the two vibrational equations. The same panels from left to right respectively correspond to $\{\sigma_1 = \sigma_2 = 1.1\}$, $\{\sigma_1 = 1.4; \quad \sigma_2 = 1.1\}$ and $\{\sigma_1 = 1.8; \quad \sigma_2 = 1.1\}$. Obviously, the obtained patterns are trains of solitonic structures whose features changes with increasing σ_1. This strongly support the fact that solitons are robust in such systems and may display different behaviors due to the interplay between nonlinear and dispersive effects. Lines (B) of Fig. 3.9 depict the case $g_2 = -0.08$ with g_1 keeping the same value as previously. σ_1 and σ_2 also keep the same values as previously. The coupling process remains effective here and the initial solitons tend to spread into radiations. However, the two excitonic parts contribute to maintain permanent energy transport under the activation of MI. The last case of Fig. 3.9, i.e., Lines (C), has been recorded for $g_2 = -0.1$. Each of the modes still displays trains of solitonic structures, except that for high values of the fractional-order parameter σ_1, the wave objects become narrow in space and highly localized. We should remind that only one of the modes has been excited and that is exactly the one that shows highly localized structures. Energy transport, to be efficient has been shown to be supported by such waves, especially during the process of replication and transcription, where the hydrogen bonds that link bases in DNA pairs are broken **[30,42,144,148–150]**. In proteins, it was shown that they may also emerge as exact solutions, depending on the used method and the corresponding biological implications **[41, 77, 89]**. However, the fractional-order parameters σ_1 and σ_2 bring about new features into wave localization in proteins, and can be used as control parameters by suitable biological processes for specific purpose.

3.2.4 Conclusion

In this part, we have studied the two-exciton energy transfer in $\alpha-$helix molecular chains, in the presence of LR dispersive interactions. We have shown that in the continuum limit, using Fourier formalism may reduce the initial discrete problem to a set of coupled

NLS equations with space-fractional derivatives. The theory of MI has thereafter been used to study the onset of solitonic structures, via the linear stability analysis, followed by direct numerical simulations for confirmation. The effect of changing the fractional-order parameters has been studied and, together with the change in the nonlinear coupling coefficient, it has been found to enhance the localization of energy, especially involving the two excitonic modes. This has been found to be in agreement with the predictions and supports once more the robustness of solitonic waves in molecular structures, especially when nonlinear and dispersive effects are involved, for specific biological purposes.

General Conclusion

Our study focused on "Energy transport and localization in complex protein structures with long-range intermolecular interactions". To achieve this, we have subdivided the presentation of our thesis into three chapters. The first chapter presents the generalities on protein chains with particular emphasis on their dynamics; first, speaking of protein chains, we first presented the amino acids and peptide bonds, followed by the structure of the proteins and finally the determination of the structure, following it; secondly, we talked about the types of proteins namely fibrous proteins and globular proteins; thirdly, the origin of the concept of the soliton has been investigated, here we have focused on the different classes of solitons and some applications of solitons; then we presented Davydov's original model; in the end we presented the literature review on models that took into account certain parameters; we will not forget to talk about the experience and applications of Davydov's model. The LRI between peptide units due to dipole-dipole interactions, inhomogeneities due to defects caused by the presence of additional molecules such as drugs, carcinogens, mutants, and dyes in specific sites of the alpha helical protein sequence make significant changes in the equations governing the dynamics of solitons in Helical Proteins. The second chapter was devoted to the investigation methodology. To achieve this, we have subdivided this chapter into three parts namely, the preliminaries in which we presented models with long-range energy modes in alpha-helix networks with inter spin coupling in a foreground and in in the background, we presented models with long-range interaction effects; subsequently the analytical method used has been presented namely the MI; in the end, the numerical method used, namely the Ronge-Kutta method. These methods might have different diagrams of the same differential equation, but they have the same purpose; that the dynamics of the system should closely correspond to the dynamics of the differential equation. The third chapter was devoted to the results of our work and the discussions. Here we have presented the effects of long range in a three-dimensional model and then the long-range dynamic effects in fractional The re-

sults have confirmed the fact that on the dynamics of solitons, a detailed study of the three-chain model has revealed that the amplitude and the width of the soliton depend on LRI's parameter. We have found that the growth rate of instability has a singular point for the long-range parameter r, where it is maximal. By using the power-law LRI, the non-locality originating from the LRI has resulted in the dynamic equations with space derivatives of fractional order. New theoretical frameworks to study exciton-phonon dynamics have been derived. The work may be interesting for all those professionals or not who want to refresh their knowledge and to obtain information or to find the appropriate keys for the understanding of biological and pathological phenomenons.

Open problems and future directions

Many interesting results have thus been obtained in the present thesis. However numerous points related to this topic remain unsolved, and then may be subject to future investigations.

• Usually we assume for LRI that each chain particle acts on all chain particles. There are systems where this assumption cannot be used. In general, the chain cannot be considered as a straight line (Davydov model). For example, the linear polymers can be represented as some compact objects. The tertiary structure of enzymes is often compact, globular shaped. In this case, we can consider that the chain particle is interacted with particles of a ball with radius R.

• We considered a three-dimensional long-range chain. For the future, the studied model will be two-dimensional at long range, and we will take into account the thermal fluctuations for the alpha-helix model in its physiological environment, then we will proceed to the numerical verification of the proposed results, where a comparison will be made. made between cases without dissipation of thermal fluctuations and that taking into account dissipation and thermal fluctuations.

• Stochastic resonance has continuously attracted considerable attention over the last two decades. The term is given to a phenomenon that is manifest in nonlinear systems whereby generally feeble input information (such as a weak signal) can be amplified and optimized by the assistance of noise. The stochastic resonance in inhomogeneous molecular chains with LRI will be studied.

• It is well known that ionizing radiation has an undeniable impact on the structure of biological molecules. The effect of ionizing radiation on the dynamics of solitons in

molecular systems such as DNA and proteins will also be studied in the near future.

Bibliography

Bibliography

[1] H. HARLEY, The origin of the world "protein", Nature, 168, 244 (1951)

[2] L. Stryer, Biochimie. 4 Auflg; Speklrum Academischer Varlag, Heidelberg (1995).

[3] S. Berrada, PLP Biotechnologie, Academie de Monpellier

[4] A. C. Scott, Phys. Rev. A **26**, 578 (1982).

[5] A. C. Scott, Phys. Rep. **217**, 1 (1992).

[6] A. S. Davydov and N. I. Kislukha, Phys. Stat. Sol. B **39**, 65 (1973).

[7] A. S. Davydov and N. I. Kislukha, Phys. Stat. Sol. B **75**, 735 (1976).

[8] A. S. Davydov, J. Theor. Biol. **38**, 559 (1973).

[9] P. L. Christiansen and A. C. Scott, *Self-trapping of vibrational energy*, (New York: Plenum Press 1990).

[10] L. Cruzeiro, J. Halding, P. L. Christiansen, O. Skovgard and A. C. Scott, Phys. Rev. A **37**, 703 (1987).

[11] L. Cruzeiro-Hansson, Phys. Rev. A **45**, 4111 (1992).

[12] L. Cruzeiro-Hansson, V. M. Kenker and A. C. Scott, Phys. Lett. A **190**, 59 (1994).

[13] W. Förner, Phys. Rev. A **44**, 2694 (1991).

[14] W. Förner, Physica D **68**, 68 (1993).

[15] W. Förner, J. Comput. Chem. **13**, 275 (1992).

[16] W. Förner, J. Phys. Condens. Matter **3**, 1915 (1991).

[17] A. C. Scott, Phys. Scr. **25**, 651 (1982).

[18] A. C. Scott, Phys. Scr. **29**, 279 (1984).

[19] A. C. Scott, Physica D **51**, 333 (1990).

[20] D. W. Brown, K. Lindenberg and B. J. West, Phys. Rev. B **35**, 6169 (1987).

[21] D. W. Brown and Z. Ivic, Phys. Rev. B **40**, 9876 (1989).

[22] D. W. Brown, K. Lindenberg and X. Wang, in *Davydov's Soliton Revisited*, edited by P. L. Christiansen and A. C. Scott (Plenum, New York, 1990).

[23] A. C. Scott, Phys. Lett. A **86**, 60 (1981).

[24] L. Cruzeiro-Hansson, J. C. Eilbeck, J. L. Marin and F. M. Russell, Phys. Lett. A **266**, 160 (2000).

[25] M. Daniel and M. M. Latha, Phys. Lett. A **252**, 92 (1999).

[26] G. R. Y. Mefire, C. B. Tabi, A. Mohamadou, H. P. F. Ekobena and T. C. Kofané, Chaos **23**, 033128 (2013).

[27] C. B. Tabi, I. Maïna, A. Mohamadou, H. P. F. Ekobena and T. C. Kofané, Europhys. Lett. **106**, 18005 (2014).

[28] C. S. Panguetna, C. B. Tabi and A. Mohamadou, Commun. Nonl. Sci. Numer. Simul. **55**, 326 (2018).

[29] C. S. Panguetna, C. B. Tabi and A. Mohamadou, Phys. Plasmas **24**, 092114 (2017).

[30] A. D. Koko, C. B. Tabi, H. P. F. Ekobena, A. Mohamadou and T. C. Kofané, Chaos **22**, 043110 (2012).

[31] H. P. F. Ekobena, C. B. Tabi, A. Mohamadou and T. C. Kofané, J. Phys.: Condens. Matter **23**, 375104 (2011).

[32] J. C. F. Mimshe, C.B Tabi, H. Edongue, H. P. Ekobena, A. Mohamadou and T. C. Kofané, Phys. Scr. **87**, 025801 (2013).

[33] C. B. Tabi, J. C. F. Mimshe, H. P. F. Ekobena, A. Mohamadou and T. C. Kofané, Eur. Phys. J. B **86**, 374 (2013).

[34] C. B. Tabi, R.Y. Ondoua, H. P. Ekobena, A. Mohamadou and T. C. Kofané, Phys. Lett. A **380**, 2374 (2016).

[35] D. Hennig, Phys. Rev. B **65**, 174302 (2002).

[36] D. N. Beratan, J. N. Onuchic and J. J. Hopfield, J. Chem. Phys. **86**, 4488 (1987).

[37] J. N. Onuchic and D. N. Beratan, J. Chem. Phys. **92**, 722 (1990).

[38] J. N. Onuchic, P. C. P. Andrade and D. N. Beratan, J. Chem. Phys. **95**, 1131 (1991).

[39] C. Turró, C.K. Chang, G.E. Leroi, R.I. Cukier and D.G. Nocera, J. Am. Chem. Soc. **114**, 4013 (1992).

[40] C. B. Tabi, A. Mohamadou and T. C. Kofané, Eur. Phys. J. E **32**, 327, (2010).

[41] A. Mvogo, G. H. Ben-Bolie and T. C. Kofané, Phys. Lett. A **378**, 2509 (2014).

[42] B. Sadjo, C. B. Tabi, H. Edongue and A. Mohamadou, Wave Motion **72**, 342 (2017).

[43] A. S. Etémé, C. B. Tabi and A. Mohamadou, Commun. Nonl. Sci. Num. Simul. **43**, 211 (2017).

[44] A. S. Etémé, C. B. Tabi and A. Mohamadou, Chaos Solit. Fract. **104**, 813 (2017).

[45] C. B. Tabi, I. Maïna, A. Mohamadou, H.P. F. Ekobena and T. C. Kofané, Physica A **435**, 1 (2015).

[46] A. S. Davydov, Soliton in molecular systems (Kluwer Academic Publishers Group, 1985, Dordrecht).

[47] S. Zdravkovic and M. V. Sataric, Physica Scripta 64, 612 (2001).

[48] J.S. Russell, *Report of the fourteenth meeting of the British Association for the Advancement of Science*, Plates XLVII-LVII, p. 311 (1845).

[49] D.J. Korteweg and H. de Vries, Phil. Mag. 39, 422 (1895).

[50] T. Dauxois and M. Peyrard, *Physics of Solitons*, Cambridge University Press, Cambridge, (2006).

[51] N.J. Zabusky and M.D. Kruskal, Phys. Rev. Lett. 15, 240(1965).

[52] C.S. Gardner et al., Phys. Rev. Lett. 19, 1095 (1967).

[53] V. E. Zakharov and A.B. Shabat, Funct. Anal. Appl. 8, 226 (1974).

[54] R.H. Enns, *It is a Nonlinear World*, Springer, New York, (2011).

[55] *Dissipative Solitons*, edited by N. Akhmediev and A. Ankiewicz (Springer, New York, 2005).

[56] M. Brambilla, L.A. Lugiato, F. Prati, L. Spinelli, and W.J. Firth, Phys. Rev. Lett. 79, 2042 (1997)

[57] J.C. Misra and M.K. Patra, Comput. Math. Appl. 54, 242 (2007).

[58] T. Heimburg and A.D. Jackson, Proc. Natl. Acad. Sci. U.S.A. **102** (2), 9790 (2005).

[59] T. Heimburg and A.D. Jackson, Biophys. Rev. Lett. 2, 57 (2007).

[60] A.L. Hodgkin and A.F. Huxley, J. Physiol. (London) 117, 500 (1952).

[61] A.S. Davydov and N.I. Kislukha, Phys. Status Solidi b **39**, 465 (1973).

[62] A.S. Davydov and N.I. Kislukha, Phys. Status Solidi b **75**, 735 (1976).

[63] A.S. Davydov, *Solitons in molecular systems*, 2nd Ed. Kluwer Academic Publishers Group, Dordrecht, (1991).

[64] V.E. Zakharov and A.B. Shabat, Zh. Eksp. Theor. Fiz. **61**, 118 (1971).

[65] A.S. Davydov, Studia Biophysicu **47**, 221 (1974).

[66] A.S. Davydov, Ukr. fiz. Zh. **20**, 179. (1975).

[67] J.M. Hyman, D.W. Mc Laughlin and A.C. Scott, Physica D **3**, 23 (1981)

[68] A.C. Scott, Phys. Scr. **25**, 651 (1982).

[69] A.C. Scott, Phys. Rev. A **26**, 578 (1982).

[70] G. Careri, U. Buontempo, F. Carta, E. Grattom and A.C. Scott, Phys. Rev. Lett. **51**, 304 (1983).

[71] A.C. Scott, Nonlinear Electrodynamics in Biological Systems ed W.R. Adey and A.F. Lawrence, New York: Plenum p 133 (1984).

[72] L. MacNeil and A.C. Scott Phys. Scr. **29**, 284 (1984).

[73] A.C. Scott, Phys. Scr. **29** 279 (1984).

[74] S. Takeno, Progr. Theor. Pkys. **71**, 395 (1984).

[75] S. Takeno, Progr. Theor. Pkys. **73**, 853 (1985).

[76] E. Simo and T.C. Kofane, Phys. Rev. E **54**, 2071 (1996).

[77] I. Sali, C. B. Tabi, H. P. F. Ekobena and T. C. Kofané, EPJ Plus **133**, 233 (2018).

[78] Lombdalh, P.S. and W.C. Kerr, Phys. Rev. Lett. **55**, 1235 (1985).

[79] L. Cruzeiro-Hansson, Phys. Rev. Lett. **73**, 2927 (1994).

[80] X.F. Pang, Phys. Rev. E. **62**, 6889 (2000).

[81] Robert Renthal and J. Taboada, Phys. Lett A. **139**, (1989).

[82] Scott P. Layne, Solitons in Biology, Los Alamos Science, (1984).

[83] E. Simo, Phys. Scr. **80**, 045801 (2009).

[84] D.R. Todorovic, Journal of Research in Physics **1**, 1 (2009).

[85] D.R. Todorovic et al., Int. J. Mod. Phys. B **31**, 5835 (2009).

[86] P. Wang, B. Tian, Y. Jiang and Y-F. Wang, Physica B **411**, 166 (2013).

[87] A. Mvogo, G.H. Ben-Bolie and T.C. Kofane, Eur. Phys. J. B **86**, 217 (2013).

[88] A. Mvogo, G.H. Ben-Bolie and T.C. Kofane, Eur. Phys. J. B **86**, 413 (2013).

[89] S. E. Madiba, C. B. Tabi, H. P. F. Ekobena and T. C. Kofané, Physica A **514**, 298, (2019).

[90] E.N.N. Aboringong and A.M. Dikandé, Eur. Phys. J. E **41**, 35, (2018).

[91] M. Daniel and M. M. Latha, Physica A **240**, 526, (1997).

[92] M. Daniel and M. M. Latha, Phy. Lett. A **252**, 92, (1999).

[93] M. Daniel, M.M. Latha, Phys. Lett. A **302**, 94 (2002).

[94] M. Daniel and M.M. Latha, Physica A **298**, 351 (2001).

[95] K. Kundu, Phys. Rev. E **61**, 5839 (2000).

[96] M.M. Latha and G. Merlin, Phys. Lett. A **376**, 938 (2012).

[97] E. Simo and T.C. Kofane, Phys. Rev. E **56**, 4751 (1997).

[98] D.C. Rau and V.A. Parsegian, Biophysics. J. **61**, 246 (1992).

[99] J. Chen and N.S. Chaudhari, Soft Comput. J. **10**, 315 (2005).

[100] K. Nagano, J. Mol. Biol. 84, 337 (1974).

[101] S.K. Sarker and J.A. Krumhansl, Phys. Rev. B **23**, 2374 (1981).

[102] Y. Ishimori, Prog. Theor. Phys. **68**, 402 (1982).

[103] M. Saha and T.C. Kofane, Chaos **22**, 013116 (2012).

[104] D. Grecu and A. Visinescu, Bulgarian J. of Phys. **27**, 1 (2000).

[105] D. Grecu and A. Visinescu and A.S. Carstea, J. Nonl. Math. Phys. **8**, 139 (2001).

[106] G.A. Baker, Phys. Rev. **122**, 1477 (1961).

[107] M. Kac and E. Helfand, J. Maths. Phys. **4**, 1078 (1963).

[108] R.B. Griffiths, *Phase Transitions and Critical Phenomena*, Vol. 1, London, (1972).

[109] A. Mvogo, G.H. Ben-Bolie, and T.C. Kofane, Phys. Lett. A **378**, 2509 (2014).

[110] I. Kourakis and P.K. Shukla, Phys. Plasmas **11**, 1384 (2004).

[111] G.P. Agrawal, *Nonlinear Fiber Optics, Optics and Photonics* (4th ed.), Academic Press, New York, (2009).

[112] F. II Ndzana, A. Mohamadou, and T.C. Kofane, Phys. Rev. E **79**, 056611 (2009).

[113] C.B. Tabi, A. Mohamadou and T.C. Kofane, Chaos **19**, 043101 (2009).

[114] H.P. Ekobena Fouda, C.B. Tabi, A. Mohamadou and T.C. Kofane, J. Phys.: Condens. Matter **23**, 375104 (2011).

[115] R.Y. Ondoua, C.B. Tabi, H.P. Ekobena Fouda, A. Mohamadou and T.C. Kofané, Eur. Phys. J. B **85**, 318 (2012).

[116] J.C. Mimshe Fewu, C.B. Tabi, H. Edongue, H.P. Ekobena Fouda and T.C. Kofane, Phys. Scr. **87**, 025801 (2013).

[117] A. Mvogo, G.H. Ben-Bolie and T.C. Kofané, Chin. Phys. B **23**, 098701 (2014).

[118] E. Yomba, Phys. Lett. A **336**, 463 (2005).

[119] E. Yomba, Chin. J. Phys. **43**, 789 (2005).

[120] E. Yomba, Chaos Solitons Fractals **26**, 785 (2005).

[121] B. Fornberg and G.B. Whitham, Phil. Trans. Roy. Soc. Lond. A **289**, 373 (1978).

[122] T.R. Taha and M.J. Ablowitz, J. Comput. Phys. **55** (2), 203-230 (1984).

[123] Z. Ivic, D. Kapor, M. Skrinjar and Z. Popovic, Phys. Rev. B **48**, 3721 (1993).

[124] C. B. Tabi, H. P. F. Ekobena and T. C. Kofané, J. Comput. Theor. Nanosci. **8**, 2220 (2011).

[125] Z. Ivic, D. Kostic, Z. Przulj and D. Kapor, J. Phys.: Condens. Matter **9**, 413 (1997).

[126] J. Tekic, Z. Ivic, S. Zekovic and Z. Przulj, Phys. Rev. E **60**,821 (1999).

[127] C. Falvo and V. Pouthier, J. Chem. Phys. **123**, 184709 (2005).

[128] C. Falvo and V. Pouthier, J. Chem. Phys. **123**, 184710 (2005).

[129] A. K. Dang, C. B. Tabi, H. P. F. Ekobena and T. C. Kofané, Int. J. Quant. Chem. **115**, 34 (2015).

[130] J. Berashevich, V. Apalkov and T. Chakraborty, J. Phys.: Condens. Matter **20**, 075104 (2008).

[131] C. B. Tabi, A. Mohamadou, and T. C. Kofané, J. Phys.: Condens. Matter **21**, 335101 (2009).

[132] C. B. Tabi, A. D. Koko, R. O. Doko, H. P. F Ekobena and TC Kofané, Physica A **442**, 498 (2016).

[133] D. Hennig, Phys. Rev. E **64**, 041908 (2001).

[134] M. Daniel and K. Deepamala, Phys. A **221**, 241 (1995).

[135] R.Y. Ondoua, C. B. Tabi, H. P. Ekobena, A. Mohamadou and T. C. Kofané, Eur. Phys. J. B **86**, 374 (2012).

[136] C. B. Tabi, R.Y. Ondoua, H. P. Ekobena, A. Mohamadou and T. C. Kofané, Phys. Lett. A **380**, 2374 (2016).

[137] V. Pouthier and C. Falvo, Phys. Rev. E **69**, 041906 (2004).

[138] M.M. Latha and G. Merlin, Phys. Lett. A **376**, 938 (2012).

[139] G. Merlin and M.M. Latha, Physica D **265**, 71 (2013).

[140] C. B. Tabi, Chaos Solit. Fract. **116**, 386 (2018).

[141] V. E. Tarasov and G. M. Zaslavsky, Commun. Nonl. Sci. Numer. Simul. **11**, 885 (2006).

[142] V. E. Tarasov and G. M. Zaslavsky, Chaos **16**, 023110 (2006).

[143] L. Zhang, Z. He, C. Contia, Z. Wang, Y. Hu, D. Lei, Y. Li and D. Fan, Commun. Nonl. Sci. Numer. Simul. **48**, 531 (2017).

[144] C. B. Tabi, A. Mohamadou and T. C. Kofané, J. Bionanosci. **2**, 89 (2008).

[145] G. P. Agrawal, *Nonlinear fiber optics*, San Diego: Academic Press; (2001).

[146] V. V. Uchaikin, *Fractional derivatives for physicists and engineers*, Berlin: Springer (2013).

[147] S. G. Samko, A. A. Kilbas and O. I. Marichev, *Fractional integrals and derivatives theory and applications*, New York: Gordon and Breach (1993).

[148] C. B. Tabi, A. Mohamadou and T. C. Kofané, Chaos **19**, 043101 (2009).

[149] C. B. Tabi, G. Bineli and A. Mohamadou, J. Biol. Phys. **41**, 391 (2015).

[150] C. B. Tabi, H. P. E. Fouda, A. Mohamadou and T. C. Kofané, Physica Scripta **83**, 035802 (2011).

List of Publications

1- **S. E. Madiba**, C.B. Tabi, H. P. F. Ekobena and T.C. Kofané, *Long-range energy modes in α-helix lattices with inter-spine coupling*, **Physica A 514 (2019) 298**.

2- C.B. Tabi, **S. E. Madiba**, H. P. F. Ekobena and T.C. Kofané, *Coupled fractional patterns of energy in α-helix proteins*, **submitted**.

Physica A 514 (2019) 298–310

Contents lists available at ScienceDirect

Physica A

journal homepage: www.elsevier.com/locate/physa

Long-range energy modes in α-helix lattices with inter-spine coupling

S.E. Madiba [a], C.B. Tabi [a,b,*], H.P.F. Ekobena [a], T.C. Kofané [c]

[a] Laboratoire de Biophysique, Département de Physique, Faculté des Sciences, Université de Yaoundé I, B.P. 812 Yaoundé, Cameroun
[b] Botswana International University of Science and Technology, Private Mail Bag 16 Palapye, Botswana
[c] Laboratoire de Mécanique, Département de Physique, Faculté des Sciences, Université de Yaoundé I, B.P. 812 Yaoundé, Cameroun

HIGHLIGHTS

- Long-range dispersive interactions are considered in a tridimensional model of α-helix proteins.
- Model equations are derived in the form of discrete and coupled nonlinear Schrödinger equations.
- Modulational instability analysis gives rise to trains of solitonic structures.
- Trains of solitons and their characteristics are sensitive to nonlinear and LR coupling effects.

ARTICLE INFO

Article history:
Received 18 February 2018
Received in revised form 8 July 2018
Available online xxxx

Keywords:
α-helix
Long-range interaction
Solitons
Energy

ABSTRACT

A system for three-strand α-helix proteins, with long-range dispersive interactions among polypeptide units, is considered. The associate improved Davydov model is shown to be fully described by a set of modified coupled discrete nonlinear Schrödinger equations, which involve long-range interactions between peptide groups along the protein strands. By means of the modulational instability theory, the competition between nonlinearity and long-range intermolecular interactions are shown to modify the domain of instability of plane waves. The impact of the competition between nonlinearity and long-range interactions, on the process of energy transport and storage, is also addressed numerically. It is shown that nonlinearity and the long-range couplings conspire to the emergence of trains of solitonic structures, when parameters are well chosen within the domain of instability of plane waves. The relevance of the improved model as well as the biological implications of the account of long-range intermolecular interactions, are discussed in the contexts of energy transport and storage in hydrogen-bonded molecular structures in general, and in α-helix proteins in particular.

1. Introduction

Many biological processes such as muscle contraction, active transport and enzyme catalysis rely on energy. This energy, which is released through the hydrolysis of adenosine triphosphate (ATP), is mainly transported and stored by proteins. Understanding the subsequent phenomena, those related to the management of energy by proteins, have been an active research topic since the pioneering work by Davydov [1]. Based on a simple formulation of the problem Davydov showed that energy is carried by solitonic structures, therefore establishing the relationship between such entities and lattice distortions.

* Corresponding author at: Botswana International University of Science and Technology, Private Mail Bag 16 Palapye, Botswana.
E-mail addresses: madibaes@yahoo.com (S.E. Madiba), conrad@aims.ac.za, tabic@biust.ac.bw (C.B. Tabi), hekobena@gmail.com (H.P.F. Ekobena), tckofane@yahoo.com (T.C. Kofané).

https://doi.org/10.1016/j.physa.2018.09.019
0378-4371/

Namely, considering the structure of α-helix proteins Davydov and Kislukha [2,3] used the exciton formalism to explain the self-trapping of the amide-I oscillations, as the consequence of the interaction between the vibrational exciton and the distortion in the protein structure resulting from the presence of the exciton. They established that as a result of the interplay between nonlinearity and dispersion, the self-trapped vibrational amide-I energy coupled to the protein structure deformation may travel as a soliton in the protein strand [4,5].

Earlier models on the issue of energy transport and storage in protein chains were focused on a structure with only one strand of hydrogen-bonded peptide units, both in the discrete and continuum regimes [1–3]. These models have been the subject of great controversy, owing to their formulation involving inconsistencies in predictions on the Davydov soliton lifetime, and more importantly its stability at the biological temperature of 300 K [6–13]. Nevertheless, numerical simulations have revealed that such solitons may be stable at 300 K, but these studies were carried out from a purely classical point of view with no consistent argument to prove their stability [4,5,14–19]. In order to solve this issue, adopting a description of the α-helix protein in terms of a biological system stabilized by three quasi-linear strands, turned out to be a suitable picture. Most of the pioneering analytical and numerical contributions in that direction can be found in Refs. [5,20,21]. In the same direction slightly modified Davydov models of α-helix proteins were addressed by Daniel and Latha [22], in which both discrete and continuum regimes were studied with a particular interest in the influence of the inter-spine coupling and its consequences on the process of energy transport and storage among the spines. Based on the fact that the process of modulational instability (MI) is a direct mechanism leading to solitons and the formation of nonlinear structures [23–27], Tabi and co-workers [28–30] showed that the process may also be envisaged in the context of three-stranded molecular structures. More recently, a generalized model of α-helix protein chains including the competition between diagonal and off-diagonal couplings was proposed [31]. The subsequent modes of energy were found to be very sensitive to the nonlinear effects introduced by the two types of couplings. In Ref. [28], using the model by Hennig [32], Tabi et al. showed that during the process of energy transport covalent bonds may be compressed, while hydrogen bonds display regular oscillating behaviors leading to favorable condition for energy transport and storage in the coupled spines via polaronic structures. Relying on data from X-ray analysis on proteins [33–35] it was also shown that the tridimensional structure is favorable to energy and particle transfer in proteins, because of the significant presence of hydrogen (H) bridges between the spines [36]. In other words the polarons that arise in protein dynamics may correspond to the energy related to the electron transport, depending on the coupling strength to vibrational motions [28,32,37]. Moreover, in recent investigations it was suggested that long-range (LR) dispersive interactions may be responsible for interesting dynamical behaviors, especially in molecular systems like DNA and proteins [38–40], neural [41,42] and cell [43] networks.

Our main objective in this paper is to show that LR dispersive interactions may enhance the efficiency of energy transport and storage in three-stranded molecules with inter-spine coupling. In this goal we shall use the theory of MI both analytically and numerically, with emphasis on the importance of the competing effects between the LR interactions among polypeptides units in individual protein helices and nonlinearity. The paper is outlined as follows: in Section 2 we introduce the model Hamiltonian, and derive the dynamical equations which are modified coupled discrete nonlinear Schrödinger (DNLS) equations. In Section 3 the theory of MI is applied to the model starting with the linear stability analysis for plane wave solutions, followed by full numerical simulations to confirm predictions of the linear stability analysis and the emergence of nonlinear wave patterns with soliton features. The last section is devoted to concluding remarks.

2. Hamiltonian model and dynamical equations

The generalized Hamiltonian for linked polypeptide chains arranged in three-dimensional helix has been proposed using Davydov's formulation [1,2]. It considers the coupling between amide-I vibration and displacements of amino-acid residues. Its tridimensional version, as proposed in Refs. [28,31,32], is given by:

$$H = H_{exc} + H_{vib} + H_{int}, \tag{1}$$

where H_{exc} is the energy associated with intramolecular excitations, H_{vib} is the contribution from the displacements of peptide groups also known as lattice vibrations; H_{int} is the interaction energy between the amide-I excitations and the displacements of peptide groups. The energy H_{exc} is defined as:

$$H_{exc} = \sum_{n,\alpha}\left[E_0\beta^{\dagger}_{n,\alpha}\beta_{n,\alpha} - \sum_{m\neq n}J_{n-m}\beta^{\dagger}_{n,\alpha}\beta_{m,\alpha} + L\left(\beta_{n,\alpha+1} + \beta_{n,\alpha-1}\right)\beta^{\dagger}_{n,\alpha}\right], \tag{2}$$

with the subscript n referring to the lattice index along a strand (or chain) α, where $\alpha = 1, 2, 3$. The expression of H_{exc} suggests that an individual amino acid will be identified by the index pair (n, α), such that $\beta_{n,\alpha}$ ($\beta^{\dagger}_{n,\alpha}$) are boson creation (annihilation) operators associated with intramolecular vibrations of the nth peptide group in the strand α. These operators satisfy the usual commutation relations for bosons i.e. $[\beta_{n,\alpha}, \beta^{\dagger}_{m,\alpha}] = \delta_{m,n}$ and $[\beta_{n,\alpha}, \beta_{m,\alpha}] = 0$. E_0 is the local amide-I vibrational energy, in this context the term $E_0\beta^{\dagger}_{n,\alpha}\beta_{n,\alpha}$ is the vibrational energy at the site (n, α). The term $\sum_{m\neq n}J_{n-m}\beta^{\dagger}_{n,\alpha}\beta_{m,\alpha}$ is the energy related to the LR interactions between molecular excitations on sites n and m, belonging to the same chain. The coupling parameter J_{n-m} is the LR transfer integral between sites n and m, here considered of the form:

$$J_{n-m} = J_0|n-m|^{-r}, \tag{3}$$

with J_0 the strength of the transfer integral and r a parameter range whose values are in the interval $[1, +\infty[$. However r covers different physical contexts, depending on its value. For example if $r \to \infty$ the LR interaction reduces to nearest-neighbor couplings, a case corresponding to the models studied in Refs. [28,32]. For $r = 5$ the LR interaction is of a dipole–dipole type, while for $r = 3$ the LR interaction is of the Coulomb type. We should stress that the strongest interaction effects are due to smaller values of r. Therefore, the case $r = 1$ is a particular one that implies strong LR forces among the peptide groups that constitute the protein lattice. This may have some direct biological consequences on the structural dynamics of the molecule and on the localization of energy. Some other contributions have recently considered the finite range interaction using the Kac–Baker potential to model intermolecular interactions, an proposed strong LR coupling to be responsible for stabilizing the protein chain structure [44].

The parameter L in formula (2) is the linear coupling energy between covalently bonded peptide groups between different strands. H_{vib} describes the vibronic dynamics of the molecular system, and includes both the radial and longitudinal displacements of the peptide units from their equilibrium positions. Note that radial and longitudinal displacements are related to the changes in radius $R \to R + v_{n,\sigma}$ and the pitch $b \to b + u_{n,\sigma}$, and feature the distortions of the covalent and hydrogen bonds respectively. This contribution to the total Hamiltonian is written as:

$$H_{vib} = \frac{1}{2}\sum_{n,\alpha}\left\{\frac{\left(P^{u}_{n,\alpha}\right)^2}{M} + \frac{\left(P^{v}_{n,\alpha}\right)^2}{M} + \kappa\left(u_{n,\alpha} - u_{n-1,\alpha}\right)^2 + \frac{1}{4}\varpi\left(v_{n,\alpha} - v_{n,\alpha-1}\right)^2\right\}. \tag{4}$$

M is the mass of a peptide group, κ and ω are the elasticity coefficients of the hydrogen and covalent bonds, respectively. $u_{n,\alpha}$ is the longitudinal displacement of the molecule parallel to the helical axis, and $v_{n,\alpha}$ the displacements along the helix radius. The quantities $P^{u}_{n,\alpha}$ and $P^{v}_{n,\alpha}$ are the momentum conjugate to $u_{n,\alpha}$ and $v_{n,\alpha}$ respectively. The vibrational and excitonic parts interact through the Hamiltonian

$$H_{int} = \sum_{n,\alpha}\left[\chi(u_{n+1,\alpha} - u_{n,\alpha}) + \frac{1}{2}\eta(v_{n,\alpha+1} - 2v_{n,\alpha} + v_{n,\alpha-1})\right]\beta^{+}_{n,\alpha}\beta_{n,\alpha}. \tag{5}$$

In Eq. (5), the terms associated with the parameters χ and η represent the diagonal coupling between the excitonic amplitude and the displacement of the peptide groups in the longitudinal and radial directions, respectively. Otherwise, the adjacent bonds oscillations are affected by the dynamics of the exciton as discussed in Refs. [28,31,32].

The following quantum state vector can be used to understand the collective excitation of the system

$$|\psi(t)\rangle = \sum_{n,\alpha} A_{n,\alpha}(t)\beta^{\dagger}_{n,\alpha}\left\{\exp\left[-\frac{i}{\hbar}\sum_{n,\alpha}\left[b_{n,\alpha}(t)P^{u}_{n,\alpha} - \phi_{n,\alpha}(t)u_{n,\alpha}\right] + \left[c_{n,\alpha}(t)P^{v}_{n,\alpha} - \pi_{n,\alpha}(t)v_{n,\alpha}\right]\right]\right\}|0\rangle, \tag{6}$$

where $\hbar$ is the Planck's constant and $|0\rangle$ is the ground-state vector. $A_{n,\alpha}(A^{*}_{n,\alpha})$ is the coherent state representation of the operators $\beta_{n,\alpha}$ $(\beta^{\dagger}_{n,\alpha})$. We have introduced $b_{n,\alpha}$ and $c_{n,\alpha}$ as the coherent state representations of $u_{n,\alpha}$ and $v_{n,\alpha}$ respectively, and $\phi_{n,\alpha}$ and $\pi_{n,\alpha}$ for their conjugate momenta $P^{u}_{n,\alpha}$ and $P^{v}_{n,\alpha}$. Moreover, the coherent state representations of the operators for $\beta_{n,\alpha}$, $\beta^{\dagger}_{n,\alpha}$, $u_{n,\alpha}$, $v_{n,\alpha}$, $P^{u}_{n,\alpha}$ and $P^{v}_{n,\alpha}$ are written as

$$\begin{aligned}
A_{n,\alpha}(t) &= \langle\psi(t)|\beta_{n,\alpha}|\psi(t)\rangle, \quad A^{*}_{n,\alpha}(t) = \langle\psi(t)|\beta^{\dagger}_{n,\alpha}|\psi(t)\rangle,\\
b_{n,\alpha}(t) &= \langle\psi(t)|u_{n,\alpha}|\psi(t)\rangle, \quad c_{n,\alpha}(t) = \langle\psi(t)|v_{n,\alpha}|\psi(t)\rangle,\\
\phi_{n,\alpha}(t) &= \langle\psi(t)|P^{u}_{n,\alpha}|\psi(t)\rangle, \quad \pi_{n,\alpha}(t) = \langle\psi(t)|P^{v}_{n,\alpha}|\psi(t)\rangle.
\end{aligned} \tag{7}$$

Ansatz Eq. (7) satisfies the normalization condition $\langle\psi(t)|\psi(t)\rangle = \sum_{n,\alpha}|A_{n,\alpha}|^2 = N$, where $|A_{n,\alpha}|^2$ characterizes the probability amplitude for finding a quantum of Amide-I energy in a particular amino acid. The Hamiltonian that gives the coherent states is written in the form

$$\langle H\rangle = \langle\psi(t)|H|\psi(t)\rangle, \tag{8}$$

which is written in the more expanded form

$$\begin{aligned}
\langle H\rangle &= \sum_{n,\alpha}\left\{A^{*}_{n,\alpha}\left[(E_0 + W)A_{n,\alpha} - \sum_{m\neq n}J_{n-m}A_{m,\alpha} - L(A_{n,\alpha+1} + A_{n,\alpha-1})\right]\right.\\
&\left. + \chi(b_{n+1,\alpha} - b_{n-1,\alpha})A^{*}_{n,\alpha}A_{n,\alpha} + \frac{1}{2}(c_{n,\alpha+1} - 2c_{n,\alpha} + c_{n,\alpha-1})A^{*}_{n,\alpha}A_{n,\alpha}\right\},
\end{aligned} \tag{9}$$

with

$$W = \frac{1}{2}\sum_{n,\alpha}\left\{\frac{\left(\phi_{n,\alpha}\right)^2}{M} + \frac{\left(\pi_{n,\alpha}\right)^2}{M} + \kappa\left(b_{n,\alpha} - b_{n-1,\alpha}\right)^2 + \frac{1}{4}\varpi\left(c_{n,\alpha} - c_{n,\alpha-1}\right)^2\right\}. \tag{10}$$

The dynamics of the system is easily understood by constructing the Heisenberg's equation of motion, i.e.,

$$i\hbar\frac{\partial}{\partial t}\langle X_{n,\alpha}\rangle = \langle [X_{n,\alpha}, H]\rangle, \tag{11}$$

where X stands for the dynamic variables $A_{n,\alpha}$, $b_{n,\alpha}$, $c_{n,\alpha}$, $\phi_{n,\alpha}$ and $\pi_{n,\alpha}$ satisfying the commutation relations $[X, X^*] = 1$ and $[\beta_{n,\alpha,P_{n,\alpha}}] = [b_{n,\alpha}, \phi_{n,\alpha}] = [\gamma_{n,\alpha}, P_{n,\alpha}] = [c_{n,\alpha}, \pi_{n,\alpha}] = i\hbar$. This leads to the following set of coupled equations:

$$\begin{aligned} i\hbar\frac{d}{dt}A_{n,\alpha}(t) &= \chi(b_{n+1,\alpha} - b_{n-1,\alpha})A_{n,\alpha} + \frac{\eta}{2}(c_{n,\alpha+1} + 2c_{n,\alpha} + c_{n,\alpha-1})A_{n,\alpha} \\ &- L(A_{n,\alpha+1} + A_{n,\alpha-1}) - \sum_{m\neq n} J_{n-m}A_{m,\alpha} \end{aligned} \tag{12}$$

$$\frac{d^2}{dt^2}b_{n,\alpha}(t) = -\kappa(b_{n+1,\alpha} - 2b_{n,\alpha} + b_{n-1,\alpha}) + \chi(|A_{n+1,\alpha}|^2 - |A_{n-1,\alpha}|^2) \tag{13}$$

$$\frac{d^2}{dt^2}c_{n,\alpha}(t) = -\frac{\varpi}{4}\left(c_{n,\alpha+1} + c_{n,\alpha-1} - 2c_{n,\alpha}\right) - \frac{\eta}{2}\left(\left|A_{n,\alpha+1}\right|^2 + \left|A_{n,\alpha-1}\right|^2 + 2\left|A_{n,\alpha}\right|^2\right). \tag{14}$$

Another fact that is not negligible in the present model is that the velocity of the intermolecular transport of excitonic energy is much lower than the velocity of sound of the acoustic bond oscillations. This causes the terms of inertia to be negligible, leading to the following adiabatic approximations:

$$\begin{aligned} b_{n,\alpha} - b_{n-1,\alpha} &= -\frac{\alpha}{\kappa}\left(A^*_{n,\alpha}A_{n-1,\alpha} + A^*_{n-1,\alpha}A_{n,\alpha}\right) + \frac{\chi}{\kappa}\left(\left|A_{n-1,\alpha}\right|^2 + \left|A_{n,\alpha}\right|^2\right) \\ b_{n+1,\alpha} - b_{n,\alpha} &= -\frac{\alpha}{\kappa}\left(A^*_{n,\alpha}A_{n+1,\alpha} + A^*_{n+1,\alpha}A_{n,\alpha}\right) + \frac{\chi}{\kappa}\left(\left|A_{n+1,\alpha}\right|^2 + \left|A_{n,\alpha}\right|^2\right) \\ c_{n,\alpha+1} + c_{n,\alpha-1} - 2c_{n,\alpha} &= \frac{2\eta}{\varpi}\left(\left|A_{n,\alpha+1}\right|^2 + \left|A_{n,\alpha-1}\right|^2 + 2\left|A_{n,\alpha}\right|^2\right), \quad \alpha = 1, 2, 3, \end{aligned} \tag{15}$$

upon which the following set of coupled equation is obtained

$$\begin{aligned} i\frac{\partial A_{n,\alpha}}{\partial t} &= -\frac{\chi^2}{\kappa}\left[|A_{n+1,\alpha}|^2 + |A_{n-1,\alpha}|^2 + 2|A_{n,\alpha}|^2\right]A_{n,\alpha} - \frac{2\eta^2}{\kappa}\left[|A_{n,\alpha-1}|^2 + |A_{n,\alpha+1}|^2 + 2|A_{n,\alpha}|^2\right]A_{n,\alpha} \\ &- \sum_{l=1}^{\infty} J'_l(A_{n+l,\alpha} + A_{n-l,\alpha}) + L(A_{n,\alpha+1} + A_{n,\alpha-1}), \quad \alpha = 1, 2, 3, \end{aligned} \tag{16}$$

which has been obtained after introducing the scaled quantities $\chi \longrightarrow \frac{\hbar}{\sqrt{M}J_0^{3/2}}\chi$, $\varpi \longrightarrow \frac{\hbar^2}{MJ_0^2}\varpi$, $\kappa \longrightarrow \frac{\hbar^2}{MJ_0^2}\kappa$, $\eta \longrightarrow \frac{\hbar^2}{MJ_0^2}\eta$, $L \longrightarrow \frac{L}{J_0}$, $t \longrightarrow \frac{J_0}{\hbar}t$. In Eqs. (16), we have simplified the LR term by considering $l = n - m$ so that the dispersion term becomes $\sum_{l=1}^{\infty} J'_l(A_{n+l,\alpha} + A_{n-l,\alpha})$, with $J'_l = |l|^{-r}$. Eqs. (16) are an ensemble of three CDNLS equations. In the same chain, there are in fact two types of couplings, i.e., the nonlinear coupling term $\frac{\chi^2}{\kappa}\left[|A_{n+1,\alpha}|^2 + |A_{n-1,\alpha}|^2 + 2|A_{n,\alpha}|^2\right]A_{n,\alpha}$ and the linear or LR coupling term $\sum_{l=1}^{\infty} J'_l(A_{n+l,\alpha} + A_{n-l,\alpha})$. Obviously, the nonlinear coupling term is restricted to nearest-neighbor peptide groups. Interestingly, interaction among adjacent spine is insured by a linear term, $L(A_{n,\alpha+1} + A_{n,\alpha-1})$, and the nonlinear term $\frac{2\eta^2}{\kappa}\left[|A_{n,\alpha-1}|^2 + |A_{n,\alpha+1}|^2 + 2|A_{n,\alpha}|^2\right]A_{n,\alpha}$. Based on this, there is indeed a competition between nonlinear and dispersive terms. However, this is not enough to confirm the emergence of solitonic structures in the proposed model. This requires more investigation related to the MI as done in the next section. For the rest of the calculations, the following set of parameter values will be used [4,28,31]: $E_0 = 0,205$ eV $= 1,55 \times 10^{-22}$ N m, $\kappa = 19.36$ N, $L = 2.46 \times 10^{-22}$ N m, $\varpi = [91.0 - 155.5]$ N m^{-1} $J = 15.47 \times 10^{-23}$ J, $I = [91.0 - 155.5]$ N m^{-1}, $M = 1.9 \times 10^{-25}$ kg, $\chi = [2 - 6] \times 10^{-11}$ N, $\eta = [0.7 - 1.2] \times 10^{-11}$ N.

3. Unstable energy patterns

The direct way to predict the emergence of nonlinear structures in physical systems is the through the activation of MI, i.e., the study of the stability of plane wave solutions. Such waves solutions are generally considered to be of the form $A_{n,\alpha} = A_{0,\alpha}e^{i(q_\alpha n - \omega_\alpha t)}$ $(\alpha = 1, 2, 3)$ where q_α and ω_α are the wavenumbers and the frequencies, respectively. The amplitudes $A_{0,\alpha}$ are assumed to be real. The solutions verify the linear dispersion relations

$$\omega_\alpha = -\frac{-4\chi^2}{\kappa}\left|A_{0,\alpha}\right|^2 - \frac{2\eta^2}{\kappa}\left[\left|A_{0,\alpha-1}\right|^2 + 2\left|A_{0,\alpha}\right|^2 + 2\left|A_{0,\alpha+1}\right|^2\right] - 2\sum_{l=1}^{\infty} J'_l \cos q_\alpha l \tag{17}$$

In order to study the stability of the plane wave solutions, we introduce small perturbations into their amplitudes in the form $A_{n,\alpha} = A_{0,\alpha}(1 + B_{n,\alpha}(t))e^{i(q_\alpha n - \omega_\alpha t)}$ $(\alpha = 1, 2, 3)$, where $B_{n,\alpha}(t)$ are the small perturbations, which, after linearizing

around the unperturbed plane waves, are governed by the set of coupled equations

$$\begin{aligned} i\frac{\partial B_{n,\alpha}}{\partial t} &= -\frac{\chi^2}{\kappa}[(B_{n+1,\alpha}+B^+_{n+1,\alpha})+(B_{n-1,\alpha}+B^+_{n-1,\alpha})+2(B_{n,\alpha}+B^+_{n,\alpha})]|A_{0,\alpha}|^2 \\ &- \frac{2\eta^2}{\kappa}[(B_{n,\alpha-1}+B^+_{n,\alpha-1})|A_{0,\alpha-1}|^2+(B_{n,\alpha+1}+B^+_{n,\alpha+1})|A_{0,\alpha+1}|^2+2(B_{n,\alpha}+B^+_{n,\alpha})|A_{0,\alpha}|^2] \\ &- \sum_{l=1}^{\infty} J'_l[(B_{n+l,\alpha}+B_{n-l,\alpha}-2B_{n,\alpha})\cos q_\alpha l - i(B_{n+l,\alpha}-B_{n-l,\alpha})\sin q_\alpha l]. \end{aligned} \tag{18}$$

Moreover, solutions for Eqs. (18) are assumed in the form $B_{n,\alpha} = a_{0,\alpha}e^{i(Qn-\Omega t)} + b^*_{0,\alpha}e^{-i(Qn-\Omega^* t)}$, with Q and Ω being the wavenumber and complex frequency of perturbation. On introducing those solutions into (18), one finds the following linear homogeneous system for $a_{0,1}$, $b_{0,1}$, $a_{0,2}$, $b_{0,2}$, $a_{0,3}$, $b_{0,3}$:

$$\begin{pmatrix} \Omega-m_{11} & m_{12} & m_{13} & m_{14} & m_{15} & m_{16} \\ m_{21} & -\Omega+m_{22} & m_{23} & m_{24} & m_{25} & m_{26} \\ m_{31} & m_{32} & \Omega+m_{33} & m_{34} & m_{35} & m_{36} \\ m_{41} & m_{42} & m_{43} & -\Omega+m_{44} & m_{45} & m_{46} \\ m_{51} & m_{52} & m_{53} & m_{54} & \Omega+m_{55} & m_{56} \\ m_{61} & m_{62} & m_{63} & m_{64} & m_{65} & -\Omega+m_{66} \end{pmatrix} \begin{pmatrix} a_{0,1} \\ b_{0,1} \\ a_{0,2} \\ b_{0,2} \\ a_{0,3} \\ b_{0,3} \end{pmatrix} = \begin{pmatrix} 0 \\ 0 \\ 0 \\ 0 \\ 0 \\ 0 \end{pmatrix}, \tag{19}$$

with the matrix elements $m_{i,j}$ being given by

$$m_{11} = -\frac{4\chi^2}{\kappa}|A_{0,1}|^2\sin^2\left(\frac{Q}{2}\right) - \frac{4\eta^2}{\kappa}|A_{0,1}|^2 - 2\sum_{l=1}^{\infty}J'_l\left\{2\sin^2\left(\frac{Ql}{2}\right)\cos q_1 l - \sin Ql\sin q_1 l\right\},$$

$$m_{12} = -\frac{4\chi^2}{\kappa}|A_{0,1}|^2\sin^2\left(\frac{Q}{2}\right) - \frac{4\eta^2}{\kappa}|A_{0,1}|^2, \quad m_{21} = \frac{2\chi^2}{\kappa}|A_{0,1}|^2\cos Q + \frac{6\eta^2}{\kappa}|A_{0,1}|^2,$$

$$m_{13} = m_{14} = m_{23} = m_{24} = m_{53} = m_{54} = m_{63} = m_{64} = \frac{2\eta^2}{\kappa}|A_{0,2}|^2,$$

$$m_{15} = m_{16} = m_{25} = m_{26} = m_{35} = m_{36} = m_{45} = m_{46} = \frac{2\eta^2}{\kappa}|A_{0,3}|^2,$$

$$m_{22} = \frac{2\chi^2}{\kappa}|A_{0,1}|^2\cos Q + \frac{6\eta^2}{\kappa}|A_{0,1}|^2 - 2\sum_{l=1}^{\infty}J'_l\left\{2\sin^2\left(\frac{Ql}{2}\right)\cos q_1 l + \sin Ql\sin q_1 l\right\},$$

$$m_{31} = m_{32} = m_{41} = m_{42} = m_{51} = m_{52} = m_{61} = m_{62} = \frac{2\eta^2}{\kappa}|A_{0,1}|^2,$$

$$m_{33} = m_{44} = -\frac{4\chi^2}{\kappa}|A_{0,2}|^2\sin^2\left(\frac{Q}{2}\right) + \frac{4\eta^2}{\kappa}|A_{0,2}|^2 - 2\sum_{l=1}^{\infty}J'_l\left\{2\sin^2\left(\frac{Ql}{2}\right)\cos q_2 l - \sin Ql\sin q_2 l\right\},$$

$$m_{34} = m_{43} = -\frac{4\chi^2}{\kappa}|A_{0,2}|^2\sin^2\left(\frac{Q}{2}\right) + \frac{4\eta^2}{\kappa}|A_{0,2}|^2, \quad m_{65} = -\frac{4\chi^2}{\kappa}|A_{0,3}|^2\sin^2\left(\frac{Q}{2}\right) + \frac{4\eta^2}{\kappa}|A_{0,3}|^2,$$

$$m_{55} = -\frac{4\chi^2}{\kappa}|A_{0,3}|^2\sin^2\left(\frac{Q}{2}\right) + \frac{4\eta^2}{\kappa}|A_{0,3}|^2 - 2\sum_{l=1}^{\infty}J'_l\left\{2\sin^2\left(\frac{Ql}{2}\right)\cos q_3 l - \sin Ql\sin q_3 l\right\},$$

$$m_{56} = -\frac{4\chi^2}{\kappa}|A_{0,3}|^2\sin^2\left(\frac{Q}{2}\right) + \frac{4\eta^2}{\kappa}|A_{0,3}|^2 - 2\sum_{l=1}^{\infty}J'_l\sin Ql\sin q_3 l,$$

$$m_{66} = -\frac{4\chi^2}{\kappa}|A_{0,3}|^2\sin^2\left(\frac{Q}{2}\right) + \frac{4\eta^2}{\kappa}|A_{0,3}|^2 - 2\sum_{l=1}^{\infty}J'_l\left\{2\sin^2\left(\frac{Ql}{2}\right)\cos q_3 l + \sin Ql\sin q_3 l\right\}.$$

The condition for the above system to admit non-trivial solutions is obtained by setting its determinant to zero. One therefore finds a sixth-order polynomials

$$\Omega^6 + P_5\Omega^5 + P_4\Omega^4 + P_3\Omega^3 + P_2\Omega^2 + P_1\Omega + P_0 = 0 \tag{20}$$

whose solutions may easily be found via symbolic computation, with the coefficients P_j being given in the Appendix. Solutions for Eq. (20) can be found analytically, using symbolic computation, but this is cumbersome are requires more

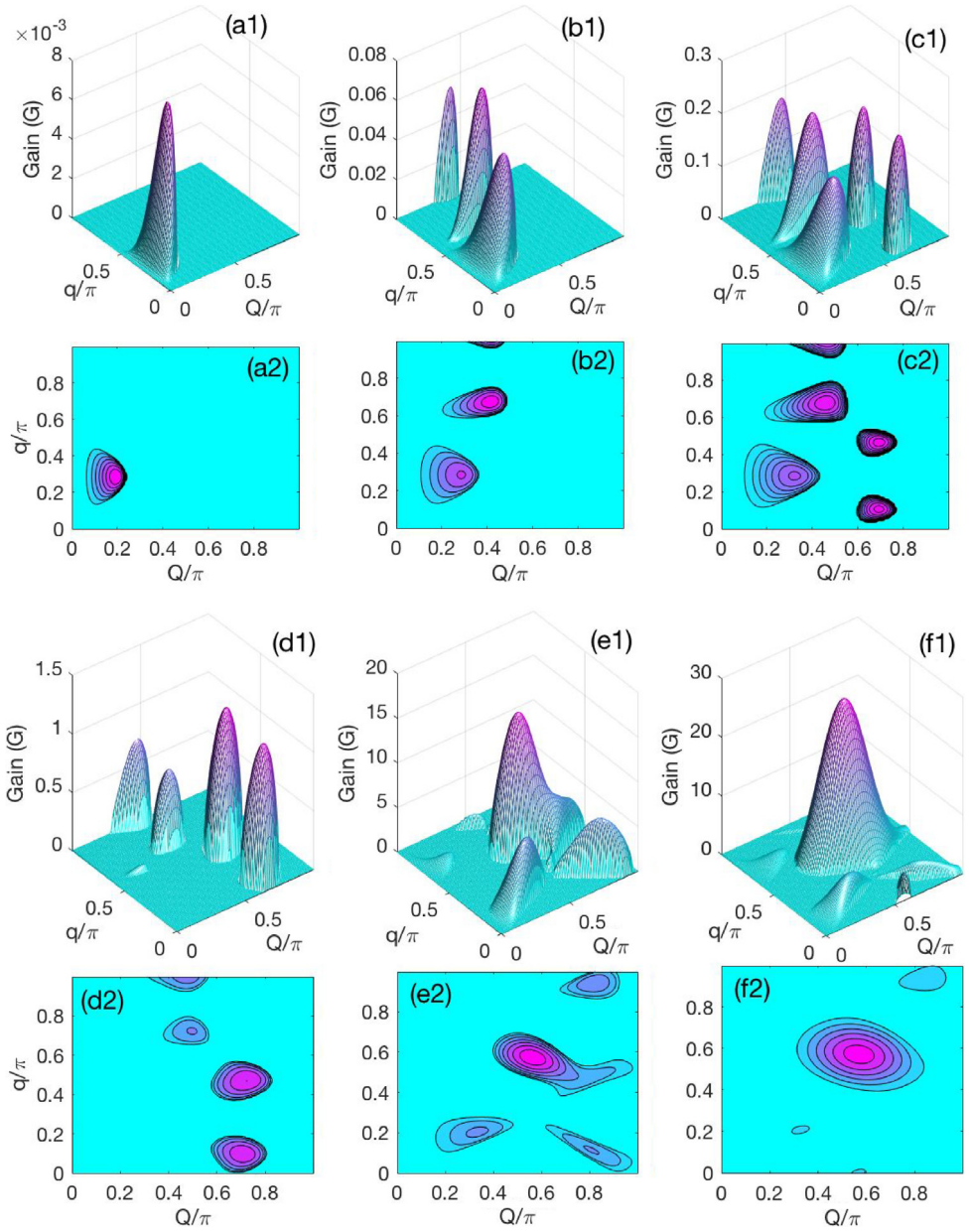

Fig. 1. The panels show plots of the MI gain, and the corresponding stability/instability diagram, versus the wavenumbers Q and q, with changing χ and the range parameter r. For $\chi = 2$, $r = 1.5$ corresponds to panels (a1) and (a2), where there is only one region of instability. For $r = 1.2$, additional instability sidebands appear for $r = 1.2$ (panels 1(b1)–(b2)), and persist for $r = 1.1$ (panels 1(c1)–(c2)). Panels (d1)–(d2), (e1)–(e2) and (f1)–(f2) corresponds to $\chi = 8$, where r takes the respective values as in the previous case. Here, under strong LR effects, the numerous number of instability regions tend to merge into one instability zone.

simplifications and the study of some few cases. A more complete investigation of the solutions requires the use of numerical schemes, which give all the possible solutions. In that respect, such solutions may be real or complex depending on the values of parameters and most of the features related to MI are due to complex solutions. For example, solutions for Ω are generally in the form $\Omega = \Omega_r + i\Omega_i$, which modifies the perturbations as $B_{n,\alpha}(t) = e^{\Omega_i t}\left[a_{0,\alpha}e^{i(Qn-\Omega_r t)} + b_{0,\alpha}e^{-i(Qn-\Omega_r t)}\right]$. Therefore, one clearly sees that the imaginary part controls the stability/instability of the plane wave solutions. The rate of instability is in general evaluated in terms of the instability gain $G(q, Q) = |\mathrm{Im}(\Omega)|$, from which the onset of MI can be detected. As already indicated while presenting the model, one should stress that the coupling among adjacent peptides is of two competitive types, i.e., the LR and the nonlinear coupling. Previous works devoted to nearest-neighbor interactions have proven that the two types of coupling indeed affect the process of energy transport and storage in the three-stranded model [28,31]. In the

rest of this particular work, we insist on the concomitant effects of LR interactions and nonlinear coupling. To proceed, we first of all consider $q_1 = q_2 = q_3 = q$ and $A_{10} = A_{20} = A_{30} = 0.1$. For weak values of the nonlinear coupling parameter, i.e., $\chi = 2$, we have the features of stability/instability given in Fig. 1. High values of the range parameter correspond to weak LR interactions and, when $r \to \infty$, the system behaves as restricted to nearest-neighbor interactions. In that respect, for $r = 1.5$, we have the gain of Fig. 1(a1) and its corresponding stability/instability diagram plotted in Fig. 1(a2), where there is only one region of instability. With decreasing r, i.e., increasing the LRI effect, additional instability sidebands appear for $r = 1.2$ (Figs. 1(b1)–(b2)), and persist for $r = 1.1$ (Figs. 1(c1)–(c2)). This shows that under weak nonlinear intra-spine interaction, LR interactions may be responsible for the explosion of the instability domain, leading to the emergence of other regions of instability. However, under strong nonlinear intra-strand coupling, the comportment is found to be different as depicted in Figs. 1(d1)–(d2), (e1)–(e2) and (f1)–(f2), where we have fixed $\chi = 8$. Panels (d1)–(d2) correspond to $r = 1.5$, value of the range parameter that gives rise to several regions of instability. Their number drops progressively with decreasing r, as shown in panels (e1)–(e2) and (f1)–(f2), for which r takes respectively the values 1.2 and 1.1. In the meantime, one should be aware that when values of parameters are picked from one of the regions of instability, the plane waves will be said to be unstable under modulation and will therefore be expected to break-up into solitonic structures. Otherwise, they will propagate with their properties not being changed, and will be said to be stable under modulation.

Beyond these information on the onset of MI, the linear stability analysis fails to predict the behaviors of solitons and nonlinear structures at long timescale. Therefore, in order to verify the accuracy of the linear stability analysis, we propose to integrate directly the set of Eqs. (16) using the fourth-order Runge–Kutta computational scheme, with periodic boundary conditions and timescale $\Delta t = 10^{-3}$. We consider the initial condition $A_{n,\alpha} = A_{0,\alpha}\left(1 + 0.01e^{iqn}\right)e^{iQn} \quad (\alpha = 1, 2, 3)$ and to start, we fix $A_{10} = 0.1$ and $A_{20} = A_{30} = 0$, with the wavenumbers q and Q taking respectively the values 0.35π and 0.28π and $\chi = 2$. Particularly, we have excited only one strand in order to observe the dynamical response of the other two strands and the effectiveness of the inter-spine coupling. The chosen values of the wavenumbers fall well inside the regions of instability depicted in Fig. 1(a1)–(a2), and are to this fact expected to support nonlinear pattern formation. This is for example confirmed by the structures obtained in Fig. 2, whose shape and characteristics are influenced by the change in the range parameter r. In general, over longtime simulation they appear and have the shape of soliton-like patterns. This is a direct proof of the accuracy between our analytical predictions and direct numerical calculations on the generic model. As only one of the spines has been excited, one notices the response from the other two strands, which obviously have the same amplitude of excitation. This has been reported in a number of recent contributions, but in the absence of LRI [28,30–32]. Nevertheless, they are the consequence of the interplay between nonlinear and dispersive effects. More precisely, the trains of waves obtained have features of pulse solitons, but while comparing Fig. 2(a1) to Figs. 2(a2) and (a3), the presence of extended waves for $|A_{n,1}|$ is a fact, while $|A_{n,2}|$ and $|A_{n,3}|$ display patterns with periodic background. Figs. 2(aj)$_{j=1,2,3}$ have been recorded for $r = 1.5$. For $r = 1.2$, the manifestations of MI are shown in Figs. 2(bj)$_{j=1,2,3}$, where the number of breathing patterns has increased. Moreover, $|A_{n,2}|$ and $|A_{n,3}|$ display some initiation of two-humped solitonic structures with filled profile, while for $|A_{n,1}|$, individual pulses of energy are visible. In Fig. 3, the calculations of Fig. 2 have been repeated, where line (A) corresponds to Figs. 2(aj)$_{j=1,2,3}$, line (B) to Figs. 2(bj)$_{j=1,2,3}$ and line (C) to Figs. 2(cj)$_{j=1,2,3}$. There, the energy density has been recorded versus space and one clearly confirms the profile depicted in Fig. 2 with changing the value of the range parameter. For small values of the later, energy is distributed among lattice sites and remains available for intrinsic lattice dynamics. Interestingly, although there is still intrinsic energy, sequences of high energy patterns emerge in the form of impulses as confirmed by line (C) of Fig. 3. The result of line (C), however, shows the robustness of energy localization in molecular models, especially monitored by solitonic structures under the influence of any factor that may modify both the intrinsic nonlinearity and the dispersion inherent to such systems. Like in DNA, the stored and transported energy is supposed to adopt a specific profile for the process of its transport to be initiated [45]. That is indeed why, when all the conditions are gathered, under the activation of MI, trains of solitons as those observed in Fig. 3, line (C), may be observed. To remind, the results of Fig. 2 and 3 have been recorded for weak nonlinear intra-spine coupling χ. In Fig. 4, we have therefore increased its value as $\chi = 8$. The obtained results suggest that for $r = 1.5$, energy patterns display periodic profiles, with the excitonic patterns $|A_{n,2}|$ and $|A_{n,3}|$ still having the same characteristics. For $r = 1.2$, the localized states described in Ref. [32] appear, due to strong coupling χ and mainly because of the strength of the LR coupling that increases. Remarkably, the spatial expansion of the obtained patterns gets restrained, compared to the case of line (A). This persists when $r = 1.1$, where the wave spatial expansion of $|A_{n,1}|$ gets more narrower, therefore involving few sequences of lattice sites. This phenomenon is ubiquitous to many molecular systems due to the strong competition between nonlinearity and dispersion. Multi-humped solitonic structures were already reported in a three-stranded model of α-helix proteins, but were shown to merge into a single structure with increasing χ. The same behavior is obvious in Fig. 5, where the value of χ has been increased to 14. In fact, the observed spectrum of behaviors is a consequence of the coupled effects of nonlinear coupling and LRI, leading to an effective transition from extended trains of waves to asymmetric solitonic humps when r becomes small, i.e., under strong LRI. Line (A) of Fig. 5 has been plotted for $r = 1.5$, line (B) for $r = 1.2$ and line (C) for $r = 1.1$. The existence of such waves in proteins was already suggested by Brown et al. [17–19] and Ivic et al. [46–48]. That was to demonstrate that due to the structural modification taking place in real proteins during energy transport, the observed structures were suitable. Falvo and Pouthier [49,50], considering a three-spine model showed that the vibron dynamics was the consequence of the competitive effects between inter-spine vibron hops, leading to some dressing effects, capable of reducing vibrational exchange between spines, the direct consequence being the emergence of energy patterns that move along a single spine, therefore reducing the system to a one-dimensional Davydov model. In contrast, the nonlinear effects present in the proposed model enhance

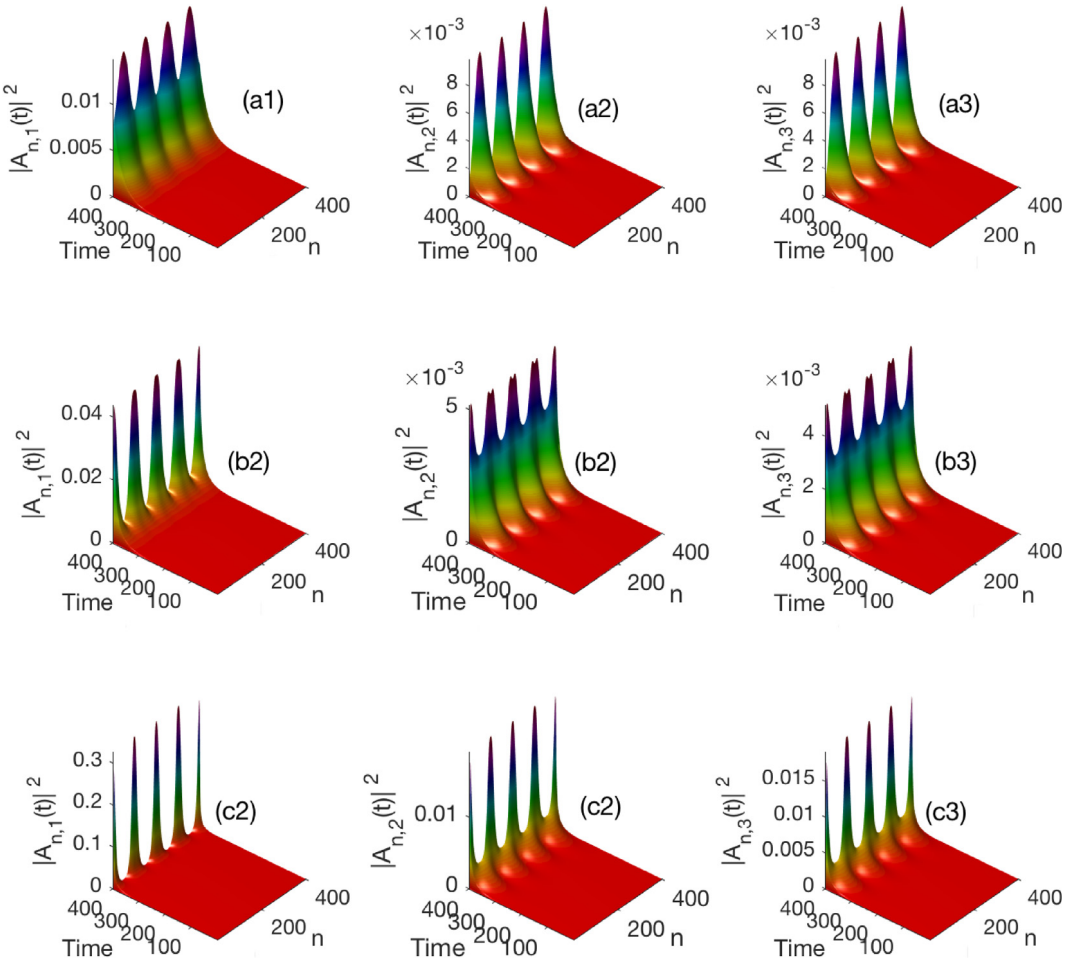

Fig. 2. Numerical energy patterns obtained for $\chi = 2$ and: $(\mathrm{aj})_{j=1,2,3}$ $r = 1.5$, $(\mathrm{bj})_{j=1,2,3}$ $r = 1.2$ and $(\mathrm{cj})_{j=1,2,3}$ $r = 1.1$, with $A_{10} = 0.1$, $A_{20} = A_{30} = 0$, $\kappa = 11$ and $\omega = 100$.

the emergence of solitonic waves that, under appropriate LR dispersive contribution in all the spines, reinforce inter-based energy storage and distribution. Indeed, the model Eqs. (16) include coupling parameters to vibrational dynamics, especially H-bonds among spines, which were already revealed to be vital for mediating electronic transport in proteins [32,36,37]. They are indeed the driving force in such a process, which to some extent is common to most of biological molecules. Due to the presence of H-bonds, charge transport in DNA may be controlled and give rise to important dynamical spectrum with appropriate biological implications [27,51–64].

4. Conclusion

This paper considered a three-stranded α-helix protein model with LR dispersive interactions and inter-spine coupling. The improved quantum model for exciton–phonon dynamics has been reduced to a set of three coupled modified DNLS equations with LR interactions. The MI analysis has thereafter been conducted, and regions of instability detected. Those regions, where the plane wave solutions are supposed to disintegrate into trains of soliton-like objects, have been found to be very sensitive to the LR and nonlinear coupling parameters, r and χ respectively. For small values of χ, strong LR interaction, i.e., small r, tends to induce additional instability sidebands which reduce to only one region when r decreases. Contrarily, for high values of χ, the spectrum of instability displays many regions of instability that are annihilated by strong LR effects. This has been confirmed numerically, using instability parameters. In that respect, it has been confirmed that when parameters fall well inside instability zones, there appear trains of solitonic entities due to the balanced effect of nonlinearity and dispersion. More importantly, for small χ, ordinary extended waves transform progressively into trains of pulses with decreasing r. Although this remains obvious for big χ and high r, more spatially restrained structures emerge under strong LR effects. This gets more pronounced when χ increases. In view of the above, solitonic structures are robust in H-bonded molecules, especially in proteins and DNA. In that respect, they may be of different significance, depending

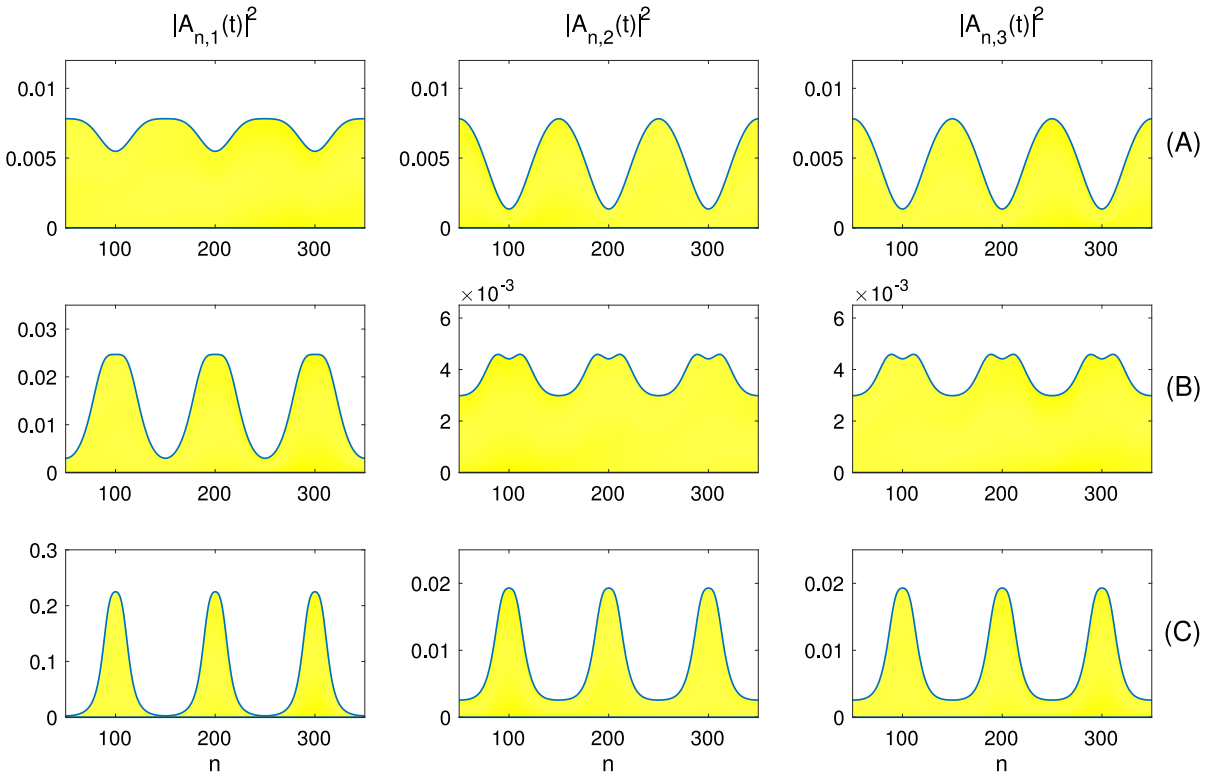

Fig. 3. Spatial energy modes corresponding to Fig. 2 at time $t = 400$, in the lattice sequence $50 \leq n \leq 350$. Line (A) is plotted for $r = 1.5$, line (B) for $r = 1.2$ and line (C) for $r = 1.1$. The other parameters are $\chi = 2, A_{10} = 0.1, A_{20} = A_{30} = 0, \kappa = 11$ and $\omega = 100$.

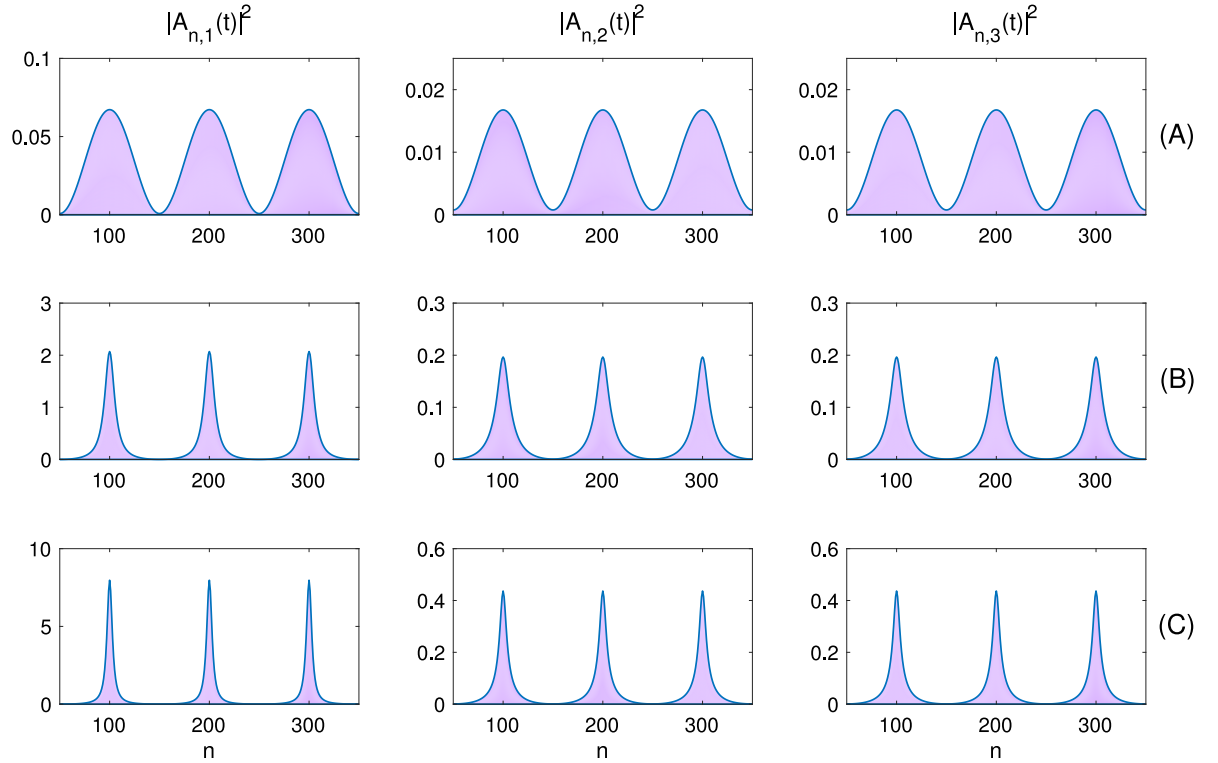

Fig. 4. Spatial energy patterns related to strong intra-spine interaction, i.e., $\chi = 8$, in the lattice sequence $50 \leq n \leq 350$ at time $t = 400$. Line (A) is plotted for $r = 1.5$, line (B) for $r = 1.2$ and line (C) for $r = 1.1$. The other parameters are $A_{10} = 0.1, A_{20} = A_{30} = 0, \kappa = 11$ and $\omega = 100$.

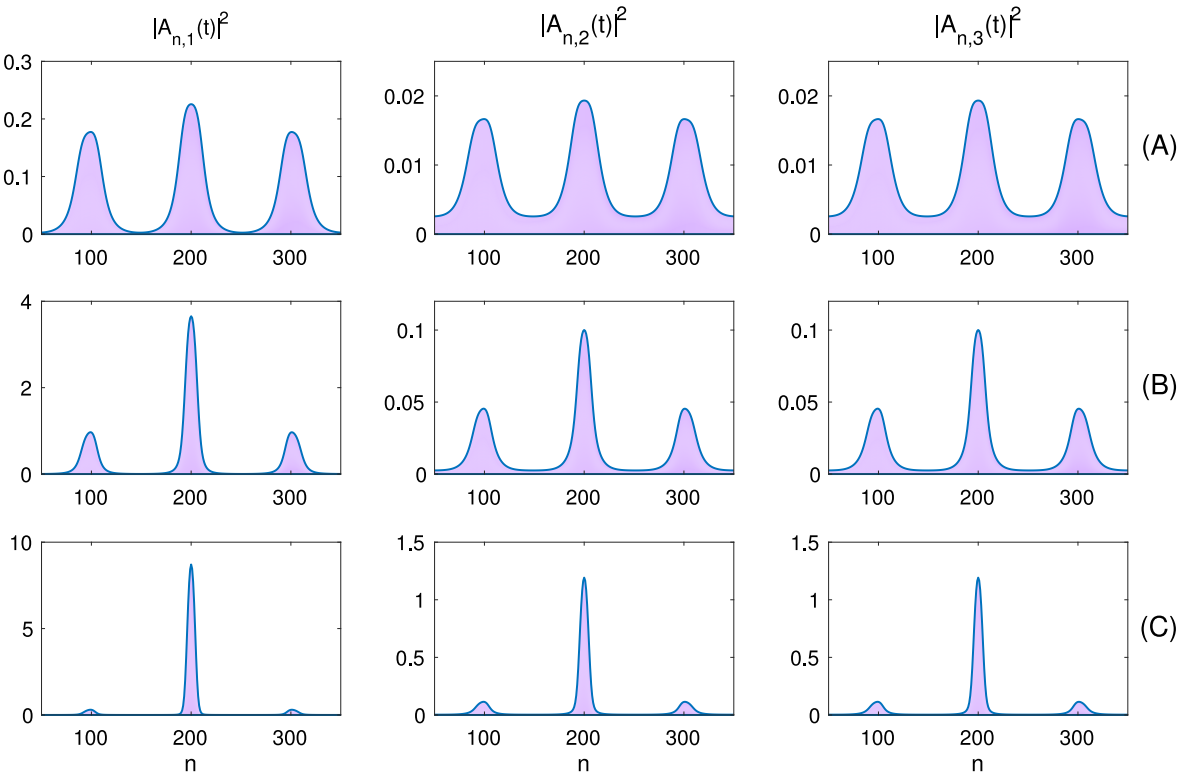

Fig. 5. Spatial energy patterns related to strong intra-spine interaction, i.e., $\chi = 14$, in the lattice sequence $50 \leq n \leq 350$ at time $t = 400$. Line (A) is plotted for $r = 1.5$, line (B) for $r = 1.2$ and line (C) for $r = 1.1$. The other parameters are $A_{10} = 0.1, A_{20} = A_{30} = 0, \kappa = 11$ and $\omega = 100$.

on the backbone structure of the studied biomolecule. However, most of the cases rely on the strong relationship between vibrational and excitonic dynamics. In DNA for example, solitonic energy patterns have been found to be more effective when the H-bonds linking the bases in pairs are compressed, leading to slight breathing oscillations of the strand under the activation of MI [27,51,53,54], and the same seems to be effective in proteins. Understanding the various mechanisms and factors related to such processes is of paramount importance both in biology and nanobioelectronic. This requires the elaboration of more suitable models, that may bring together as many interactions as possible, including those related to the direct molecular environment of the protein such as thermal fluctuations, dissipation and LR coupling among peptide groups. Investigations in those directions are ongoing.

Acknowledgments

Rich comments and relevant suggestions from the referees are acknowledged. The work by CBT is supported by the Botswana International University of Science and Technology, Republic of Botswana under the grant DVC/RDI/2/1/16I (25). CBT thanks the Kavli Institute for Theoretical Physics (KITP), University of California Santa Barbara (USA), for invitation.

Appendix. Coefficients of Eq. (20)

$$
\begin{aligned}
P_5 &= m_{22} + m_{44} - m_{55} - m_{33} + m_{66} - m_{11},\\
P_4 &= m_{22}m_{33} + m_{22}m_{11} + m_{22}m_{55} + m_{44}m_{55} + m_{55}m_{66} - m_{56}m_{65} + m_{33}m_{66} + m_{33}m_{44} - m_{33}m_{55}\\
&\quad - m_{33}m_{66} - m_{22}m_{44} + m_{11}m_{66} + m_{11}m_{44} - m_{11}m_{55} - m_{11}m_{33} - m_{44}m_{66} - m_{12}m_{21} - m_{34}^2,\\
P_3 &= -m_{22}m_{33}m_{44} + m_{22}m_{11}m_{55} + m_{22}m_{56}m_{65} + m_{34}^2m_{66} - m_{34}^2m_{55}\\
&\quad + m_{11}m_{33}m_{66} + m_{11}m_{33}m_{44} - m_{22}m_{11}m_{44} + m_{22}m_{11}m_{33}\\
&\quad - m_{22}m_{11}m_{66} - m_{44}m_{55}m_{66} - m_{33}m_{44}m_{66} + m_{33}m_{4}m_{55} + m_{33}m_{55}m_{66}\\
&\quad - m_{11}m_{33}m_{55} - m_{33}m_{56}m_{65} + m_{11}m_{55}m_{66} + m_{44}m_{56}m_{65} - m_{11}m_{44}m_{66} - m_{11}m_{34}^2\\
&\quad + m_{11}m_{44}m_{55} - m_{22}m_{56}m_{66} + m_{22}m_{34}^2 - m_{11}m_{56}m_{65}
\end{aligned}
$$

$$
\begin{aligned}
P_2 = {} & m_{11}m_{44}m_{56}m_{65} - m_{11}m_{33}m_{44}m_{66} + m_{11}m_{33}m_{44}m_{55} + m_{11}m_{33}m_{55}m_{66} - m_{11}m_{33}m_{56}m_{65} \\
& - m_{12}m_{15}m_{31}m_{66} - 2m_{34}m_{13}m_{55}m_{15} - m_{13}m_{44}m_{65}m_{15} + m_{13}m_{44}m_{15}m_{66} \\
& + m_{13}m_{44}m_{55}m_{15} - m_{13}m_{44}m_{15}m_{56} - m_{11}m_{44}m_{55}m_{66} \\
& + m_{31}m_{22}m_{33}m_{13} - m_{31}m_{65}m_{15}m_{11} + m_{31}m_{15}m_{11}m_{66} - m_{31}m_{22}m_{65}m_{15} \\
& + m_{31}m_{22}m_{15}m_{66} + m_{12}m_{21}m_{55}m_{66} - m_{12}m_{21}m_{56}m_{65} + m_{12}m_{21}m_{33}m_{44} \\
& + m_{12}m_{21}m_{33}m_{66} - m_{12}m_{21}m_{33}m_{55} - m_{12}m_{21}m_{44}m_{66} + m_{12}m_{21}m_{44}m_{55} \\
& + m_{22}m_{33}m_{44}m_{66} - m_{22}m_{33}m_{44}m_{55} - m_{22}m_{33}m_{55}m_{66} - m_{15}m_{31}m_{21}m_{66} \\
& + 2m_{34}m_{13}m_{15}m_{56} + m_{33}m_{44}m_{56}m_{65} - m_{33}m_{13}m_{65}m_{15} + m_{33}m_{13}m_{15}m_{66} \\
& - m_{33}m_{13}m_{15}m_{56} + m_{33}m_{13}m_{55}m_{15} + 2m_{34}m_{13}m_{65}m_{15} - 2m_{34}m_{13}m_{15}m_{66} \\
& - m_{22}m_{34}^2m_{66} - m_{22}m_{11}m_{34}m_{55} - m_{22}m_{15}m_{55}m_{66} + m_{22}m_{11}m_{56}m_{65} \\
& - m_{22}m_{11}m_{33}m_{44} - m_{22}m_{11}m_{33}m_{66} + m_{22}m_{11}m_{33}m_{55} - m_{33}m_{44}m_{55}m_{66} \\
& + m_{56}m_{21}m_{15}m_{31} + m_{22}m_{11}m_{34}^2 - m_{34}^2m_{56}m_{65} + m_{22}m_{34}^2m_{55} \\
& + m_{34}^2m_{55}m_{66} + m_{11}m_{34}^2m_{66} - m_{12}m_{21}m_{34}^2 - m_{11}m_{34}^2m_{55} - m_{21}m_{55}m_{15}m_{31} \\
& + m_{15}m_{31}m_{65}m_{21} + m_{31}m_{13}m_{11}m_{44} - 2m_{31}m_{34}m_{13}m_{11} + m_{31}m_{22}m_{13}m_{44} \\
& - 2m_{31}m_{22}m_{34}m_{13} + m_{31}m_{33}m_{13}m_{11} + m_{22}m_{33}m_{56}m_{65} + m_{22}m_{11}m_{44}m_{66} \\
& - m_{31}m_{21}m_{13}m_{44} + 2m_{31}m_{21}m_{34}m_{13} - m_{31}m_{21}m_{33}m_{13} + m_{31}m_{55}m_{15}m_{11} \\
& - m_{31}m_{15}m_{11}m_{56} + m_{31}m_{22}m_{55}m_{15} - m_{31}m_{22}m_{15}m_{56} + m_{22}m_{44}m_{55}m_{66} \\
& - m_{12}m_{55}m_{15}m_{31} + m_{12}m_{56}m_{15}m_{31} + m_{12}m_{15}m_{31}m_{65} - m_{12}m_{33}m_{13}m_{31} \\
& - m_{12}m_{13}m_{31}m_{44} + 2m_{12}m_{34}m_{13}m_{31} - m_{22}m_{44}m_{56}m_{65}
\end{aligned}
$$

$$
\begin{aligned}
P_1 = {} & m_{22}m_{11}m_{34}^2m_{55} + m_{22}m_{34}^2m_{56}m_{65} - m_{22}m_{34}^2m_{55}m_{66} - m_{12}m_{21}m_{34}^2m_{55} \\
& + m_{12}m_{21}m_{34}^2m_{66} + 2m_{31}m_{21}m_{34}m_{13}m_{55} + m_{11}m_{34}^2m_{55}m_{66} \\
& - m_{22}m_{11}m_{34}^2m_{66} - m_{11}m_{34}^2m_{56}m_{65} + m_{31}m_{22}m_{44}m_{65}m_{15} \\
& + m_{31}m_{33}m_{15}m_{11}m_{66} - m_{31}m_{33}m_{65}m_{15}m_{11} + m_{12}m_{21}m_{33}m_{44}m_{55} \\
& - m_{31}m_{22}m_{44}m_{15}m_{66} - m_{31}m_{44}m_{55}m_{15}m_{11} + m_{31}m_{22}m_{33}m_{15}m_{66} \\
& - m_{31}m_{22}m_{33}m_{65}m_{15} + m_{31}m_{44}m_{15}m_{11}m_{56} + m_{31}m_{21}m_{33}m_{15}m_{56} - m_{31}m_{21}m_{33}m_{55}m_{15} \\
& - m_{11}m_{33}m_{44}m_{55}m_{66} + m_{22}m_{11}m_{33}m_{56}m_{65} - m_{22}m_{11}m_{33}m_{55}m_{66} \\
& - m_{22}m_{11}m_{33}m_{44}m_{55} + m_{22}m_{11}m_{33}m_{44}m_{66} - m_{22}m_{11}m_{44}m_{56}m_{65} \\
& + m_{22}m_{11}m_{44}m_{55}m_{66} + m_{11}m_{33}m_{44}m_{56}m_{65} - m_{11}m_{33}m_{13}m_{15}m_{56} \\
& + m_{11}m_{33}m_{13}m_{15}m_{66} - m_{11}m_{33}m_{13}m_{65}m_{15} - m_{12}m_{33}m_{13}m_{31}m_{55} \\
& + m_{11}m_{33}m_{13}m_{55}m_{15} + m_{12}m_{13}m_{31}m_{44}m_{66} + m_{12}m_{33}m_{13}m_{31}m_{66} \\
& + m_{12}m_{44}m_{15}m_{31}m_{66} + m_{12}m_{44}m_{55}m_{15}m_{31} - m_{12}m_{44}m_{15}m_{31}m_{65} \\
& - m_{12}m_{44}m_{56}m_{15}m_{31} - m_{12}m_{13}m_{31}m_{44}m_{55} - m_{12}m_{33}m_{15}m_{31}m_{66} \\
& - m_{12}m_{33}m_{55}m_{15}m_{31} + m_{12}m_{33}m_{15}m_{31}m_{65} + m_{12}m_{33}m_{56}m_{15}m_{31} - m_{11}m_{13}m_{44}m_{15}m_{56} \\
& + m_{11}m_{13}m_{44}m_{55}m_{15} + m_{11}m_{13}m_{44}m_{15}m_{66} - m_{11}m_{13}m_{44}m_{65}m_{15} + m_{22}m_{13}m_{44}m_{15}m_{56} \\
& - m_{22}m_{13}m_{44}m_{55}m_{15} - m_{22}m_{13}m_{44}m_{15}m_{66} + m_{22}m_{13}m_{44}m_{65}m_{15} \\
& - m_{22}m_{33}m_{13}m_{55}m_{15} + m_{22}m_{33}m_{13}m_{15}m_{56} - m_{22}m_{33}m_{13}m_{15}m_{66} \\
& + m_{22}m_{33}m_{13}m_{65}m_{15} - m_{22}m_{33}m_{44}m_{56}m_{65} + m_{22}m_{33}m_{44}m_{55}m_{66} \\
& - 2m_{11}m_{34}m_{13}m_{15}m_{66} + 2m_{11}m_{34}m_{34}m_{65}m_{15} - m_{12}m_{21}m_{33}m_{44}m_{66} \\
& + m_{12}m_{21}m_{44}m_{56}m_{65} - m_{12}m_{21}m_{44}m_{55}m_{66} - m_{31}m_{44}m_{15}m_{11}m_{66} + m_{31}m_{44}m_{65}m_{15}m_{11} \\
& + m_{31}m_{22}m_{33}m_{13}m_{55} - m_{31}m_{22}m_{33}m_{13}m_{66} + m_{31}m_{33}m_{13}m_{11}m_{55} \\
& - m_{31}m_{33}m_{13}m_{11}m_{66} + m_{31}m_{22}m_{13}m_{44}m_{55} - m_{31}m_{22}m_{13}m_{44}m_{66} + m_{31}m_{13}m_{11}m_{44}m_{55} \\
& - m_{31}m_{13}m_{11}m_{44}m_{66} + 2m_{31}m_{34}m_{13}m_{11}m_{66} + 2m_{22}m_{34}m_{13}m_{55}m_{15} \\
& - 2m_{22}m_{34}m_{13}m_{15}m_{56} + 2m_{22}m_{34}m_{13}m_{15}m_{66} - 2m_{22}m_{34}m_{13}m_{65}m_{15} \\
& - 2m_{12}m_{34}m_{13}m_{31}m_{66} + 2m_{12}m_{34}m_{13}m_{31}m_{55} - 2m_{11}m_{34}m_{13}m_{55}m_{15} \\
& + 2m_{11}m_{34}m_{13}m_{15}m_{56} - 2m_{31}m_{22}m_{34}m_{13}m_{55} + 2m_{31}m_{22}m_{34}m_{13}m_{66} \\
& - 2m_{31}m_{34}m_{13}m_{11}m_{55} - m_{12}m_{21}m_{33}m_{56}m_{65} + m_{31}m_{33}m_{55}m_{15}m_{11} \\
& - m_{31}m_{33}m_{15}m_{11}m_{56} + m_{31}m_{21}m_{33}m_{13}m_{66} + m_{12}m_{21}m_{33}m_{55}m_{66} \\
& + m_{31}m_{21}m_{33}m_{65}m_{15} - 2m_{31}m_{21}m_{34}m_{13}m_{66} + m_{31}m_{21}m_{44}m_{15}m_{66} \\
& - m_{31}m_{21}m_{44}m_{15}m_{56} + m_{31}m_{21}m_{44}m_{55}m_{15} + m_{31}m_{21}m_{13}m_{44}m_{66} \\
& + m_{31}m_{22}m_{33}m_{55}m_{15} + m_{31}m_{22}m_{44}m_{15}m_{56} - m_{31}m_{21}m_{44}m_{65}m_{15} - m_{31}m_{22}m_{44}m_{55}m_{15} \\
& - m_{31}m_{21}m_{33}m_{13}m_{55} - m_{31}m_{22}m_{33}m_{15}m_{56} - m_{31}m_{21}m_{13}m_{44}m_{55} - m_{31}m_{21}m_{33}m_{15}m_{66},
\end{aligned}
$$

$$P_0 = P_0^{(1)} + P_0^{(1)} + P_0^{(2)},$$

with

$$
\begin{aligned}
P_0^{(1)} &= m_{12}m_{21}m_{34}^2m_{55}m_{66} - m_{12}m_{21}m_{34}^2m_{56}m_{65} - m_{12}m_{21}m_{33}m_{44}m_{55}m_{66} + m_{12}m_{21}m_{33}m_{44}m_{56}m_{65}\\
&- m_{12}m_{21}m_{33}m_{13}m_{65}m_{15} + m_{12}m_{21}m_{33}m_{13}m_{15}m_{66} - m_{12}m_{21}m_{33}m_{13}m_{15}m_{56}\\
&+ m_{12}m_{21}m_{33}m_{13}m_{55}m_{55} + 2m_{12}m_{21}m_{34}m_{13}m_{65}m_{15} - 2m_{12}m_{21}m_{34}m_{13}m_{15}m_{66}\\
&+ 2m_{12}m_{21}m_{34}m_{13}m_{15}m_{56} - 2m_{12}m_{21}m_{34}m_{13}m_{55}m_{15} - m_{12}m_{34}^2m_{55}m_{15}m_{31}\\
&- m_{12}m_{34}^2m_{15}m_{31}m_{66} + m_{12}m_{34}^2m_{56}m_{15}m_{31} + m_{12}m_{34}^2m_{15}m_{31}m_{65} - m_{12}m_{21}m_{13}m_{44}m_{65}m_{15}\\
&+ m_{12}m_{21}m_{13}m_{44}m_{15}m_{66} + m_{12}m_{21}m_{13}m_{44}m_{55}m_{15} - m_{12}m_{21}m_{13}m_{44}m_{15}m_{56}\\
&- m_{22}m_{11}m_{34}^2m_{55}m_{66} + m_{22}m_{11}m_{34}^2m_{56}m_{65} - 4m_{31}m_{21}m_{34}m_{13}m_{65}m_{15}\\
&+ 4m_{31}m_{21}m_{34}m_{13}m_{15}m_{66} - 4m_{31}m_{21}m_{34}m_{13}m_{15}m_{56} + 4m_{31}m_{21}m_{34}m_{13}m_{55}m_{15}\\
&+ 2m_{31}m_{21}m_{13}m_{44}m_{65}m_{15} - 2m_{31}m_{21}m_{13}m_{44}m_{15}m_{66} - 2m_{31}m_{21}m_{13}m_{44}m_{55}m_{15}\\
&+ 2m_{31}m_{21}m_{13}m_{44}m_{15}m_{56} + m_{31}m_{21}m_{13}m_{44}m_{55}m_{66} - m_{31}m_{21}m_{13}m_{44}m_{56}m_{65} - 2m_{31}m_{21}m_{34}m_{13}m_{55}m_{66}\\
&+ 2m_{31}m_{21}m_{34}m_{13}m_{56}m_{65} + m_{31}m_{21}m_{33}m_{13}m_{55}m_{66} - m_{31}m_{21}m_{33}m_{13}m_{56}m_{65}\\
&+ 2m_{31}m_{21}m_{33}m_{13}m_{65}m_{15} - 2m_{31}m_{21}m_{33}m_{13}m_{15}m_{66} + 2m_{31}m_{21}m_{33}m_{13}m_{15}m_{56}.\\
P_0^{(2)} &= -2m_{31}m_{21}m_{33}m_{13}m_{55}m_{15} - m_{31}m_{21}m_{33}m_{44}m_{65}m_{15} + m_{31}m_{21}m_{33}m_{44}m_{15}m_{66}\\
&- m_{31}m_{34}^2m_{65}m_{15}m_{11} + m_{31}m_{34}^2m_{15}m_{11}m_{66}\\
&+ m_{31}m_{22}m_{34}^2m_{15}m_{66} - m_{31}m_{22}m_{34}^2m_{65}m_{15} + m_{31}m_{21}m_{33}m_{44}m_{55}m_{15}\\
&- m_{31}m_{21}m_{33}m_{44}m_{15}m_{56} + m_{31}m_{34}^2m_{55}m_{15}m_{11}\\
&- m_{31}m_{34}^2m_{15}m_{11}m_{56} - m_{31}m_{22}m_{34}^2m_{15}m_{56} + m_{31}m_{22}m_{34}^2m_{55}m_{15}\\
&+ m_{22}m_{11}m_{33}m_{44}m_{55}m_{66} - m_{22}m_{11}m_{33}m_{44}m_{56}m_{65} + m_{22}m_{11}m_{33}m_{13}m_{65}m_{15}\\
&- m_{22}m_{11}m_{33}m_{13}m_{15}m_{66} + m_{22}m_{11}m_{33}m_{13}m_{15}m_{56}\\
&- m_{22}m_{11}m_{33}m_{13}m_{55}m_{15} - 2m_{22}m_{11}m_{34}m_{13}m_{65}m_{15} + 2m_{22}m_{11}m_{34}m_{13}m_{15}m_{66}\\
&- 2m_{22}m_{11}m_{34}m_{13}m_{15}m_{56} + 2m_{22}m_{11}m_{34}m_{13}m_{55}m_{15} + m_{22}m_{11}m_{13}m_{44}m_{65}m_{15}\\
&- m_{22}m_{11}m_{13}m_{44}m_{15}m_{66} - m_{22}m_{11}m_{13}m_{44}m_{55}m_{15}\\
&+ m_{22}m_{11}m_{13}m_{44}m_{15}m_{56} - 2m_{12}m_{13}m_{44}m_{15}m_{31}m_{66} + 2m_{12}m_{13}m_{44}m_{15}m_{31}m_{65}\\
&- 4m_{12}m_{34}m_{13}m_{15}m_{31}m_{65} + 4m_{12}m_{34}m_{13}m_{15}m_{31}m_{66} + 2m_{12}m_{34}m_{13}m_{31}m_{56}m_{65}\\
&- m_{12}m_{33}m_{13}m_{31}m_{56}m_{65} + m_{12}m_{33}m_{13}m_{31}m_{55}m_{66}\\
&+ m_{12}m_{13}m_{31}m_{44}m_{55}m_{66} + 2m_{12}m_{33}m_{13}m_{15}m_{31}m_{65} - 2m_{12}m_{33}m_{13}m_{15}m_{31}m_{66}\\
&- m_{12}m_{33}m_{44}m_{56}m_{15}m_{31} - m_{12}m_{33}m_{44}m_{15}m_{31}m_{65} + m_{12}m_{33}m_{44}m_{55}m_{15}m_{31}\\
&+ m_{12}m_{33}m_{44}m_{15}m_{31}m_{66} - 2m_{12}m_{34}m_{13}m_{31}m_{55}m_{66}\\
&- 4m_{12}m_{34}m_{13}m_{56}m_{15}m_{31} + 4m_{12}m_{34}m_{13}m_{55}m_{15}m_{31} - m_{12}m_{13}m_{31}m_{44}m_{56}m_{65}\\
&- 2m_{12}m_{13}m_{44}m_{55}m_{15}m_{31} + 2m_{12}m_{13}m_{44}m_{56}m_{15}m_{31} + 2m_{12}m_{33}m_{13}m_{56}m_{15}m_{31}\\
&- 2m_{12}m_{33}m_{13}m_{55}m_{15}m_{31} - m_{31}m_{21}m_{34}^2m_{15}m_{66}.
\end{aligned}
$$

$$
\begin{aligned}
P_0^{(2)} &= + m_{31}m_{21}m_{34}^2m_{65}m_{15} + m_{31}m_{21}m_{34}^2m_{15}m_{56} - m_{31}m_{21}m_{34}^2m_{55}m_{15} - m_{31}m_{13}m_{11}m_{44}m_{55}m_{66}\\
&+ m_{31}m_{13}m_{11}m_{44}m_{56}m_{65} + 2m_{31}m_{34}m_{13}m_{11}m_{55}m_{66} - 2m_{31}m_{34}m_{13}m_{11}m_{56}m_{65}\\
&+ 4m_{31}m_{34}m_{13}m_{65}m_{15}m_{11} - 4m_{31}m_{34}m_{13}m_{15}m_{11}m_{66} + 4m_{31}m_{34}m_{13}m_{15}m_{11}m_{56}\\
&- 4m_{31}m_{34}m_{13}m_{55}m_{15}m_{11} - 2m_{31}m_{13}m_{44}m_{65}m_{15}m_{11}\\
&+ 2m_{31}m_{13}m_{44}m_{15}m_{11}m_{66} + 2m_{31}m_{13}m_{44}m_{55}m_{15}m_{11} - 2m_{31}m_{13}m_{44}m_{15}m_{11}m_{56}\\
&+ 4m_{31}m_{22}m_{34}m_{13}m_{65}m_{15} - 4m_{31}m_{22}m_{34}m_{13}m_{15}m_{66} + 4m_{31}m_{22}m_{34}m_{13}m_{15}m_{56}\\
&- 4m_{31}m_{22}m_{34}m_{13}m_{55}m_{15} - 2m_{31}m_{22}m_{13}m_{44}m_{65}m_{15}\\
&+ 2m_{31}m_{22}m_{13}m_{44}m_{15}m_{66} + 2m_{31}m_{22}m_{13}m_{44}m_{55}m_{15} - 2m_{31}m_{22}m_{13}m_{44}m_{15}m_{56}\\
&- m_{31}m_{22}m_{13}m_{44}m_{55}m_{66} + m_{31}m_{22}m_{13}m_{44}m_{56}m_{65} + 2m_{31}m_{22}m_{34}m_{13}m_{55}m_{66}\\
&- 2m_{31}m_{22}m_{34}m_{13}m_{56}m_{65} - m_{31}m_{33}m_{13}m_{11}m_{55}m_{66}\\
&+ m_{31}m_{33}m_{13}m_{11}m_{56}m_{65} - 2m_{31}m_{33}m_{13}m_{65}m_{15}m_{11} + 2m_{31}m_{33}m_{13}m_{15}m_{11}m_{66}\\
&- 2m_{31}m_{33}m_{13}m_{15}m_{11}m_{56} + 2m_{31}m_{33}m_{13}m_{55}m_{15}m_{11} - m_{31}m_{22}m_{33}m_{13}m_{55}m_{66}\\
&+ m_{31}m_{22}m_{33}m_{13}m_{56}m_{65} - 2m_{31}m_{22}m_{33}m_{13}m_{65}m_{15}\\
&+ 2m_{31}m_{22}m_{33}m_{13}m_{15}m_{66} - 2m_{31}m_{22}m_{33}m_{13}m_{15}m_{56} + 2m_{31}m_{22}m_{33}m_{13}m_{55}m_{15}\\
&+ m_{31}m_{33}m_{44}m_{65}m_{15}m_{11} - m_{31}m_{33}m_{44}m_{15}m_{11}m_{66} + m_{31}m_{22}m_{33}m_{44}m_{65}m_{15}\\
&- m_{31}m_{22}m_{33}m_{44}m_{15}m_{66} - m_{31}m_{33}m_{44}m_{55}m_{15}m_{11}\\
&+ m_{31}m_{33}m_{44}m_{15}m_{11}m_{56} - m_{31}m_{22}m_{33}m_{44}m_{55}m_{15} + m_{31}m_{22}m_{33}m_{44}m_{15}m_{56}.
\end{aligned}
$$

References

[1] A.S. Davydov, J. Theoret. Biol. 38 (1973) 559.
[2] A.S. Davydov, N.I. Kislukha, Phys. Status Solidi B 39 (1973) 65.
[3] A.S. Davydov, N.I. Kislukha, Phys. Status Solidi B 75 (1976) 735.

[4] A.C. Scott, Phys. Rev. A 26 (1982) 578.
[5] A.C. Scott, Phys. Rep. 217 (1992) 1.
[6] P.L. Christiansen, A.C. Scott, Self-Trapping of Vibrational Energy, Plenum Press, New York, 1990.
[7] L. Cruzeiro, J. Halding, P.L. Christiansen, O. Skovgard, A.C. Scott, Phys. Rev. A 37 (1987) 703.
[8] L. Cruzeiro-Hansson, Phys. Rev. A 45 (1992) 4111.
[9] L. Cruzeiro-Hansson, V.M. Kenker, A.C. Scott, Phys. Lett. A 190 (1994) 59.
[10] W. Förner, Phys. Rev. A 44 (1991) 2694.
[11] W. Förner, Physica D 68 (1993) 68.
[12] W. Förner, J. Comput. Chem. 13 (1992) 275.
[13] W. Förner, J. Phys.: Condens. Matter. 3 (1991) 1915.
[14] A.C. Scott, Phys. Scr. 25 (1982) 651.
[15] A.C. Scott, Phys. Scr. 29 (1984) 279.
[16] A.C. Scott, Physica D 51 (1990) 333.
[17] D.W. Brown, K. Lindenberg, B.J. West, Phys. Rev. B 35 (1987) 6169.
[18] D.W. Brown, Z. Ivic, Phys. Rev. B 40 (1989) 9876.
[19] D.W. Brown, K. Lindenberg, X. Wang, in: P.L. Christiansen, A.C. Scott (Eds.), Davydov's Soliton Revisited, Plenum, New York, 1990.
[20] A.C. Scott, Phys. Lett. A 86 (1981) 60.
[21] L. Cruzeiro-Hansson, J.C. Eilbeck, J.L. Marin, F.M. Russell, Phys. Lett. A 266 (2000) 160.
[22] M. Daniel, M.M. Latha, Phys. Lett. A 252 (1999) 92.
[23] G.R.Y. Mefire, C.B. Tabi, A. Mohamadou, H.P.F. Ekobena, T.C. Kofané, Chaos 23 (2013) 033128.
[24] C.B. Tabi, I. Maïna, A. Mohamadou, H.P.F. Ekobena, T.C. Kofané, Europhys. Lett. 106 (2014) 18005.
[25] C.S. Panguetna, C.B. Tabi, T.C. Kofané, Commun. Nonl. Sci. Numer. Simul. 55 (2018) 326.
[26] C.S. Panguetna, C.B. Tabi, T.C. Kofané, Phys. Plasmas 24 (2017) 092114.
[27] A.D. Koko, C.B. Tabi, H.P.F. Ekobena, A. Mohamadou, T.C. Kofané, Chaos 22 (2012) 043110.
[28] C.B. Tabi, J.C.F. Mimshe, H.P.F. Ekobena, A. Mohamadou, T.C. Kofané, Eur. Phys. J. B 86 (2013) 374.
[29] H.P.F. Ekobena, C.B. Tabi, A. Mohamadou, T.C. Kofané, J. Phys.: Condens. Matter 23 (2011) 375104.
[30] J.C.F. Mimshe, C.B. Tabi, H. Edongue, H.P. Ekobena, A. Mohamadou, T.C. Kofané, Phys. Scr. 87 (2013) 025801.
[31] C.B. Tabi, R.Y. Ondoua, H.P. Ekobena, A. Mohamadou, T.C. Kofané, Phys. Lett. A 380 (2016) 2374.
[32] D. Hennig, Phys. Rev. B 65 (2002) 174302.
[33] D.N. Beratan, J.N. Onuchic, J.J. Hopfield, J. Chem. Phys. 86 (1987) 4488.
[34] J.N. Onuchic, D.N. Beratan, J. Chem. Phys. 92 (1990) 722.
[35] J.N. Onuchic, P.C.P. Andrade, D.N. and Beratan, J. Chem. Phys. 95 (1991) 1131.
[36] C. Turró, C.K. Chang, G.E. Leroi, R.I. Cukier, D.G. Nocera, J. Am. Chem. Soc. 114 (1992) 4013.
[37] D. Hennig, Phys. Rev. E 64 (2001) 041908.
[38] T.C. Tabi, Eur. Phys. J. E 32 (2010) 327.
[39] A. Mvogo, G.H. Ben-Bolie, T.C. Kofané, Phys. Lett. A 378 (2014) 2509.
[40] B. Sadjo, C.B. Tabi, H. Edongue, A. Mohamadou, Wave Motion 72 (2017) 342.
[41] A.S. Etémé, C.B. Tabi, A. Mohamadou, Commun. Nonlinear Sci. Numer. Simul. 43 (2017) 211.
[42] A.S. Etémé, C.B. Tabi, A. Mohamadou, Chaos Solitons Fractals 104 (2017) 813.
[43] C.B. Tabi, I. Maïna, A. Mohamadou, H.P.F. Ekobena, T.C. Kofané, Physica A 435 (2015) 1.
[44] E.N.N. Aboringong, A.M. Dikandé, Eur. Phys. J. E 41 (2018) 35.
[45] C.B. Tabi, H.P.F. Ekobena, T.C. Kofané, J. Comput. Theor. Nanosci. 8 (2011) 2220.
[46] Z. Ivic, D. Kapor, M. Skrinjar, Z. Popovic, Phys. Rev. B 48 (1993) 3721.
[47] Z. Ivic, D. Kostic, Z. Przulj, D. Kapor, J. Phys.: Condens. Matter 9 (1997) 413.
[48] J. Tekic, Z. Ivic, S. Zekovic, Z. Przulj, Phys. Rev. E 60 (1999) 821.
[49] C. Falvo, V. Pouthier, J. Chem. Phys. 123 (2005) 184709.
[50] C. Falvo, V. Pouthier, J. Chem. Phys. 123 (2005) 184710.
[51] A.K. Dang, C.B. Tabi, H.P.F. Ekobena, T.C. Kofané, Int. J. Quantum Chem. 115 (2015) 34.
[52] J. Berashevich, V. Apalkov, T. Chakraborty, J. Phys.: Condens. Matter 20 (2008) 075104.
[53] C.B. Tabi, A. Mohamadou, T.C. Kofané, J. Phys.: Condens. Matter 21 (2009) 335101.
[54] C.B. Tabi, A.D. Koko, R.O. Doko, H.P.F. Ekobena, T.C. Kofané, Physica A 442 (2016) 498.

Coupled Fractional Patterns of Energy in $\alpha-$helix Proteins

C. B. Tabi [1,2*], S. E. Madiba[1†], H. P. F. Ekobena[1‡] and T. C. Kofané[3§]

[1]Botswana International University of Science and Technology, Private Mail Bag 16 Palapye, Botswana
[2]Laboratoire de Biophysique, Département de Physique, Faculté des Sciences, Université de Yaoundé I, B.P. 812 Yaoundé, Cameroun
[3]Laboratoire de Mécanique, Département de Physique, Faculté des Sciences, Université de Yaoundé I, B.P. 812 Yaoundé, Cameroun

July 8, 2020

Abstract

Coupled fractional nonlinear Schrödinger equations are derived from a two-exciton energy transfer model of $\alpha-$helix proteins. Space-fractional terms are due to the presence of long-range intermolecular interactions. The linear stability analysis of plane wave solutions reveals the existence of regions of instability, where solitonic waves can emerge as the consequence of the competition between nonlinear and dispersive effects. The parametric expansion of the growth rate of instability is found to be sensitive to the variations in the fractional-order parameters and the nonlinear coupling coefficient. Numerical evidence of analytical predictions is given via the long-time emergence and behavior of solitonic structures, whose characteristics change with variations in the fractional-order parameters.

*Corresponding author: conrad@aims.ac.za or tabic@biust.ac.bw (C. B. Tabi)
†madibaes@yahoo.com (S. E. Madiba)
‡hekobena@gmail.com (H. P. F. Ekobena)
§tckofane@yahoo.com (T. C. Kofané)

Keywords: $\alpha-$helix; Fractional dispersion; Solitons; Two exciton.

---

1 Introduction

In the last decades, the understanding of energy transport and storage in biomolecules has received a remarkable development mainly based on the seminal contribution of Davydov [1]. It has been well-established that the energy which is transported via proteins originates from the hydrolysis of adenosine triphosphate (ATP) [1]. Namely, considering the structure of $\alpha-$helix proteins, Davydov and Kislukha [2, 3] used the exciton formalism to explain the self-trapping of the amide-I oscillations as the consequence of the interaction between the vibrational exciton and the distortion in the protein structure, resulting from the presence of the exciton. They established that the interplay between nonlinearity and dispersion may favor solitons to travel in the protein strand and carry the self-trapped vibrational amide-I energy. Many of the contributions that followed focussed on the existence of only one exciton state [4, 5, 6, 7, 8, 9, 10, 11, 12, 13]. Works by Pouthier and Falvo [16, 17, 18] however insisted on the existence of at least two excited states as a way of stabilizing the self-trapped energy. Merlin and Latha [19, 20] also addressed such aspects and rather showed, based on a paper from Ekobena et al. [8], that anharmonicity may play an important role when more that one excitations are considered. The soliton that are usually obtained in this context are solutions of coupled nonlinear Schrödinger (NLS) equations, each describing a specific excitonic state [7, 9, 10, 13, 21]. Attention has been given recently to protein structures with long-range (LR) intermolecular interactions, leading to space-fractional NLS equations [21, 22]. In this framework, Tarasov and Zaslavsky [23, 24] have shown that in the presence of power-law LR interactions, it was possible to reduce a purely discrete problem to its space-fractional formulation. A three-stranded model of $\alpha-$helix proteins was used recently as an example by Mvogo et al. [21], but further

approximations were made to recover a classical set of coupled NLS equations, therefore avoiding the complexity imposed by the fractional terms. More recently, the modulational instability (MI) of a fractional NLS equation was addressed, where Zhang et al. [25] showed that the fractional-order parameter may have important influence on the onset and long-time evolution of nonlinear modulated patterns. Tabi [22] also studied the MI of plane wave in an $\alpha-$helix model and brought out the effect of the fractional derivative on the process of energy transport and storage along a single protein strand. This work is a generalization of such a model, i.e., when more that one excitonic degree of freedom is considered. We show that for a two-exciton model, transport and storage of energy can fully be described by a set of nonlinearly coupled space-fractional NLS equations. The linear stability analysis of their plane wave solutions is then performed with emphasis on the effect of changing both the fractional-order parameters and the coefficient of nonlinearity. Numerical experiments are used to confirm the analytical predictions through the long-time behaviors of the subsequent modulated trains of waves. Concluding remarks end the paper.

2 Model and dynamical equation

2.1 Model

The generalized Hamiltonian corresponding to the dynamics of two excitons in a protein lattice has been proposed in some recent works as an improvement of the Davydov model [1, 2]. In the presence of LR intrachain molecular interaction between molecular excitations, the Hamiltonian writes

$$\begin{aligned} H = \sum_n \Big[& \hbar\omega_0 (A_n^\dagger A_n + B_n^\dagger B_n) - \sum_{m\neq n} J_{n-m}^{(1)} (A_n^\dagger A_m + A_n A_m^\dagger) - \sum_{m\neq n} J_{n-m}^{(1)} (B_n^\dagger B_m + B_n B_m^\dagger) \\ & + \frac{g_1}{2} (A_n^\dagger A_n^\dagger A_n A_n + B_n^\dagger B_n^\dagger B_n B_n) + g_2 A_n^\dagger A_n B_n^\dagger B_n \Big], \end{aligned} \tag{1}$$

with the subscript n referring to the lattice index along the strand (or chain). The expression of H suggests that an individual amino acid will be identified by the index pair n, such that A_n $(A_n^\dagger)$

and B_n ($B_n^\dagger$) are boson creation (annihilation) operators associated with intramolecular vibrations of the nth peptide group. These operators satisfy the usual commutation relations for bosons, i.e., $[A_n, A_m^\dagger] = \delta_{m,n}$, $[A_n, A_m] = 0$, $[B_n, B_m^\dagger] = \delta_{m,n}$ and $[B_n, B_m] = 0$. $\hbar\omega_0$ is the local amide-I vibrational energy, and the terms $\hbar\omega_0 A_n^\dagger A_n$ and $\hbar\omega_0 B_n^\dagger B_n$ are the vibrational energies at the site n from the two exciton bound states. The terms $\sum_{m\neq n} J_{n-m}^{(1)}(A_n^\dagger A_m + A_n A_m^\dagger)$ and $\sum_{m\neq n} J_{n-m}^{(2)}(B_n^\dagger B_m + B_n B_m^\dagger)$ are the energies related to the LR interactions between molecular excitations on sites n and m. The coupling parameters $J_{n-m}^{(1)}$ and $J_{n-m}^{(2)}$ are the LR transfer integrals between sites n and m, here considered of the form [26, 27, 28, 29]:

$$J_{n-m}^{(1)} = J_1|n-m|^{-s_1} \quad \text{and} \quad J_{n-m}^{(2)} = J_2|n-m|^{-s_2}, \tag{2}$$

with J_1 and J_2 being the strengths of the transfer integral between the chain and each of the excitations. s_i ($i = 1, 2$) are range parameters whose values belong to the interval $[1, +\infty[$. However s_i cover different physical contexts, depending on its value. For example if $s_i \to \infty$, the LR interaction reduces to nearest-neighbor couplings. For $s_i = 5$, the LR interaction is of a dipole-dipole type, while for $s_i = 3$, the LR interaction is of the Coulomb type. We should stress that the strongest interaction effects are due to smaller values of s_i.

We make use of the Heisenberg formulation and obtain the following exciton equations:

$$i\hbar\frac{\partial A_n}{\partial t} = \hbar\omega_0 A_n - \sum_{m\neq n} J_{n-m}^{(1)} A_m + (g_1 A_n A_n^\dagger + g_2 B_n B_n^\dagger)A_n, \tag{3a}$$

$$i\hbar\frac{\partial B_n}{\partial t} = \hbar\omega_0 B_n - \sum_{m\neq n} J_{n-m}^{(2)} B_m + (g_1 B_n B_n^\dagger + g_2 A_n A_n^\dagger)B_n. \tag{3b}$$

In order to study coherent states, it will be useful to rewrite Eq.(3) in terms of eigenfunctions of the operators A_n, $A_n^\dagger$, B_n and $B_n^\dagger$ so that, if the Glauber coherent states $|\{\alpha_n\}\rangle = \prod_n |\alpha_n\rangle$, $A_n|\alpha_n\rangle = \alpha_n|\alpha_n\rangle$, $|\{\beta_n\}\rangle = \prod_n |\beta_n\rangle$ and $B_n|\beta_n\rangle = \beta_n|\beta_n\rangle$ are introduced [30], the set of Eqs.(3)

becomes

$$i\hbar\frac{\partial\alpha_n}{\partial t} = \hbar\omega_0\alpha_n - \sum_{m\neq n} J^{(1)}_{n-m}\alpha_m + (g_1|\alpha_n|^2 + g_2|\beta_n|^2)\alpha_n, \tag{4a}$$

$$i\hbar\frac{\partial\beta_n}{\partial t} = \hbar\omega_0\beta_n - \sum_{m\neq n} J^{(2)}_{n-m}\beta_m + (g_2|\alpha_n|^2 + g_1|\beta_n|^2)\beta_n. \tag{4b}$$

Eqs.(4) are a set of nonlinearly coupled NLS equations with LR dispersive interactions. When $g_2 = 0$, the two equations will be completely decoupled and will reduce to individual discrete NLS equations. For instance, we can get rid of the terms $\hbar\omega_0\alpha_n$ and $\hbar\omega_0\beta_n$ via the gauge transformations $\alpha_n(t) = u_n(t)e^{-i\omega_0 t}$ and $\beta_n(t) = v_n(t)e^{-i\omega_0 t}$. This yields

$$i\frac{\partial u_n}{\partial t} = -\sum_{m\neq n} J^{(1)}_{n-m}u_m + (g_1|u_n|^2 + g_2|v_n|^2)u_n, \tag{5a}$$

$$i\frac{\partial v_n}{\partial t} = -\sum_{m\neq n} J^{(2)}_{n-m}v_m + (g_2|u_n|^2 + g_1|v_n|^2)v_n, \tag{5b}$$

where we have further made the change of variable $t \to t/\hbar$.

2.2 The coupled NLS equation with fractional derivative

In order to obtain the fractional-derivative formulation of Eqs.(5), we introduce the functions [21, 23, 24]

$$\phi(k,t) = \sum_{m=-\infty}^{+\infty} e^{-iknd}u_n(t), \quad \psi(k,t) = \sum_{m=-\infty}^{+\infty} e^{-iknd}v_n(t) \quad \text{and} \quad J(k) = \sum_{m=-\infty}^{+\infty} e^{-iknd}J_n, \tag{6}$$

where the parameter k is a wavenumber, d is the lattice spacing and J_n is given by Eq. (2). Inversely, the functions $u_n(t)$ and $u_n(t)$ are respectively related to $\phi(k,t)$ and $\psi(k,t)$ through the relations

$$u_n(t) = \int_{-\pi}^{\pi} e^{iknd}\phi(k,t)dk \quad \text{and} \quad v_n(t) = \int_{-\pi}^{\pi} e^{iknd}\psi(k,t)dk. \tag{7}$$

In the continuum approximation, i.e., $u_n(t) \to u(x,t)$ and $v_n(t) \to v(x,t)$, with $x = nd$, when $k \to 0$, relations (6) and (7) become

$$\begin{aligned} \phi(k,t) &= \int_{-\infty}^{+\infty} e^{-ikx} u(x,t)dx, \quad \psi(k,t) = \int_{-\infty}^{+\infty} e^{-ikx} v(x,t)dx, \\ u(x,t) &= \frac{1}{2\pi}\int_{-\infty}^{+\infty} e^{ikx}\phi(k,t)dk, \quad v(x,t) = \frac{1}{2\pi}\int_{-\infty}^{+\infty} e^{ikx}\psi(k,t)dk. \end{aligned} \tag{8}$$

Applying all the above to Eq.(5) in the continuum approximation leads to

$$i\frac{\partial u(x,t)}{\partial t} = -J_1(0)u(x,t) - \int_{-\infty}^{+\infty} dydx K_1(x-y)\frac{\partial u(x,t)}{\partial x} + \left(g_1|u(x,t)|^2 + g_2|v(x,t)|^2\right)u(x,t) \tag{9a}$$

$$i\frac{\partial v(x,t)}{\partial t} = -J_2(0)v(x,t) - \int_{-\infty}^{+\infty} dydx K_2(x-y)\frac{\partial v(x,t)}{\partial x} + \left(g_2|u(x,t)|^2 + g_1|v(x,t)|^2\right)v(x,t), \tag{9b}$$

where the Kernels $K_i(x)$ $(i = 1, 2)$ are given by

$$K_i(x) = \frac{1}{\pi}\int_{-\infty}^{+\infty} e^{ikx}\frac{G_i(k)}{k^2}dk, \quad i = 1, 2, \tag{10}$$

with $G_i(k) = J_i(0) - J_i(k)$, $J_i = \zeta(s_i)^{-1}$, with the $\zeta-$function being given by $\zeta = \sum_{1=1}^{\infty} n^{-s}$. For the specific case where $2 \leq s_i < 3$, the function $G(k)$ is in the form

$$G_i(k) = \frac{\pi J_i}{\Gamma(\sigma_i + 1)\sin\left(\frac{\pi\sigma_i}{2}\right)}|k|^{\sigma_i}, \tag{11}$$

where where $\Gamma(\sigma)$ is the $\Gamma-$function, with $\sigma = s - 1$ and $\Gamma(\sigma + 1) = \sigma\Gamma(\sigma)$. Therefore, given the possible values of s, the values of σ will be found between 1 and 2. Under such considerations, the continuum equations (9) become

$$i\frac{\partial u(x,t)}{\partial t} = -J_1(0)u(x,t) - P_1\frac{\partial^{\sigma_1}}{\partial|x|^{\sigma_1}}u(x,t) + \left(g_1|u(x,t)|^2 + g_2|v(x,t)|^2\right)u(x,t), \tag{12a}$$

$$i\frac{\partial v(x,t)}{\partial t} = -J_2(0)v(x,t) - P_2\frac{\partial^{\sigma_2}}{\partial|x|^{\sigma_2}}v(x,t) + \left(g_2|u(x,t)|^2 + g_1|v(x,t)|^2\right)v(x,t), \tag{12b}$$

where the coefficients P_i $(i = 1, 2)$ are given by

$$P_1 = \frac{\pi J_1}{\Gamma(\sigma_1 + 1)\sin\left(\frac{\pi\sigma_1}{2}\right)} \quad \text{and} \quad P_2 = \frac{\pi J_2}{\Gamma(\sigma_2 + 1)\sin\left(\frac{\pi\sigma_2}{2}\right)}. \tag{13}$$

The Riesz fractional derivatives are given by [31, 32]

$$\frac{\partial^{\sigma_1}}{\partial|x|^{\sigma_1}}u(x,t) = -\frac{1}{2\pi}\int_{-\infty}^{+\infty}|k|^{\sigma_1}\phi(k,t)dk \quad \text{and} \quad \frac{\partial^{\sigma_2}}{\partial|x|^{\sigma_2}}v(x,t) = -\frac{1}{2\pi}\int_{-\infty}^{+\infty}|k|^{\sigma_2}\psi(k,t)dk. \tag{14}$$

By making use of the gauge transfomations $u(x,t) \to u(x,t)e^{iJ_1 t}$ and $v(x,t) \to v(x,t)e^{iJ_2 t}$, we finally obtain

$$i\frac{\partial u(x,t)}{\partial t} = -P_1\frac{\partial^{\sigma_1}}{\partial|x|^{\sigma_2}}u(x,t) + \left(g_1|u(x,t)|^2 + g_2|v(x,t)|^2\right)u(x,t), \tag{15a}$$

$$i\frac{\partial v(x,t)}{\partial t} = -P_2\frac{\partial^{\sigma_2}}{\partial|x|^{\sigma_2}}v(x,t) + \left(g_2|u(x,t)|^2 + g_1|v(x,t)|^2\right)v(x,t), \tag{15b}$$

which is a set of coupled NLS equations with space-fractional derivatives. Obviously, the dispersion terms P_i are functions of the fractional-order parameters σ_i. However, the Riesz fractional derivative is also expressed as [31, 32]

$$\frac{\partial^{2\sigma}}{\partial|x|^{\sigma}}f(x,t) = -\left(-\frac{\partial^2}{\partial|x|^2}\right)^{\sigma/2}f(x,t) = -\frac{1}{2\cos\left(\frac{\pi\sigma}{2}\right)}\left[{}_{-\infty}\mathcal{D}_x^{\sigma}f(x,t) + {}_{x}\mathcal{D}_{+\infty}^{\sigma}f(x,t)\right], \tag{16}$$

where ${}_{-\infty}\mathcal{D}_x^{\sigma}f(x,t)$ and ${}_{x}\mathcal{D}_{+\infty}^{\sigma}f(x,t)$, are the left- and right-side Riemann-Liouville fractional derivatives of order σ, that are respectively given by [31, 32]

$$\begin{aligned} {}_{x}\mathcal{D}_{+\infty}^{\sigma}f(x,t) &= \frac{1}{\Gamma(n-\sigma)}\frac{\partial^n}{\partial x^n}\int_{-\infty}^{x}\frac{f(\xi,t)d\xi}{(x-\xi)^{\sigma-x+1}}, \\ {}_{-\infty}\mathcal{D}_x^{\sigma}f(x,t) &= \frac{(-1)^n}{\Gamma(n-\sigma)}\frac{\partial^n}{\partial x^n}\int_{-\infty}^{x}\frac{f(\xi,t)d\xi}{(\xi-x)^{\sigma-x+1}}. \end{aligned} \tag{17}$$

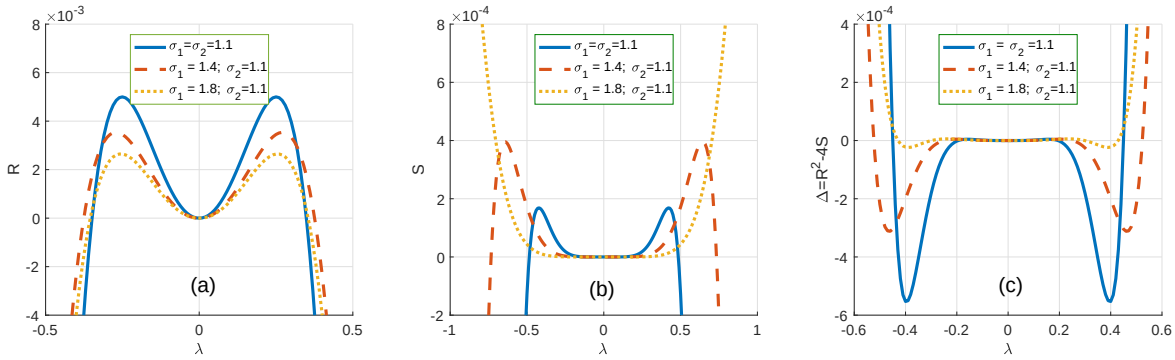

Figure 1: The panels show plots of the of the coefficients R and S of Eq. (22) and its discriminant $\Delta = R^2 - 4S$, versus the perturbation wavenumber λ. The fractional-order parameters change as shown in the legends, with $g_1 = g_2 = -0.05$ and $J_1 = J_2 = 0.08$.

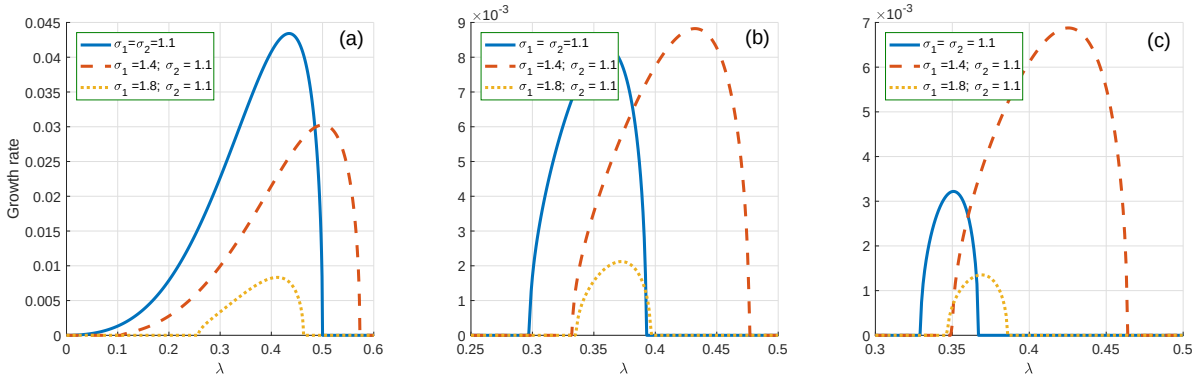

Figure 2: The panels show plots of the MI growth rate (25) versus the perturbation wavenumber λ. (a) corresponds to $g_1 = -0.5$, (b) to $g_1 = -0.1$ and (c) to $g_1 = -0.08$. We have fixed $g_2 = -0.05$, while the fractional-order parameters change as displayed by the legends, with $J_1 = J_2 = 0.08$.

3 Modulational instability analysis

The set of Eqs.(15) admits the plane waves $u(x,t) = u_0 e^{i\omega_1 t}$ and $v(x,t) = v_0 e^{i\omega_2 t}$ as solutions, with the frequencies and amplitudes u_0 and v_0 being related by

$$\omega_1 = -(g_1|u_0|^2 + g_2|v_0|^2) \text{ and } \omega_2 = -(g_1|v_0|^2 + g_2|u_0|^2). \tag{18}$$

We consider small perturbations χ_1 and χ_2 into the above solutions, i.e., $u(x,t) = u_0(1+\chi_1(x,t))e^{i\omega_1 t}$ and $v(x,t) = v_0(1+\chi_2(x,t))e^{i\omega_2 t}$. This leads, after linearizing around the unperturbed plane waves, to the set of equations

$$i\frac{\partial}{\partial t}\chi_1(x,t) = -P_1\frac{\partial^{\sigma_1}}{\partial|x|^{\sigma_1}}\chi_1(x,t) + g_1|u_0|^2(\chi_1+\chi_1^*) + g_2|v_0|^2(\chi_2+\chi_2^*), \tag{19a}$$

$$i\frac{\partial}{\partial t}\chi_2(x,t) = -P_2\frac{\partial^{\sigma_2}}{\partial|x|^{\sigma_2}}\chi_2(x,t) + g_1|v_0|^2(\chi_2+\chi_2^*) + g_2|u_0|^2(\chi_1+\chi_1^*) \tag{19b}$$

for the perturbations. Moreover, the problem can be efficiently solved by separating real from imaginary parts, i.e., $\chi_1 = a_1 + ib_1$ and $\chi_2 = a_2 + ib_2$, leading to the equations

$$\begin{aligned}
\frac{\partial}{\partial t}a_1(x,t) &= -P_1\frac{\partial^{\sigma_1}}{\partial|x|^{\sigma_1}}b_1(x,t),\\
\frac{\partial}{\partial t}b_1(x,t) &= P_1\frac{\partial^{\sigma_1}}{\partial|x|^{\sigma_1}}a_1(x,t) - 2g_1|u_0|^2a_1(x,t) - 2g_2|v_0|^2a_2(x,t),\\
\frac{\partial}{\partial t}a_2(x,t) &= -P_2\frac{\partial^{\sigma_2}}{\partial|x|^{\sigma_2}}b_2(x,t),\\
\frac{\partial}{\partial t}b_2(x,t) &= P_2\frac{\partial^{\sigma_2}}{\partial|x|^{\sigma_2}}a_2(x,t) - 2g_1|v_0|^2a_2(x,t) + 2g_2|u_0|^2a_1(x,t).
\end{aligned} \tag{20}$$

Solutions for Eqs.(20) can be considered in the form of the following Fourier transfroms:

$$\begin{aligned}
\tilde{a}_1(\lambda,\Omega) &= \int\int_{-\infty}^{+\infty} a_1(x,t)e^{i(\lambda x+\Omega t)}dxdt,\\
\tilde{a}_2(\lambda,\Omega) &= \int\int_{-\infty}^{+\infty} a_2(x,t)e^{i(\lambda x+\Omega t)}dxdt,\\
\tilde{b}_1(\lambda,\Omega) &= \int\int_{-\infty}^{+\infty} b_1(x,t)e^{i(\lambda x+\Omega t)}dxdt,\\
\tilde{b}_2(\lambda,\Omega) &= \int\int_{-\infty}^{+\infty} b_2(x,t)e^{i(\lambda x+\Omega t)}dxdt.
\end{aligned} \tag{21}$$

Replacing the above solutions into Eqs.(20) leads to a homogeneous system for $\tilde{a}_1$, $\tilde{b}_1$, $\tilde{a}_2$ and $\tilde{b}_2$. The condition for such a system to admit non-trivial solutions is obtained by setting its determinant to zero, which leads to the nonlinear dispersion relation

$$\Omega^4 - R\Omega^2 + S = 0, \tag{22}$$

where

$$\begin{aligned}
R &= P_2|\lambda|^{\sigma_2}(2g_1|v_0|^2 - P_2|\lambda|^{\sigma_2}) + P_1|\lambda|^{\sigma_1}(2g_1|u_0|^2 - P_1|\lambda|^{\sigma_1}),\\
S &= P_1P_2|\lambda|^{\sigma_1+\sigma_2}\left[4g_2^2|u_0|^2|v_0|^2 - (P_1|\lambda|^{\sigma_1} - 2g_1|u_0|^2)(P_2|\lambda|^{\sigma_2} - 2g_1|v_0|^2)\right].
\end{aligned} \tag{23}$$

Obviously, the coefficients of the dispersion relation (22) depend on the fractional-order parameters σ_1 and σ_2. However, the plane wave solutions will remain stable if the conditions $R > 0$, $S > 0$ and $\Delta = R^2 - 4S > 0$ are simultaneously satisfied. In order to find the intervals of parameters where such condition can be satisfied, we have plotted R, S and Δ in Fig. 1 versus the perturbation wavenumber λ.

The condition $R > 0$ is studied in Fig. 1(a), where the stability region is found in the interval $0 < \lambda < \lambda_+$. However, depending on the value of the fractional-order parameters σ_1 and σ_2, that interval can get expanded or reduced. It gets expanded for $\sigma_1 = 1.4$ and $\sigma_2 = 1.1$, and drops for $\sigma_1 = 1.8$ and $\sigma_2 = 1.1$.

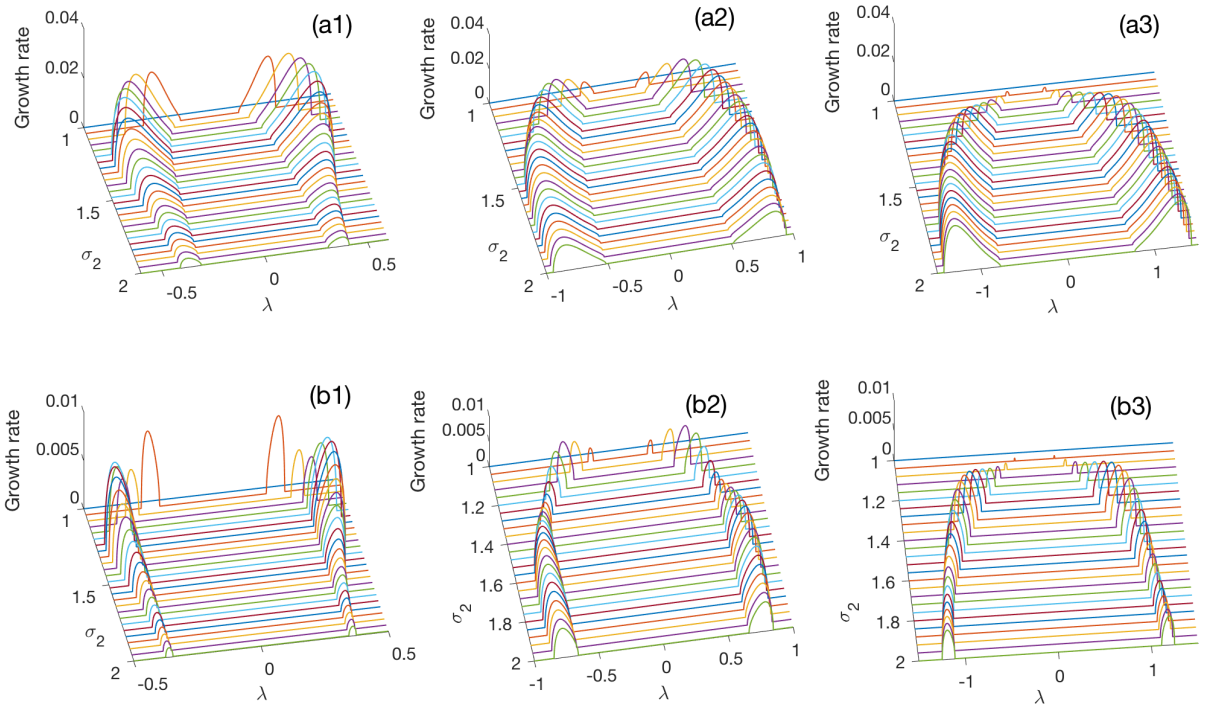

Figure 3: Plots of the MI growth rate versus the perturbation wavenumber λ and the fractional-order parameter σ_2. Panels $(\mathrm{aj})_{j=1,2,3}$ correspond to $g_1 = -0.5$ and $g_2 = -0.05$, and panels $(\mathrm{bj})_{j=1,2,3}$ gives Γ for $g_1 = -0.08$ and $g_2 = -0.05$. Columns (a1)-(b1) are obtained for $\sigma_1 = 1.1$, (a2)-(b2) for $\sigma_1 = 1.4$ and (a3)-(b3) for $\sigma_1 = 1.8$, with $J_1 = J_2 = 0.08$.

The condition $S > 0$ is addressed in Fig. 1(b). For $\{\sigma_1 = \sigma_2 = 1.1\}$ and $\{\sigma_1 = 1.4; \sigma_2 = 1.1\}$, there is an interval $\lambda_- < \lambda < \lambda_+$ (with $\lambda_- > 0$) where wave stability is expected. However, there is a change of behavior for $\{\sigma_1 = 1.8; \sigma_2 = 1.1\}$, where stable plane wave are possible in the interval $\lambda_- < \lambda < \infty$.

The discriminant Δ has been plotted in Fig. 1(c). The plane wave will remain stable where Δ is positive. Its sign changes with the fractional-order parameters. Under such a condition, Eq. (22) admits two solutions given by

$$\Omega_+^2 = \frac{1}{2}\left(R + \sqrt{R^2 - 4S}\right), \quad \Omega_-^2 = \frac{1}{2}\left(R - \sqrt{R^2 - 4S}\right). \tag{24}$$

On the other hand, if $\Delta = R^2 - 4S < 0$, there exists a domain of the wavenumber λ for which Ω^2 is negative. In this range, the solution of (22) are complex so that Ω^2 has a nonvanishing imaginary part. The plane waves will be unstable if this imaginary part of Ω is positive, causing the perturbation to grow exponentially. Then, the plane wave tends to self-modulate with a wavenumber λ corresponding to the growth rate

$$\Gamma = \mathrm{Im}\left(\Omega_\pm^2\right) = \pm\frac{1}{2}\sqrt{4S - R^2}. \tag{25}$$

The above growth rate of instability implies that the condition $\sqrt{4S - R^2} > 0$ should be satisfied for wave instability to take place. The growth rate of instability (25) is plotted in Fig. 2, versus the wavenumber λ, where the effect of the fractional-order parameters is obvious. To plot Fig. 2(a), we have fixed $g_2 = -0.5$ and $\sigma_2 = 1.1$. For $\sigma_1 = \sigma_2 = 1.1$, the plane wave is unstable in the region $0 < \lambda < 0.5$ which gets extended to $0 < \lambda < 0.58$ for $\sigma_1 = 1.4$. For $\sigma_1 = 1.8$, the region of instability gets reduced and restricted to the interval $0.26 < \lambda < 0.48$. The same behavior is obvious in all the other cases, where $g_2 = -0.1$ (Fig. 2(b)) and $g_2 = -0.05$ (Fig. 2(c)), but with a delocalization phenomenon of the instability domain. To remind, g_2 is the nonlinear coupling parameter between Eqs. (15a) and (15b), which when set to zero reduces the system to ordinary

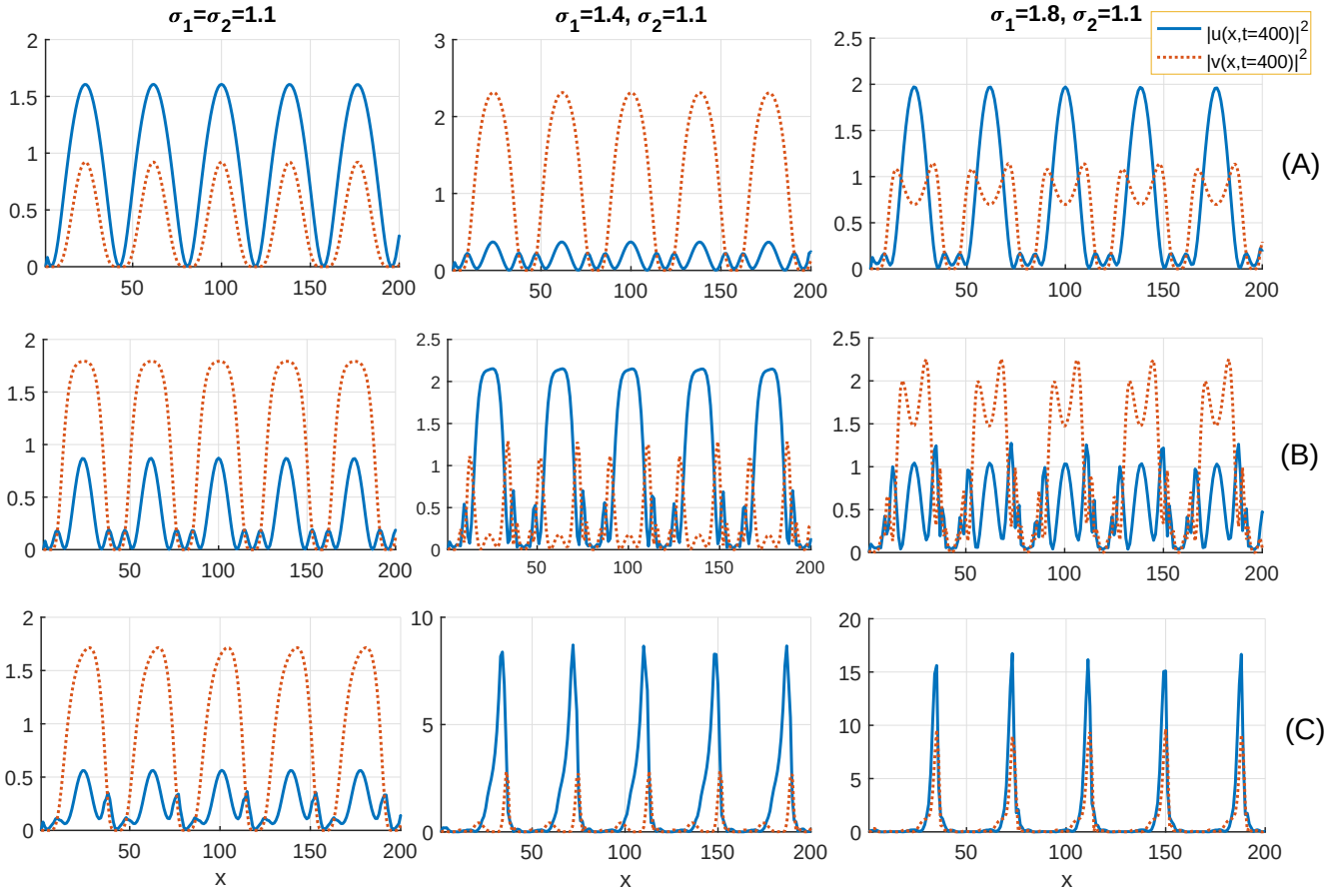

Figure 4: Plane wave modulation in the two-exciton chain for: Line (A) $g_1 = g_2 = -0.05$, Line (B) $g_1 = -0.08$ and $g_2 = -0.05$, and Line (C) $g_1 = -0.1$ and $g_2 = -0.05$. The first column on the left correspond to $\sigma_1 = \sigma_2 = 1.1$. The middle column corresponds to $\sigma_1 = 1.4$ and $\sigma_2 = 1.1$, and the right column corresponds to $\sigma_1 = 1.8$ and $\sigma_2 = 1.1$. We have fixed $\lambda = 0.3$ and $J_1 = J_2 = 0.08$.

fractional NLS equations. Its interplay with space-fractional terms (or fractional dispersion) is responsible for the emergence of regions of instability as further confirmed by the growth rate diagrams plotted in Fig. 3, where the upper line corresponds to $g_2 = -0.5$ and the lower line to $g_2 = -0.08$. Therefore, when parameters fall inside regions of instability, the plane wave solutions will be said to be unstable under modulation. Otherwise, the plane wave solutions will be expected

to remain stable, keeping their initial characteristics. Further details on the instability features of the plane wave solutions are given in Fig. 4, where the fractional CNLS Eqs.(15) have been solved numerically using the standard split-step Fourier method [33]. In order to verify both the dispersive and nonlinear coupling effects, we have assumed $v_0 = 0$ as initial condition of Eq. (15b), while the initial condition for Eq. (15a) is considered to be a perturbed plane wave solution with the perturbation wavenumber $\lambda = 0.3$. Lines (A) of Fig. 4 correspond to the case $g_1 = g_2 = -0.05$, where g_2 is the nonlinear coupling coefficient between the two vibrational equations. The same panels from left to right respectively correspond to $\{\sigma_1 = \sigma_2 = 1.1\}$, $\{\sigma_1 = 1.4; \quad \sigma_2 = 1.1\}$ and $\{\sigma_1 = 1.8; \quad \sigma_2 = 1.1\}$. Obviously, the obtained patterns are trains of solitonic structures whose features changes with increasing σ_1. This strongly support the fact that solitons are robust in such systems and may display different behaviors due to the interplay between nonlinear and dispersive effects. Lines (B) of Fig. 4 depict the case $g_2 = -0.08$ with g_1 keeping the same value as previously. σ_1 and σ_2 also keep the same values as previously. The coupling process remains effective here and the initial solitons tend to spread into radiations. However, the two excitonic parts contribute to maintain permanent energy transport under the activation of MI. The last case of Fig. 4, i.e., Lines (C), has been recorded for $g_2 = -0.1$. Each of the modes still displays trains of solitonic structures, except that for high values of the fractional-order parameter σ_1, the wave objects become narrow in space and highly localized. We should remind that only one of the modes has been excited and that is exactly the one that shows highly localized structures. Energy transport, to be efficient has been shown to be supported by such waves, especially during the process of replication and transcription, where the hydrogen bonds that link bases in DNA pairs are broken [12, 29, 34, 35, 36, 37]. In proteins, it was shown that they may also emerge as exact solutions, depending on the used method and the corresponding biological implications [13, 21, 38]. However, the fractional-order parameters σ_1 and σ_2 bring about new features into wave localization

in proteins, and can be used as control parameters by suitable biological processes for specific purpose.

4 Concluding remarks

In this paper, we have studied the two-exciton energy transfer in $\alpha-$helix molecular chains, in the presence of LR dispersive interactions. We have shown that in the continuum limit, using Fourier formalism may reduce the initial discrete problem to a set of coupled NLS equations with space-fractional derivatives. The theory of MI has thereafter been used to study the onset of solitonic structures, via the linear stability analysis, followed by direct numerical simulations for confirmation. The effect of changing the fractional-order parameters has been studied and, together with the change in the nonlinear coupling coefficient, it has been found to enhance the localization of energy, especially involving the two excitonic modes. This has been found to be in agreement with the predictions and supports once more the robustness of solitonic waves in molecular structures, especially when nonlinear and dispersive effects are involved, for specific biological purposes.

Acknowledgements

This work is supported by the Botswana International University of Science and Technology under the grant **DVC/RDI/2/1/16I (25)**. I thank the Kavli Institute for Theoretical Physics (KITP), University of California Santa Barbara (USA), where this work was supported in part by the National Science Foundation Grant no.**NSF PHY-1748958**, NIH Grant no.**R25GM067110**, and the Gordon and Betty Moore Foundation Grant no.**2919.01**.

References

[1] A. S. Davydov, J. Theor. Biol. **38** (1973) 559.

[2] A. S. Davydov and N. I. Kislukha, Phys. Stat. Sol. B **39** (1973) 65.

[3] A. S. Davydov and N. I. Kislukha, Phys. Stat. Sol. B **75** (1976) 735.

[4] A. C. Scott, Phys. Rev. A **26** (1982) 578.

[5] A. C. Scott, Phys. Rep. **217** (1992) 1.

[6] M. Daniel and K. Deepamala, Phys. A **221** (1995) 241

[7] R.Y. Ondoua, C. B. Tabi, H. P. Ekobena, A. Mohamadou and T. C. Kofané, Eur. Phys. J. B **86** (2012) 374.

[8] H. P. F. Ekobena, C. B. Tabi, A. Mohamadou and T. C. Kofané, J. Phys.: Condens. Matter **23** (2011) 375104.

[9] C. B. Tabi, J. C. F. Mimshe, H. P. F. Ekobena, A. Mohamadou and T. C. Kofané, Eur. Phys. J. B **86** (2013) 374.

[10] J. C. F. Mimshe, C. B. Tabi, H. Edongue, H. P. F. Ekobena, A. Mohamadou and T. C. Kofané, Physica Scripta **87** (2013) 025801.

[11] C. B. Tabi, R.Y. Ondoua, H. P. Ekobena, A. Mohamadou and T. C. Kofané, Phys. Lett. A **380** (2016) 2374.

[12] B. Sadjo, C. B. Tabi, H. Edongue and A. Mohamadou, Wave Motion **72** (2017) 342.

[13] I. Sali, C. B. Tabi, H. P. F. Ekobena and T. C. Kofané, EPJ Plus **133** (2018) 233.

[14] M. Daniel and M. M. Latha, Phys. Lett. A **252** (1999) 92.

[15] E. N. N. Aboringong and A. M. Dikandé, Eur. Phys. J. E **41** (2018) 35.

[16] V. Pouthier and C. Falvo, Phys. Rev. E **69** (2004) 041906.

[17] C. Falvo and V. Pouthier, J. Chem. Phys. **123** (2005) 184710.

[18] C. Falvo and V. Pouthier, J. Chem. Phys. **122** (2005) 041701.

[19] M.M. Latha and G. Merlin, Phys. Lett. A **376** (2012) 938.

[20] G. Merlin and M.M. Latha, Physica D **265** (2013) 71.

[21] A. Mvogo, G. H. Ben-Bolie and T. C. Kofané, Phys. Lett. A **378** (2014) 2509.

[22] C. B. Tabi, Chaos Solit. Fract. **116** (2018) 386.

[23] V. E. Tarasov and G. M. Zaslavsky, Commun. Nonl. Sci. Numer. Simul. **11** (2006) 885.

[24] V. E. Tarasov and G. M. Zaslavsky, Chaos **16** (2006) 023110.

[25] L. Zhang, Z. He, C. Contia, Z. Wang, Y. Hu, D. Lei, Y. Li and D. Fan, Commun. Nonl. Sci. Numer. Simul. **48** (2017) 531.

[26] A. S. Etémé, C. B. Tabi and A. Mohamadou, Commun. Nonl. Sci. Num. Simul. **43** (2017) 211.

[27] A. S. Etémé, C. B. Tabi and A. Mohamadou, Chaos Solit. Fract. **104** (2017) 813.

[28] C. B. Tabi, I. Maïna, A. Mohamadou, H.P. F. Ekobena and T. C. Kofané, Physica A **435** (2015) 1.

[29] C. B. Tabi, A. Mohamadou and T. C. Kofané, J. Bionanosci. **2** (2008) 89.

[30] R. J. Glauber, Phys. Rev. **131** (1958) 776.

[31] V. V. Uchaikin, *Fractional derivatives for physicists and engineers*, Berlin: Springer (2013).

[32] S. G. Samko, A. A. Kilbas and O. I. Marichev, *Fractional integrals and derivatives theory and applications*, New York: Gordon and Breach (1993).

[33] G. P. Agrawal, *Nonlinear fiber optics*, San Diego: Academic Press; 2001.

[34] A. D. Koko, C. B. Tabi, H. P. F. Ekobena, A. Mohamadou and T. C. Kofané, Chaos **22** (2012) 043110.

[35] C. B. Tabi, A. Mohamadou and T. C. Kofané, Chaos **19** (2009) 043101.

[36] C. B. Tabi, G. Bineli and A. Mohamadou, J. Biol. Phys. **41** (2015) 391.

[37] C. B. Tabi, H. P. E. Fouda, A. Mohamadou and T. C. Kofané, Physica Scripta **83** (2011) 035802.

[38] S. E. Madiba, C. B. Tabi, H. P. F. Ekobena and T. C. Kofané, Physica A **514** (2019) 298.